



Development of a Low-Cost, Portable Lab-on-a-Disc PCR Instrument

Project Portfolio

Candidate: Conor Michael Curley
Student ID: 19467152
Course Code: MEIM5
Date: 26 March 2025

M.Eng. in Mechatronic Engineering

School of Electronic Engineering

School of Mechanical & Manufacturing Engineering

Core Deliverable
IEEE Conference Paper

Development of a Low-Cost, Portable Lab-on-a-Disc PCR Instrument

Conor M. Curley, Dublin City University

Abstract— This document details the development of a centrifugal microfluidic platform to facilitate the polymerase chain reaction. Microfluidic platforms represent an attractive opportunity for the development of low-cost, point-of-care diagnostic assays, a principle that is explored throughout this paper. First, prior work on the topic of microfluidic assays, microfluidic PCR, and PCR temperature control systems is explored. Subsequently, detail is provided on the design and fabrication of a novel and innovative centrifugal microfluidic platform for PCR, along with validation procedures and an experimental protocol. Finally, the results of the work detailed within this paper are presented and discussed.

I. INTRODUCTION

The Polymerase Chain Reaction (PCR) is vital to the field of diagnostics, permitting the rapid amplification of genetic material for the purposes of parthenogen identification, genetic sequencing, and forensics. However, traditional PCR equipment is expensive and bulky, inhibiting its use in point-of-care settings and in the developing world. On the other hand, Centrifugal microfluidic devices exploit rotational forces to implement automatic sample handling and complex diagnostic processes in a disc-shaped platform. This approach stands as a pivotal advancement in point-of-care diagnostics, enabling rapid, high-bandwidth, equipment-free testing.

Microfluidic devices have been designed to streamline assay protocols such that little-to-no personnel training is required, substantially reduce sample volumes, enhanced control over fluid behavior, and reduce reaction time. PCR is tackled frequently in Microfluidic literature; however, the demand remains for a low-cost, portable PCR instrument suitable for use in point-of-care settings and in the developing world. However, a modern focus on point-of-care testing and diagnostics in the developing world has opened an opportunity for additional research in the area of microfluidic PCR.

Significant work has been undertaken to migrate existing diagnostic assays to microfluidic platforms. Previous work on the topic gives significant insight into the current state of the art in microfluidic PCR. Much of the existing research tends towards droplet-based qualitative or digital PCR, which results in an assay that is more suitable for laboratory settings. Significant research has also been conducted on novel and innovative heating elements to support PCR thermocycling, continuously miniaturizing elements of the instrument that would be bulky and expensive in traditional instruments.

The method proposed within this paper represents a contribution to low-cost, energy-efficient, point-of-care devices, designed for regions where access to traditional laboratory commodities may be limited. The research aim is to create a centrifugal microfluidic PCR platform using an innovative PCB-based temperature control system. The instrument will be capable of completing a quantitative PCR assay, controlled wirelessly through a web-based user interface

II. PRIOR WORK

Solutions have previously been developed for low-cost, point-of-care microfluidic devices, in some cases, even in domestic settings. Andres W. Martinez et al would develop the first practical application of a paper-based assay used in the detection of glucose and protein[1]. The process involved the application of an indicator compound to patterning paper. The paper was subsequently dipped into an artificial urine solution consisting of glucose and bovine serum albumin. The resulting reaction would cause the color of the paper to change, indicating a positive assay. Paper-based lateral flow devices were used ubiquitously on a global scale in the detection of SARS-CoV-2 during the COVID-19 pandemic. In these devices, a preprocessed sample is loaded onto a sample pad. Subsequently, capillary action carries the sample across a porous membrane, upon which test and control lines, containing an indicator, are overlayed. Upon reaching these lines, the sample reacts with the indicator, providing a visual indication of the result[2].

Droplet based microfluidic devices have been used to improve diagnostic devices in a range of areas, as detailed in a comprehensive review conducted by Amirfar et al[3]. The earliest implementation, one also significant to this thesis, was in the polymerase chain reaction (PCR). Numerous researchers have contributed a range of process improvements since the inception of DBMD. Zubaite et al introduced a method of isolating, amplifying, and condensing DNA molecules in 3pL droplets using an integrated T-junction droplet generator. Stark et al implemented a process for a microfluidic platform combining DNA extraction and quantitative PCR. Pellegrino et al introduced a microfluidic device capable of sequencing DNA derived from acute myeloid leukemia tumors. Azizi et al designed a high-precision assay to detect *Salmonella typhimurium* using a droplet-based LAMP instrument.

Moschou et al would later propose a centrifugal microfluidic quantitative PCR reaction is achieved using a microfluidic chip[4]. The sample was exposed to 30 temperature cycles, each composed of three distinct steps. Each temperature zone is controlled by an individual resistive

microheater. The sample was pumped through 1.45m of microchannels by a laboratory syringe pump. The resulting instrument exhibited a total power consumption of only 2.4W, while successful DNA amplification was demonstrated after only 5 minutes.

A challenge, however, present itself in the thermocycling mechanism of a PCR instrument. Traditionally, a PCR cycle is composed of two distinct temperature stages, denaturation at 94 degrees and annealing and extension at 74 degrees, although the number of stages and the precise temperature set-points for each stage vary depending on the author's method. However, poor thermal management may allow any of the stages to fall out of operating range, resulting the production of unwanted byproducts. It can then be inferred that the selection of an appropriate heating element is paramount to the successful creation of a PCR instrument. In traditional thermo-cyclers, the heating and cooling is permitted though a conventional heating block, which is incompatible with centrifugal microfluidics. A thermocycler proposed by Xie et al introduced a method utilizing magnetic induction heating[5], requiring a constant pumped-supply of cool water. Other researchers have proposed the use of Peltier plates to both heat and cool the sample. In a method proposed by Nasser et al[6], a 50W Peltier element is integrated to heat and cool a PMMA chip. Peltier elements, however, consume large amounts of power and require bulking heatsinks. Wang et al proposed a novel heating method using liquid metal as a medium for heat exchange which, while innovative, is impractical. In a paper published by Talebi et al, a PCB-based heater was proposed as a heating element for a continuous-flow PCR chip[7]. The chip was fabricated from PMMA, containing microfluidic channels in a serpentine pattern. A PCB with integrated heating elements was then placed over the chip, such that half of each channel was covered by the high-temperature heating element, and the other was covered by the low-temperature heating element. The result was a heater capable of transitioning the sample between two temperature zones at a near-instant rate, without the requirement for pumping or active cooling.

III. TECHNICAL DESCRIPTION

The solution proposed in this paper is composed of a self-enclosed centrifugal microfluidic PCR instrument based on the Lab-on-a-Disc platform. The instrument is composed of a range of components, including a microfluidic disc, centrifuge, heating element, spectrometry system, and user interface. The internal elements of the instrument are controlled by a central control system. The fabrication and implementation of these elements will be described in this section.

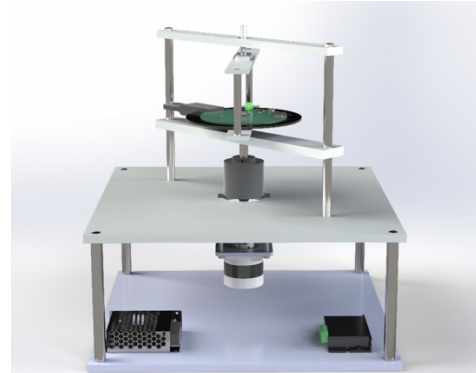


Figure 1 A render of the instrument

A. Chassis

The chassis for the instrument is adapted from a previous final-year project[8], featuring a platform, slirping for power transmission, and mount for a motor.

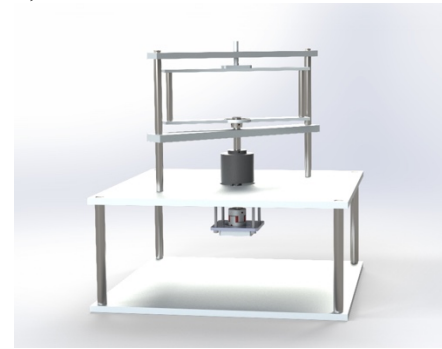


Figure 2 The existing chassis

B. Central Control System

The central control system (CCS) is responsible for governing the function of the instrument and reporting vital information to the user. In essence, the CCS manages the control of peripheral control systems (PCSS), including the centrifuge and the heater, and also acquisition of data from sensors such as the spectral sensor. The CCS is capable of communicating with the user interface over the WebSockets protocol.

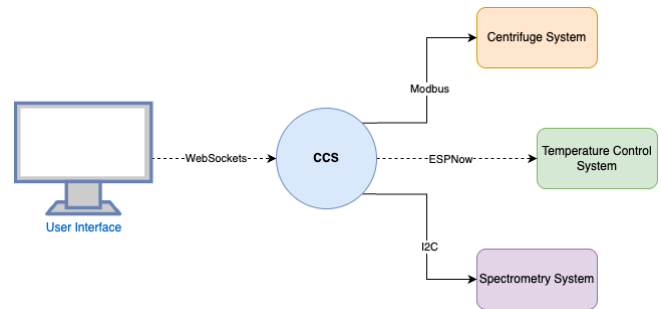


Figure 3 Overview of the communications structure used in the CCS

The CCS also encompasses the power system for the instrument. The instrument is powered by both 24V/14A and 5V/7A power supplies. The 24V power supply was salvaged from a broken Ender3 3D printer, while the 5V supply (Meanwell LRS-35-5) was purchased new from StepperOnline.

C. Microfluidic Disc

The primary objective of this project is to create an instrument capable of supporting a PCR assay. As such, the determination was made that a disc capable of supporting the simplest form of PCR, end-point PCR, should be designed first. In order to support an end-point PCR reaction, the disc must contain reservoirs to hold the sample before and after the reaction and channels to perform the reaction in.

Regardless of the type of PCR undertaken, the reaction requires the sample to be exposed repeatedly to heating and cooling cycles, between the temperatures of 74°C and 94°C. While heating a liquid between the two temperatures listed previously in itself is not a difficult task, cooling presents a unique challenge. To circumvent this issue, a unique solution is proposed. If the volume of the channels is reduced, the thermal mass for the fluid is reduced, consequently reducing the energy required to heat the fluid and the energy loss required to cool the fluid. To achieve this reduction in volume, the channels are cut from PSA rather than PMMA, permitting a channel height of only 0.086mm. This results in a thermal diffusion time of only 150ms.

In addition to temperature modulation, the rate of change in temperature is also a significant factor. The channels must be designed to physically support the modulation of temperature at a rapid rate. A dual-layer design was selected as the appropriate design for this project.

The progression of liquid through the microfluidic channels is dependent on the pressure exerted on the liquid, which in turn is dependent on the difference between the radial locations of the start of the liquid and the end of the liquid. Given that the liquid in the channels on the top layer will flow radially outward, down through a via, and return radially inward, the relative pressure on the fluid in the channels on the bottom layer will cancel that of the channels in the top layer. If a volume of the sample is less than or equal to the total volume of the channels, the input reservoir will empty before the sample can progress to the output reservoir, the pressure on the sample will fall to zero, causing the reaction to stall. To work around this, a volume equal to V_{total} of low-density, immiscible liquid such as mineral oil is added to the input reservoir, and as such, the input reservoir will require a total volume of the sample and the mineral oil.

$$V_{total} = N_{cyc} \cdot (A \cdot L_t + A \cdot L_b + 2 \cdot A \cdot L_v)$$

$$V_{total} = 5.83 \times 10^{-5} \text{ m}^3$$

D. Centrifuge

A centrifuge is a laboratory instrument that is used to separate the contents of a mixture based on their relative densities by subjecting them to rapid rotation. This generates outward acceleration on denser components. In this project, outward acceleration is required to propel the sample through microfluidic reservoirs. As such, a centrifuge mechanism is required. Key design components of the centrifuge include a motor, motor driver, and microcontroller. The CCS and centrifuge are designed to communicate over Modbus.



Figure 4 The spindle mechanism of the instrument

In order to couple the disc to the drive mechanism, a spindle has been adapted from existing chassis. The spindle is mounted to the chassis using a sliring, permitting the rotation of the spindle and power transmission to the rotating body. A shaft connects the spindle to a motor through a jaw coupling.

A suitable BLDC motor capable of driving the disc at 3000RPM with 0.23Nm of torque was selected (StepperOnline, 57BLR50-24-01). In line with the manufacturer's recommendations, a suitable motor driver (StepperOnline, BLD-305S) was also selected.

E. Heating

Given that a regulated temperature is required for a PCR reaction, a temperature control system is required to regulate the temperature of the heating element. A PCB heater has been designed and fabricated for the purposes of this project. The design of the heater is made difficult by virtue of the number of viable entry points into calculating heater parameters. Additionally, drawing a heater composed of a large number of repeating traces is quite tedious. Consequently, a solution was designed to identify the optimal design for the heater.

The heater PCB was designed using KiCad, a software that facilitates both schematic and PCB design. A schematic was drawn to demonstrate connections between the numerous components on the board. The primary microcontroller on the board is an ESP-S3 module. A USB-micro connector, as well as reset and boot buttons, are provided for programming over the ESP32-S3's integrated USB-OTG driver. The board is supplied with a 5V connection via terminal blocks, which is stepped down to a suitable voltage for the ESP32-S3 by a 3V3 regulator. A MOSFET is used to switch power to the heater trace to control heating. The temperature of the heater is acquired via a digital temperature sensor. The PCB itself was produced by JLCPCB.



Figure 5 A render of the PCB heater

In order to control the temperature of the heater, a combination of Bang-Bang control and Pulse-Width Modulation (PWM) control is used. The Bang-Bang controller will turn the heater fully on until the target temperature is reached, at which point, the PWM controller will take over, turning the heater on and off in cycles to maintain the set-point. While likely not as accurate as PID control, this type of control will be able to maintain the temperatures required of this heater. In both cases, feedback from the temperature sensor is used as the reference for the temperature of the heater.

E. Spectrometry

A fluorophore (EVARuby) will be used to qualify the result of the PCR reactions undertaken by the instrument. As such, the spectrometry system is designed as a C-shaped assembly, to be attached to the spindle support. The assembly may be rotated over the disc once the PCR reaction is complete. The system is designed such that the C-shaped assembly covers the sample reservoir, preventing extraneous light from entering the reservoir while analysis is underway. A blue LED (C503B-BCN-CV0Z0461) with a peak emission wavelength of 470nm projects light onto the sample from the bottom of the disc through a blue gel filter. This light illuminates the sample, causing fluorescence. The fluorescent emission projects upwards towards the top of the disc, through a red gel filter, and into a spectral sensor (Adafruit AS7341).

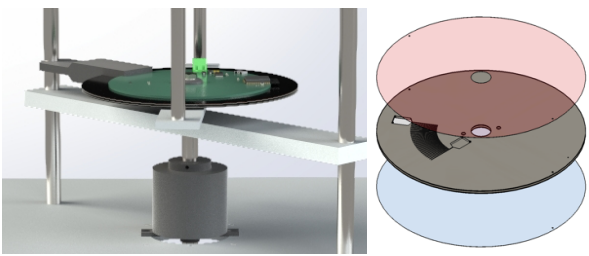


Figure 6 The spectrometry element of the instrument (left), the stacked configuration of gel filters (right)

F. User Interface

A fundamental objective of this project is to provide a professional, usable interface for interacting with and receiving data from the instrument. This objective is fulfilled with a web-based user interface, which communicates with the instrument in real-time wirelessly over the WebSocket protocol.

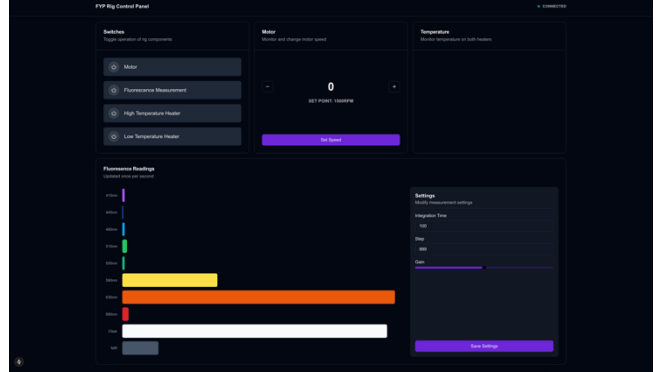


Figure 7 The user interface for the instrument

The user interface is built as a single-page application. The home page contains a range of cards, each with unique functions. An indicator in the top right of the screen shows whether there is an active WebSocket connection to the instrument. An image of the interface on startup is shown in Figure X. An image of the interface while the instrument is running is shown in Figure Y. "Switches" allows the user to control boolean actions, such as turning on the motor or activating the heaters. "Motor" allows the user to view the actual speed of the motor and adjust the speed set-point. "Temperature" allows the user to view the actual temperature of both heaters. "Fluorescence Readings" allows the user to view a plot of the most recent readings from the spectral sensor. The user can also adjust spectral sensor parameters in the menu to the right of the card.

G. Experimental Procedure

The experimental procedure for this project is composed of two components. First, each of the components of the instrument must be validated to ensure they meet the requirements of the project. After the instrument is validated, an assay may be conducted in order to gather experimental results.

The centrifuge is validated via the user interface. The motor is enabled and set to a range of speeds. The actual speed of the motor given by the motor driver is compared to the set-point. If the reported values match that of the set-point, the validation test is considered successful. The disc is validated through the use of dyed water. A distilled water and food dye mixture is added to the reservoir using a pipette. The motor is enabled, and the disc is rotated at a range of angular velocities. If the sample is able to flow through the channels unimpeded, without leaks, the validation test is considered successful. The heater is validated through the use of a FLIR thermal camera and the user interface. The heater is assigned a set-point, and the temperature rise is observed both through a thermal camera

and on the user interface. If the disc maintains a set point without under- or overshoot, and the values reported by the user interface and the thermal camera align, the validation test is considered successful.

Once the instrument is validated as detailed above, a PCR assay will be completed on the instrument. The PCR assay will be completed per the following experimental protocol. The sample is prepared using PCR master mix and a measure of EVARuby (Biotium), per the relevant protocols. A $200\mu L$ sample is loaded onto the disc using a micropipette, followed by a layer of mineral oil. The rig is enclosed to prevent injury from moving components over the course of the assay. The heaters are set to preheat to the relevant temperature set-points. Once the heaters are at temperature, the motor is enabled, and rotation is started. Once the sample has been processed, the instrument is stopped and locked-out. The fluorescence sensor is moved into position and fluorescence data is recorded.

IV. DISCUSSION

An instrument capable of undertaking a microfluidic PCR assay has been designed. Many of the elements of the instrument have been constructed and implemented, including the centrifuge, microfluidic disc, and spectrometry system. A centrifuge system has been built, including a BLDC motor and motor driver. Communication over Modbus has been successfully implemented such that a remote user interface can control and receive vital information from the motor driver.

A microfluidic disc has been fabricated, capable of providing a medium for an end-point PCR reaction. During fabrication, it was noted that the laser did not provide enough precision to accurately cut the 0.5mm vias between the top and bottom PSA layers. While the disc was unable to be validated due to component delays, this likely would have given rise to further issues in testing. Consequently, further work is required to design the disc such that it is compatible with the manufacturing facilities available.

A spectrometry system has been created with the capacity to qualify the result of DNA amplification resulting from the PCR assay. Due to shipping issues, it was not possible to obtain the EVARuby fluorophore in advance of the project deadline. As such, it was not possible to validate the functionality of the system.

A PCB heating element has been designed, capable of regulating the temperature of the sample over the course of a PCR assay. Unfortunately, due to a miscommunication in the manufacturing process, the fabrication of the PCB heaters was delayed until the 26th of March 2025. This issue arose as both metric and imperial systems share the same naming convention for SMD component sizes. An imperial 0205 capacitor was selected in error, when the actual capacitor should have been metric 0205. This resulted in the capacitor being oversized, and consequently not aligning properly with the relevant solder pad on the PCB. This resulted in back-and-forth communication with the supplier to resolve the issue, inevitably resulting in significant delays.

As a result, it was not possible to fully assemble the instrument and complete a PCR assay. However, I plan to

continue work on this instrument in a PhD capacity to address the original research goals outlined in this paper. In the future, I also plan to implement a qualitative PCR assay on the instrument.

APPENDIX

All CAD/CAM and software files are available in the project repository.

Available at https://github.com/conorcurley5/FYP_Files

REFERENCES AND FOOTNOTES

A. References

- [1] A. W. Martinez, S. T. Phillips, M. J. Butte, and G. M. Whitesides, "Supporting Information for".
- [2] L. Syedmoradi, M. Daneshpour, M. Alvandipour, F. A. Gomez, H. Hajighassem, and K. Omidfar, "Point of care testing: The impact of nanotechnology," *Biosens. Bioelectron.*, vol. 87, pp. 373–387, Jan. 2017, doi: 10.1016/j.bios.2016.08.084.
- [3] "Droplet-based microfluidics in biomedical applications - IOPscience." Accessed: Mar. 26, 2025. [Online]. Available: <https://iopscience.iop.org/article/10.1088/1758-5090/ac39a9/pdf>
- [4] D. Moschou *et al.*, "All-plastic, low-power, disposable, continuous-flow PCR chip with integrated microheaters for rapid DNA amplification," *Sens. Actuators B Chem.*, vol. 199, pp. 470–478, Aug. 2014, doi: 10.1016/j.snb.2014.04.007.
- [5] Y. Xie *et al.*, "A Thermal Cycler Based on Magnetic Induction Heating and Anti-Freezing Water Cooling for Rapid PCR," *Micromachines*, vol. 15, no. 12, p. 1462, Nov. 2024, doi: 10.3390/mi15121462.
- [6] G. A. Nasser, A. L. Abdel-Mawgood, A. A. Abouelsoud, H. Mohamed, S. Umezawa, and A. M. R. F. El-Bab, "New cost effective design of PCR heating cycler system using Peltier plate without the conventional heating block," *J. Mech. Sci. Technol.*, vol. 35, no. 7, pp. 3259–3268, Jul. 2021, doi: 10.1007/s12206-021-0646-5.
- [7] F. Talebi, H. Ghafoorifard, S. Ghafouri-Fard, and A. Jahanshahi, "A straight-forward, inexpensive, low power continuous-flow μPCR chip using PCB-based heater electrodes with uniform temperature distribution," *Sens. Actuators Phys.*, vol. 333, p. 113220, Jan. 2022, doi: 10.1016/j.sna.2021.113220.
- [8] S. Fairbrother, "Redesign of a Test Rig and Implementation of Bioassay," Oct. 2023.

Conor M. Curley (Student, Dublin City University), photograph and biography not available at the time of publication.

Appendix One

Status Report



Ollscoil Chathair
Bhaile Átha Cliath
Dublin City University

Portable Lab Instrument 5th Year Project Status Report

20 Nov 2024

Conor Curley

MEng in Mechatronic Engineering
Advisor: David Kinahan

Table of Contents

Portable Lab Instrument	1
5 th Year Project Status Report	1
Table of Contents.....	<i>Error! Bookmark not defined.</i>
Table of Figures	2
Introduction.....	3
Background	3
Proposed Solution.....	4
Lab-on-a-Disc.....	4
Temperature Control System.....	5
Spectrometry System.....	6
Project Plan	7
Success Criteria	7
References	8

Table of Figures

Figure 1: A technical drawing of a prototype microfluidic disc (to be revised)	5
Figure 2: An exploded view of the Temperature Control System assembly.....	5
Figure 3: A plot of the optical properties of the proposed spectrometry instrument (blue: excitation source, dotted orange: excitation wavelength of EvaRuby, filled orange: emission wavelength of EvaRuby, outlined orange: measurement wavelength of spectral sensor)	6
Figure 4: An image of a Gantt chart describing planned actions for this project. .	7

Introduction

The Polymerase Chain Reaction (PCR) is a diagnostic technique that facilitates the amplification of a DNA sample in-vitro, first discovered in 1986 by Mullis et. al[1]. PCR is commonly used world-wide to support genetic sequencing[2], detection of genetic mutations[3], and diagnosis of a wide range of diseases, including COVID-19[4], Hepatitis[5], and HIV[6].

Modern PCR instruments provide immense value to the medical industry, however, there are several issues that stifle further adoption. In general, conventional PCR instruments require a large upfront investment[7]. Conventional PCR instruments are also typically quite large, reducing portability[8]. As a result, in regions where formal laboratory environments are not available, PCR testing may not be feasible. Furthermore, these PCR instruments typically consume large amounts of power[9], restricting their usage in regions where electricity is limited.

This proposal aims to find a solution to these issues in the form of a centrifugal microfluidic lab-on-a-disc instrument is proposed. The device will be capable of qualitative PCR, and the fundamental principles of the instrument will be designed with portability, cost, and power efficiency in mind.

Background

Until 1986, the most promising method for DNA synthesis and amplification was de novo synthesis[10], taking inspiration from genetic engineering principles to synthesize DNA via the recombination of existing fragments using oligonucleotide kinase and DNA ligase.

Mullis et al.[1] raised an issue with de novo synthesis where an accurate sequence of DNA could not be synthesized unless the template was already sequenced and understood. Mullis et al. would go on to propose a solution to this problem: the Polymerase Chain Reaction. The technique, referred to as end-point PCR (EP-PCR) in modern literature, involved the use of a DNA template and a primer. A primer is a complementary sequence of nucleotides, ideally 18-24, to a specific area of interest in the target template strand[11]. EP-PCR was takes place over three distinct stages, as described by the authors.

Denaturation allows the separating of a DNA template strand into two single-stranded DNA molecules (ssDNA). This involves the application of heat to break the hydrogen bonds that hold the strands together. The enzyme helicase is responsible for this action in a biological environment[12]. This stage typically occurs over 2 minutes with the sample heated to 90°C.

Annealing describes a process where a primer bonds to a complementary oligonucleotide sequence on an ssDNA molecule. The term is used in literature to describe PCR-specific hybridisation[13]. This stage typically takes place over 2 minutes with the sample incubated at 30°C.



Extension refers to the DNA polymerase enzyme transcribing a new strand of DNA from the template ssDNA. DNA Polymerase I attaches to the template strand at the 3' end of the primer and extends the complementary strand in the 3' direction of the new strand[14]. Extension is an active process, requiring the presence of dATP as a source of energy. DNA polymerase also requires four nucleotides (thymidine monophosphate, adenosine monophosphate, cytidine monophosphate, and guanosine monophosphate) as cofactors to support this reaction. This stage typically takes place over 2 minutes with the sample incubated at 30°C.

These stages compose one PCR "cycle". In total, 20-27 cycles were conducted by the authors on human DNA. In practice, the total number of cycles required varies depending on the amplification requirements[15].

An issue present in the technique proposed by Mullis et al is the use of DNA polymerase I. This enzyme has a heat inactivation temperature of 37-80°C, resulting in denaturation during the initial stage of the PCR cycle[16]. Consequently, fresh DNA polymerase I was required to be added prior to each cycle. Saiki et al. determined a resolution to this issue in a 1988 paper, proposing the use of thermostable Taq polymerase[17], discovered in the thermophilic bacteria *Thermus aquaticus*[18]. This enzyme has an active temperature range of 70-75°C[19], with a heat inactivation temperature of 95°C, affording it the ability to survive exposure to high temperatures at the denaturation stage of a PCR cycle.

Higuchi et al. would devise a separate, primarily quantitative method in 1993[20]. Termed as "Kinetic PCR", although later named qPCR or real-time PCR (RT-PCR)[21], the paper details the use of a video camera to discreetly monitor the fluorescence of the reactants after each PCR cycle. In samples with positive amplification, the level of light emission via fluorescence is directly proportional to the quantity of target DNA in the solution. Since the quantity of target DNA increases exponentially by a factor of 2 with each cycle, the original quantity of target DNA can also be accurately inferred.

Proposed Solution

As mentioned above, the proposed solution to the stated problem is the creation of a centrifugal microfluidic device, capable of facilitating flowing PCR. The instrument will be composed of a Lab-on-a-Disc reaction vessel, a temperature control system, and a spectrometry system. Each element of the proposed solution will be explored in the subsequent sections.

Lab-on-a-Disc

Microfluidics is a field that focuses on the manipulation and control of the flow fluids through very small channels, typically with dimensions measured in micrometers[22]. A particular focus of the microfluidic field is Lab-on-a-Chip technology. Using a series of very small channels and microfluidic valves, this technology can effectively miniaturise and integrate multiple laboratory processes onto a single chip[23]. Given the small size of these devices, the volume of sample required to run an assay is quite low.

Centrifugal microfluidics is a branch of microfluidics in which the centrifugal force imposed on a rotating body is utilized to moderate the flow of fluid through microfluidic channels[24]. This technology is commonly referred to as Lab-on-a-Disc.

A PCR assay requires rapid switching between at least two set temperature points[1]. In a Lab-on-a-Disc system with channels bearing a rectangular cross-section, the flow rate of the fluid (Q) is given by:

$$Q = \frac{h^3 w \Delta p}{12\eta L} \left[1 - 0.630 \frac{h}{w} \right], \text{ for } h < w$$

As shown above, the flow rate is proportional to the change in pressure (p)[25]. Given that the pressure exerted on the sample is given by:

$$p = \rho \omega^2 \left(\frac{r^2 - r_0^2}{2} \right)$$

it can be inferred that the pressure imposed on the fluid is proportional to the angular velocity (w) of the disc[26]. Given this, the flow rate of the fluid is related to the angular velocity of the disc. Since the angular velocity can be controlled by the drive system, the flow rate can also therefore be controlled. This makes lab-on-a-disc an ideal solution for this instrument, as the flow rate control of the assays ensures samples are under the correct reaction conditions for the correct period.

Temperature Control System

PCR instruments rely on precise and rapid temperature cycling to amplify DNA effectively. Numerous methods of temperature control are used in modern PCR instruments, such as Peltier thermoelectric elements[27], resistive heaters[28], microwaves[29], and lasers[30]. In this project, a silicone heater has been selected as a low cost and ease of control.

Silicone heaters are a type of resistive heater, consisting of a thin nichrome film between two sheets of silicone rubber[31]. As a current is passed through the nichrome film, heat is generated. The heat is then uniformly dispersed across the surface by the silicone sheets.

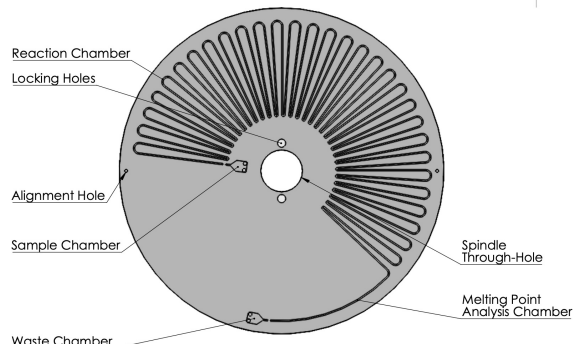


Figure 1: A technical drawing of a prototype microfluidic disc (to be revised)

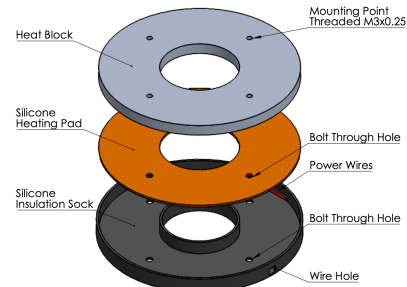


Figure 2: An exploded view of the Temperature Control System assembly

The silicone heaters will be attached to an aluminium heat block as pictured in Figure X. The heat block will house a thermocouple to provide temperature feedback to the control system. This heat block will be pressed against the lab-on-a-disc to heat the sample in the reaction channel. The small volume of liquid in the channels reduces the time taken to reach each stage's temperature, resulting in rapid temperature change ability.

Spectrometry System

When Ethidium Bromide (EtBr), an intercalating agent[32], is introduced into solution during a PCR reaction, it is integrated into the synthesized DNA molecule between each pair of nucleic bases during extension. EtBr fluoresces with excitation from ultraviolet light[33], and thus was used in PCR as an indicator of DNA amplification. While EtBR is used less frequently in modern assays, intercalating dyes remain most common type of fluorophores, with the most common being SYBR green[34].

Most fluorophores, however, have a relatively small ‘stokes-shift’ (the distance between the local maxima of the absorption and emission spectra for a fluorophore[35]). This results in the requirement for expensive optical filters for differentiating light from the excitation source and the fluorophore emission. As a result, a fluorophore with a large stokes shift was identified: EvaRuby (Excitation:480, Emission: 613 nm[36]). This fluorophore allows the use of colour gel filters, and spectral sensors, both of which are significantly lower in cost than their high-precision counterparts (dichroic filters and spectrographs respectively).

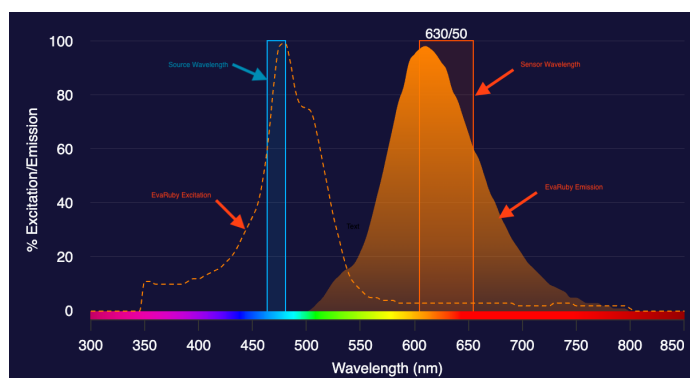


Figure 3: A plot of the optical properties of the proposed spectrometry instrument (blue: excitation source, dotted orange: excitation wavelength of EvaRuby, filled orange: emission wavelength of EvaRuby, outlined orange: measurement wavelength of spectral sensor)

Project Plan

A Gantt chart describing the plan for this project is presented in Figure X with a time unit of one day. The timeline for the Semester 2 phase of this project is January 13th to March 23rd 2025.

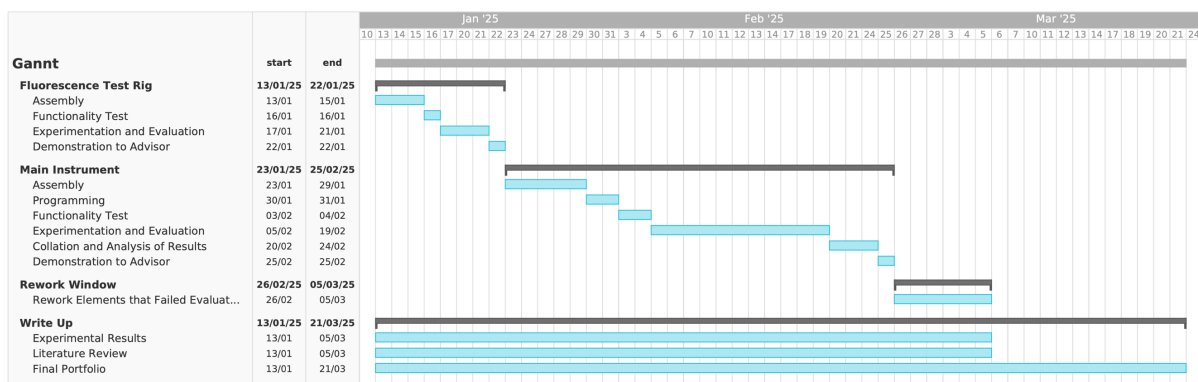


Figure 4: An image of a Gantt chart describing planned actions for this project.

Success Criteria

This project will be considered successful if the following criteria are met:

- A lab-on-a-disc is produced, capable of facilitating a flowing PCR reaction.
- A drive assembly and control system is produced, capable of:
 - accelerating the rotation of the disc to a set point.
 - controlling the angular velocity of the disc at a set point.
- A temperature control system is produced, capable of:
 - rapidly heating and cooling the sample between two set points.
 - controlling the temperature of the sample at a set point.
- A spectrometry instrument is produced, capable of:
 - emitting light in a narrow band of wavelengths.
 - measuring the intensity of light emission in a narrow band of wavelengths.
 - filtering out redundant wavelengths of light.
- Each of the items listed above should function in tandem to produce a laboratory instrument capable of completing a 40-cycle qualitative flowing PCR reaction.

References

- [1] K. Mullis, F. Falloona, S. Scharf, R. Saiki, G. Horn, and H. Erlich, "Specific enzymatic amplification of DNA in vitro: the polymerase chain reaction," *Cold Spring Harb. Symp. Quant. Biol.*, vol. 51 Pt 1, pp. 263–273, 1986, doi: 10.1101/sqb.1986.051.01.032.
- [2] U. B. Gyllensten, "PCR and DNA sequencing," *BioTechniques*, vol. 7, no. 7, pp. 700–708, 1989.
- [3] P. J. Sykes, S. H. Neoh, M. J. Brisco, E. Hughes, J. Condon, and A. A. Morley, "Quantitation of targets for PCR by use of limiting dilution," *BioTechniques*, vol. 13, no. 3, pp. 444–449, Sep. 1992.
- [4] N. Gupta *et al.*, "Point-of-Care PCR Assays for COVID-19 Detection," *Biosensors*, vol. 11, no. 5, Art. no. 5, May 2021, doi: 10.3390/bios11050141.
- [5] D. R. Gretsch, "Diagnostic tests for hepatitis C," *Hepatology*, vol. 26, no. S3, pp. 43S-47S, Dec. 1997, doi: 10.1002/hep.510260708.
- [6] "A Novel PCR Assay for Quantification of HIV-1 RNA | Journal of Virology." Accessed: Nov. 20, 2024. [Online]. Available: <https://journals.asm.org/doi/full/10.1128/jvi.00006-13>
- [7] P.-L. Quan, M. Sauzade, and E. Brouzes, "dPCR: A Technology Review," *Sensors*, vol. 18, no. 4, Art. no. 4, Apr. 2018, doi: 10.3390/s18041271.
- [8] S. Petralia and S. Conoci, "PCR Technologies for Point of Care Testing: Progress and Perspectives," *ACS Sens.*, vol. 2, no. 7, pp. 876–891, Jul. 2017, doi: 10.1021/acssensors.7b00299.
- [9] J. Lim, S. Jeong, M. Kim, and J.-H. Lee, "Battery-operated portable PCR system with enhanced stability of Pt RTD," *PLOS ONE*, vol. 14, no. 6, p. e0218571, Jun. 2019, doi: 10.1371/journal.pone.0218571.
- [10] J. E. Davies and H. G. Gassen, "Synthetic Gene Fragments in Genetic Engineering—The Renaissance of Chemistry in Molecular Biology," *Angew. Chem. Int. Ed. Engl.*, vol. 22, no. 1, pp. 13–31, Jan. 1983, doi: 10.1002/anie.198300131.
- [11] F. J. Bollum, "'Primer' in DNA Polymerase Reactions," in *Progress in Nucleic Acid Research and Molecular Biology*, vol. 1, J. N. Davidson and W. E. Cohn, Eds., Academic Press, 1963, pp. 1–26. doi: 10.1016/S0079-6603(08)60637-6.
- [12] S. W. Matson, D. W. Bean, and J. W. George, "DNA helicases: Enzymes with essential roles in all aspects of DNA metabolism," *BioEssays*, vol. 16, no. 1, pp. 13–22, 1994, doi: 10.1002/bies.950160103.
- [13] Y. Yin and X. S. Zhao, "Kinetics and Dynamics of DNA Hybridization," *Acc. Chem. Res.*, vol. 44, no. 11, pp. 1172–1181, Nov. 2011, doi: 10.1021/ar200068j.
- [14] G. T. Walker, M. C. Little, J. G. Nadeau, and D. D. Shank, "Isothermal in vitro amplification of DNA by a restriction enzyme/DNA polymerase system.," *Proc. Natl. Acad. Sci.*, vol. 89, no. 1, pp. 392–396, Jan. 1992, doi: 10.1073/pnas.89.1.392.
- [15] J. Rameckers, S. Hummel, and B. Herrmann, "How Many Cycles Does a PCR need? Determinations of Cycle Numbers Depending on the Number of Targets and the Reaction Efficiency Factor," *Naturwissenschaften*, vol. 84, no. 6, pp. 259–262, Jun. 1997, doi: 10.1007/s001140050393.
- [16] "Reference to 2.7.7.7; Id = 643606 - BRENDA Enzyme Database - BRENDA Enzyme Database." Accessed: Nov. 20, 2024. [Online]. Available: <https://www.brenda-enzymes.org/literature.php?e=2.7.7.7&r=643606>
- [17] R. K. Saiki *et al.*, "Primer-directed enzymatic amplification of DNA with a thermostable DNA polymerase," *Science*, vol. 239, no. 4839, pp. 487–491, Jan. 1988, doi: 10.1126/science.2448875.
- [18] A. Chien, D. B. Edgar, and J. M. Trela, "Deoxyribonucleic acid polymerase from the extreme thermophile *Thermus aquaticus*," *J. Bacteriol.*, vol. 127, no. 3, pp. 1550–1557, Sep. 1976.
- [19] "Reference to 2.7.7.7; Id = 643634 - BRENDA Enzyme Database - BRENDA Enzyme Database." Accessed: Nov. 20, 2024. [Online]. Available: <https://www.brenda-enzymes.org/literature.php?e=2.7.7.7&r=643634>

- [20] R. Higuchi, C. Fockler, G. Dollinger, and R. Watson, "Kinetic PCR analysis: real-time monitoring of DNA amplification reactions," *Biotechnol. Nat. Publ. Co.*, vol. 11, no. 9, pp. 1026–1030, Sep. 1993, doi: 10.1038/nbt0993-1026.
- [21] J. Mackay, "Introduction to kinetic (real-time) PCR," *Methods Mol. Biol. Clifton NJ*, vol. 353, pp. 167–176, 2007, doi: 10.1385/1-59745-229-7:167.
- [22] J. Cottet and P. Renaud, "Chapter 1 - Introduction to microfluidics," in *Drug Delivery Devices and Therapeutic Systems*, E. Chappel, Ed., in *Developments in Biomedical Engineering and Bioelectronics*. , Academic Press, 2021, pp. 3–17. doi: 10.1016/B978-0-12-819838-4.00014-6.
- [23] A. Pradeep, J. Raveendran, and T. G. S. Babu, "Chapter Five - Design, fabrication and assembly of lab-on-a-chip and its uses," in *Progress in Molecular Biology and Translational Science*, vol. 187, 1 vols., A. Pandya and V. Singh, Eds., in *Micro/Nanofluidics and Lab-on-Chip Based Emerging Technologies for Biomedical and Translational Research Applications - Part B*, vol. 187. , Academic Press, 2022, pp. 121–162. doi: 10.1016/bs.pmbts.2021.07.021.
- [24] M. Tang, G. Wang, S.-K. Kong, and H.-P. Ho, "A Review of Biomedical Centrifugal Microfluidic Platforms," *Micromachines*, vol. 7, no. 2, p. 26, Feb. 2016, doi: 10.3390/mi7020026.
- [25] H. Bruus, *Theoretical Microfluidics*. London, England: Oxford University Press, 2007.
- [26] D. Kinahan, "Introduction to Lab on a Disc,"
- [27] X. Qiu and J. Yuan, "Temperature Control for PCR Thermocyclers Based on Peltier-Effect Thermolectric," in *2005 IEEE Engineering in Medicine and Biology 27th Annual Conference*, Jan. 2005, pp. 7509–7512. doi: 10.1109/IEMBS.2005.1616249.
- [28] C. Yu, W. Liang, I. Kuan, C. Wei, and W. Gu, "Fabrication and characterization of a flow-through PCR device with integrated chromium resistive heaters," *J. Chin. Inst. Chem. Eng.*, vol. 38, no. 3, pp. 333–339, May 2007, doi: 10.1016/j.jcice.2007.05.001.
- [29] C. Fermér, P. Nilsson, and M. Larhed, "Microwave-assisted high-speed PCR," *Eur. J. Pharm. Sci.*, vol. 18, no. 2, pp. 129–132, Feb. 2003, doi: 10.1016/S0928-0987(02)00252-X.
- [30] H. Kim, S. Dixit, C. J. Green, and G. W. Faris, "Nanodroplet real-time PCR system with laser assisted heating," *Opt. Express*, vol. 17, no. 1, p. 218, Jan. 2009, doi: 10.1364/OE.17.000218.
- [31] P. Selvakumar, A. Abubakkar, A. Tamilvanan, and T. Rajagopal, "Design, Fabrication And Testing Of Prototype Of An Anti-Hypothermic Flexible Body Heater," vol. 8, no. 10, 2019.
- [32] N. V. Bhagavan and C.-E. Ha, "Chapter 21 - Structure and Properties of DNA," in *Essentials of Medical Biochemistry (Second Edition)*, N. V. Bhagavan and C.-E. Ha, Eds., San Diego: Academic Press, 2015, pp. 381–400. doi: 10.1016/B978-0-12-416687-5.00021-X.
- [33] "Spectrum [Ethidium Bromide] | AAT Bioquest." Accessed: Nov. 20, 2024. [Online]. Available: https://www.aatbio.com/fluorescence-excitation-emission-spectrum-graph-viewer/ethidium_bromide
- [34] H. Gudnason, M. Dufva, D. D. Bang, and A. Wolff, "Comparison of multiple DNA dyes for real-time PCR: effects of dye concentration and sequence composition on DNA amplification and melting temperature," *Nucleic Acids Res.*, vol. 35, no. 19, p. e127, Oct. 2007, doi: 10.1093/nar/gkm671.
- [35] "10.3.2: The Stokes Shift," Chemistry LibreTexts. Accessed: Nov. 20, 2024. [Online]. Available: https://chem.libretexts.org/Courses/Providence_College/CHM_331_Advanced_Analytical_Chemistry_1/10%3A_Molecular_Luminescence_Spectrometry/10.03%3A_Applications_of_Photoluminescence_Methods/10.3.02%3A_The_Stokes_Shift
- [36] "Product Information - EvaRuby™ Dye, 20X in Water." biotium, Oct. 27, 2021. Accessed: Nov. 20, 2024. [Online]. Available: <https://biotium.com/wp-content/uploads/2021/10/PI-31079.pdf>

Appendix Two

In-Depth Literature Review, Background, Design, and Experimental Procedure

Table of Contents

<i>Table of Tables</i>	3
<i>Table of Figures</i>	4
<i>Literature Review</i>	6
Microfluidics	6
Principles	7
Microfluidic Platform Architectures.....	8
Dipstick Devices.....	8
Lateral Flow Devices	9
Droplet-Based Devices	10
Centrifugal Devices	11
Nucleic Acid Testing.....	13
Background	13
DNA Amplification	15
PCR	16
Advancements in PCR.....	17
Types of PCR	20
Methods of Temperature Control in PCR	22
Technical Background	25
Heating	29
Control Systems	31
Spectrometry	33
Electronics	35
Communications Protocols	37
Software	41
<i>Design and Implementation</i>	42
Central Control System.....	42
Software Implementation.....	42
Power System Implementation	44
Microfluidic Disc	45
Channel Dimensions	45
Channel Pattern	47
Reservoir Design.....	47
Centrifuge	49
Heating	56
Fabrication.....	62

Spectrometry	63
Spectral Sensor Selection	63
Fabrication	65
User Interface	69
Design.....	69
Communications Implementation.....	70
Experimental Procedure.....	73
Validation.....	73
Centrifuge	73
Disc	73
Heater.....	73
Experimental Protocol	73
References	75

Table of Tables

Table 1 A table describing different PCB heaters	30
Table 2 A table describing the components of a PID controller	32
Table 3 A table describing the different methods of optical filtering	33
Table 4 A table describing the different types of optical filters.	34
Table 5 A table outlining the parts of a BLDC motor	35
Table 6 A table describing Modbus frame structure	37
Table 7 A table describing each segment in a Modbus frame.	38
Table 8 A table describing TTL frame structure	39
Table 9 A table showing the properties of the selected BLDC motor	52
Table 10 A table showing the properties of the selected motor driver.....	52
Table 11 A table showing available motor functions	55
Table 12 A table showing the registers for each function	55
Table 13 Table of design parameters for the PCB heater.....	57
Table 14 A table showing the pattern in heater trace increments	57
Table 15 A table showing final PCB parameters	58
Table 16 A table detailling the files sent to the manufacturer.....	62
Table 17 A table showing the fabrication parameters used for the PCB	62
Table 18 A table showing available spectrometry functions	67

Table of Figures

Figure 1 Left: Bio-Rad T100 Thermal Cycler[4], right: Abbott ID Now Microfluidic PCR Device[5]	6
Figure 2 Lab on a Chip[7], (right) Lab on a Disc[8]	8
Figure 3 A dispstick urine test [11]	8
Figure 4 A lateral flow test [14].....	9
Figure 5 A glucose monitoring pin-prick test [15]	9
Figure 6 Sample droplets in a microfluidic device[10].....	10
Figure 7 Forces on a microfluidic disc [21]	11
Figure 8 A microfluidic disc featuring reservoirs, channels, and valves[21]	11
Figure 9 Operation of a dissolvable film valve[21]	12
Figure 10 Structure of a DNA molecule [23].....	13
Figure 11 Action of helicase (left) and DNA Polymerase (right) [23]	14
Figure 12 Formation and sealing of Okazaki fragments [23].....	14
Figure 13 Original PCR mechanism proposed by Mullis et al [23].....	16
Figure 14 Thermus aquaticus [28].....	17
Figure 15 Gel-electrophoresis result from the PCR experiment carried out by Mullis et al [23]	18
Figure 16 SYBR Green (left)[34], EVARuby (right)[35]	19
Figure 17 Absorption and emission spectral for SYBR Green (left)[38] and EVARuby (right)[39]	20
Figure 18 The experimental protocol used by Higuchi et al[31]	20
Figure 19 The experimental protocol used by Sykes et al[40].....	21
Figure 20 The experimental protocol used by Moschou et al[40].....	22
Figure 21 Experimental assembly used by Xie et al [41].....	23
Figure 22 Experimental assembly used by Nasser et al[42]	23
Figure 23 Experimental assembly used by Wang et al[3]	23
Figure 24 Experimental designs used by Talebi et al: left: PCB-based heater, right: PMMA chip[43]	24
Figure 25 Forces on a microfluidic disc [19]	25
Figure 26 Visual representation of centrifugal pressure.....	26
Figure 27 Left: PMMA sheets[47], right: laser cutter[48]	27
Figure 28 Left: roll of PSA[51], right: plotter cutter[52].....	27
Figure 29 Hot-roller laminator [53].....	28
Figure 30 Left: channel in microfluidic disc, right: reservoir in microfluidic disc	28
Figure 31 A printed-circuit board [56].....	29
Figure 32 Example of a serpentine PCB heater trace.....	30

Figure 33 Optical electromagnetic spectrum [63].....	33
Figure 34 Left: laboratory-grade optical filters, right: gel filters[65]	34
Figure 35 CCS communications architecture.....	42
Figure 36 Left: power supply circuit diagram, right: WAGO 221 level connector [79]	44
Figure 37 The microfluidic disc designed for this project.....	45
Figure 38 Example of channels and reservoir cut from PSA	46
Figure 39 Left: disc revision 4 channel pattern, right: disc revision 1 channel pattern	47
Figure 40 The instrument's centrifuge mechanism	49
Figure 41The instrument's centrifuge mechanism with spindle highlighted.....	50
Figure 42 Measure statistics from Solidworks, showing mass moment of interial along the Y-axis.....	51
Figure 43 Wiring diagram for the motor and driver.....	53
Figure 44 Communications workflow for motor control	54
Figure 45 Left: example of how an arc is defined in KiCAD, right: the complete heater trace	58
Figure 46 Left: a render of the completed PCB, right: a PCB layout schematic of the PCB .	59
Figure 47 Left: spectrometry system assembly, right: stacked gel filters over disc	63
Figure 48 Hamamatsu C12666MA micro-spectrometer[82]	64
Figure 49 Left: AS72651 spectral sensor[83], right: optical response of the AS72651[84]..	64
Figure 50 Left: AS7341 spectral sensor[85], right: frequency response of the AS7341[86].	65
Figure 51 An image of the spectrometry system with the spectrometer head highlighted..	65
Figure 52 Circuit diagram for the spectrometry system	66
Figure 53 Communications architecture for the spectrometry system.....	67
Figure 54 Communications architecture to send data from the spectrometry system to the user interface.....	68
Figure 55 An image of the user interface	69
Figure 56 An image of the user interface in operation.....	70

Literature Review

Microfluidics

Microfluidics is a field of study within fluid dynamics with a focus on the manipulations of fluids at a sub-millimeter scale. The field arose out of a desire to manipulate diagnostic samples on a cell-length scale in-vitro. Initial developments in the field took inspiration from innovative processes used in the semiconductor industry to create micro-electromechanical systems (MEMS). Advancements in microfluidics since its inception have allowed for the development of rapid, cost-effective diagnostic tools that operate on micro-scale sample volumes, typically integrating numerous laboratory processes into a single device[1], [2].

Microfluidics involves the exploitation of phenomena experienced in liquids at the microscopic scale, which are typically not experienced in macro-scale analysis. Precise control of fluid mechanics that given rise to these phenomena, including diffusion, convection, and capillary action enables the automated, micro-scale implementation of laboratory processes[1].

Initial microfluidic devices were initially only utilized in the engineering community as proof-of-concept experiments to replace macro-scale assays. However, in the years since its inception, the field has developed as a fundamental tool in diagnostic analysis, aiding in detection of countless varieties of infectious diseases. The low-cost development opportunities that microfluidics provides also opens up the possibility for use in diagnostics in the developing world, for which traditional laboratory processes are incompatible[3].



Figure 1 Left: Bio-Rad T100 Thermal Cycler[4], right: Abbott ID Now Microfluidic PCR Device[5]

Traditional laboratory equipment typically bears the requirement for comparatively large sample volumes, long processing times, bulky instruments, large capital investment, high maintenance costs, rigorous training protocols. In contrast, microfluidic devices have been designed to streamline assay protocols such that little-to-no personnel training is required, substantially reduce sample volumes, enhanced control over fluid behavior, and reduce reaction time. Microfluidic devices may also offer enhanced scalability via the implementation of assay multiplexing on a single device, similar to the multiplexing capacity provided by multi-well plates[3].

Devices have been developed conforming to a range of different platforms, including domestic dipstick or pin-prick glucose tests for patients with diabetes. The usage of lateral flow tests was observed on global scale in the diagnosis of SARS-COV-2 during the COVID-19 pandemic. Droplet-based microfluidic devices are used to facilitate diagnostic tests on increasingly small sample volumes. As both academic research and industry adoption increases, microfluidics continuously migrates from an engineering proof-of-concept to an industry standard in field of rapid diagnostics.

Principles

At the micro-scale, fluid viscosity has a greater impact fluid behavior than inertia. The micro-channels prevalent in microfluidics give rise to a small Reynolds number, resulting in laminar flow, a phenomenon in which fluid moves in parallel layers. This phenomenon permits the usage of diffusion as an effective solution to moving and mixing solutes. The importance of diffusion, the random thermal motion of molecules, and convection, the motion as a result of bulk fluid motion, is governed by the Peclet number[1].

The large ratio of surface area to volume observed in micro-channels leads to an increased impact of fluid surface tension on fluid behavior. The most significant motive phenomenon that arises from the impact of surface tension is capillary action. As the size of a system is reduced, the impact of capillary forces on fluid motion can exceed that of fluid viscosity. This action is governed by the Capillary number. If the interactions between capillary action and fluid viscosity are balanced, the phenomenon may give rise to novel methods of pumping and droplet manipulation[1].

Micro-scale fluid volumes permit efficient heat transfer. Volume is directly correlated to the heat energy required to increase the temperature of a liquid[6]. Therefore, as volume decreases, so does thermal mass, resulting in more efficient heating. Another advantage of this mechanic is the opportunity for significantly increased thermal gradients, potentially reducing reaction byproducts. Therefore, the homogenous heating and rapid temperature gradients are easily achievable in microfluidic systems.

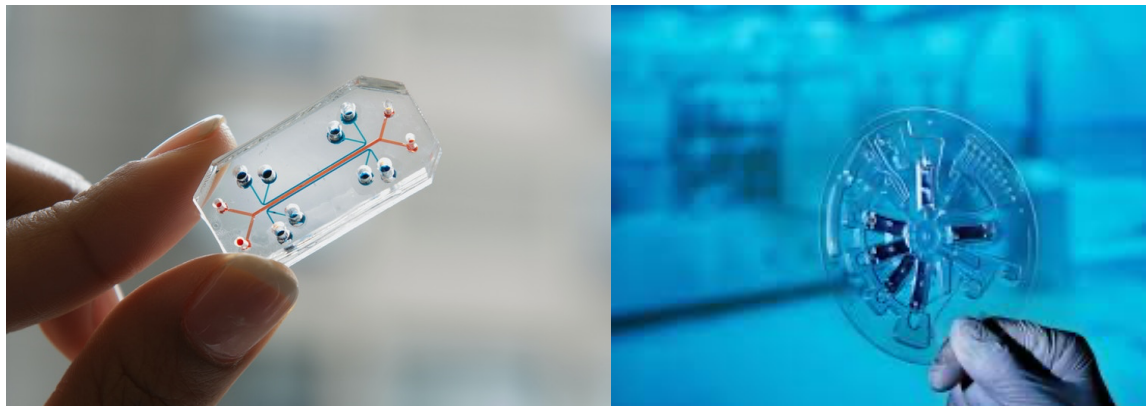


Figure 2 Lab on a Chip[7], (right) Lab on a Disc[8]

The implementation of these concepts to develop complex micro-channels structures within microfluidic devices allows for the integration of multiple laboratory processes into a single device, as seen in the areas of Lab-on-a-Chip (LoaC) and Lab-on-a-Disc (LoaD, previously referred to as Lab-on-a-CD). Additional research has led to the development of mechanisms for mixing, metering, and droplet manipulation[9], [10].

Microfluidic Platform Architectures

Dipstick Devices



Figure 3 A dispstick urine test [11]

Paper-based microfluidic devices have been developed for the rapid detection of biological markers. Muller and Clegg introduced the first implementation of paper-based microfluidic channels in 1945[3].

Later on Andres W. Martinez et al would develop the first practical application of a paper-based assay used in the detection of glucose and protein[12]. The process involved the application of an indicator compound to patterning paper. The paper was subsequently

dipped into an artificial urine solution consisting of glucose and bovine serum albumin. The resulting reaction would cause the color of the paper to change, indicating a positive assay.

Lateral Flow Devices

Lateral flow devices are another example of low-cost, rapid diagnostic microfluidic devices. Capillary action is typically used to move a sample from a loading point across an indicator or into an electronic device[13].



Figure 4 A lateral flow test [14]

Paper-based lateral flow devices were used ubiquitously on a global scale in the detection of SARS-CoV-2 during the COVID-19 pandemic[15]. In these devices, a preprocessed sample is loaded onto a sample pad. Subsequently, capillary action carries the sample across a porous membrane, upon which test and control lines, containing an indicator, are overlayed. Upon reaching these lines, the sample reacts with the indicator, providing a visual indication of the result.

Pinprick microfluidic device are examples of electronic lateral flow devices, functioning by extracting a small volume of blood from the user[13], typically a from finger via a small needle. The sample is subsequently transported through the needle and into the device for analysis through capillary action. These devices are commonly used in domestic settings, particularly in the quantification of blood glucose levels in patients with diabetes[16].



Figure 5 A glucose monitoring pin-prick test [15]

Droplet-Based Devices

Droplet-based microfluidic devices (DBMD) involve the precise control of micro-scale droplets of liquid. Droplets are formed from a sample and typically coated in a separate immiscible liquid to prevent droplets from mixing. This property explicitly permits analysis on individual droplets without the possibility of cross-contamination[10].

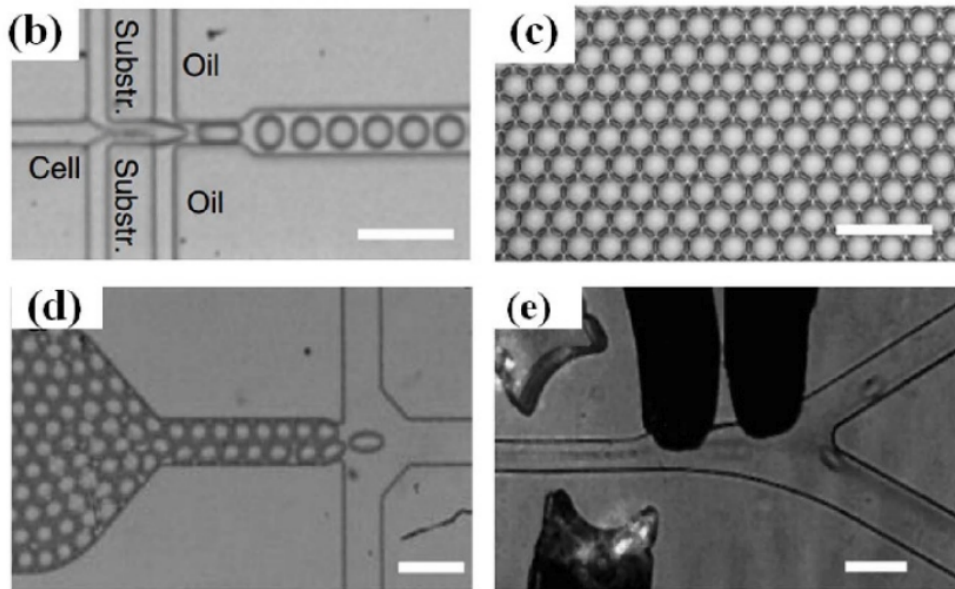


Figure 6 Sample droplets in a microfluidic device[10]

Precise design is used to produce geometries within the device which cause droplets to form due to surface-induced instability. This design may be tuned to achieve the desired droplet frequency, monodispersity, and size. The flow of two fluids, typically a sample and an oil, is controlled using an actuator to give rise to immiscibility in the droplets produced by the device, as shown in Figure 6. Droplets may be manipulated through the device with a range of different motive forces, including magnetism, temperature, hydraulic resistance, and valving. Droplets can be combined and mixed through coalescence, utilizing channel geometry, fluid properties, temperature control, and electricity[10].

DBMD have been used to improve diagnostic devices in a range of areas, as detailed in a comprehensive review conducted by Amirfar et al [10]. The earliest implementation, one also significant to this thesis, was in the polymerase chain reaction (PCR). Numerous researchers have contributed a range of process improvements since the inception of DBMD. Zubaite et al introduced a method of isolating, amplifying, and condensing DNA molecules in 3pL droplets using an integrated T-junction droplet generator[17]. Stark et al implemented a process for a microfluidic platform combining DNA extraction and quantitative PCR[18]. Pellegrino et al introduced a microfluidic device capable of

sequencing DNA derived from acute myeloid leukemia tumors[19]. Azizi et al designed a high-precision assay to detect *Salmonella typhimurium* using a droplet-based LAMP instrument[20].

Centrifugal Devices

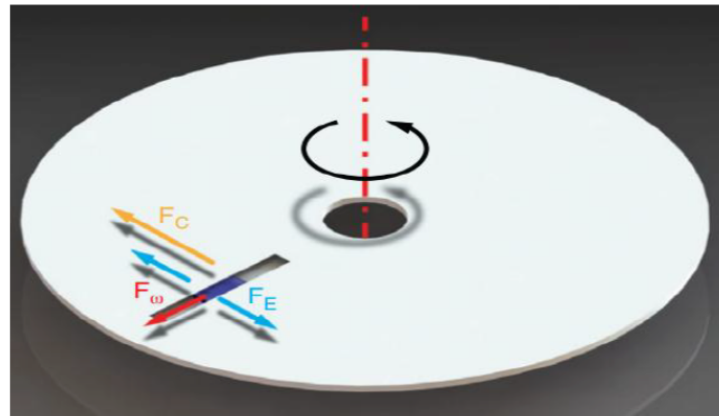


Figure 7 Forces on a microfluidic disc [21]

Centrifugal microfluidic devices exploit rotational forces to implement automatic sample handling and complex diagnostic processes in a disc-shaped platform as shown in Figure 7. This approach particular stands as a pivotal advancement in point-of-care diagnostics, enabling rapid, high-bandwidth, equipment-free testing[9].

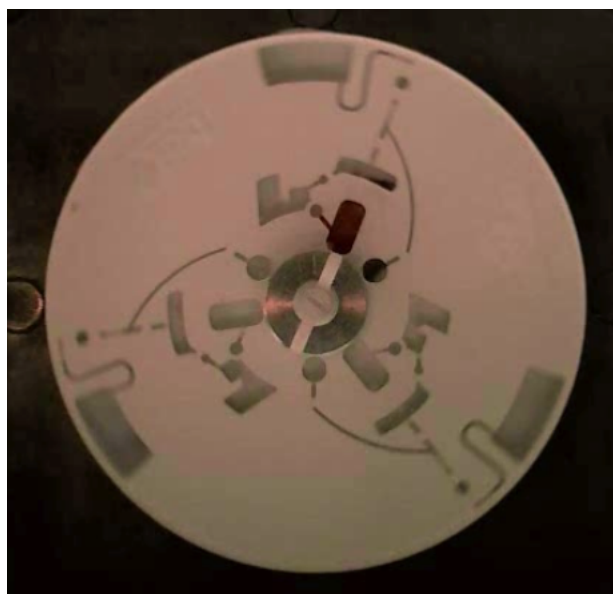


Figure 8 A microfluidic disc featuring reservoirs, channels, and valves[21]

The core component of a centrifugal microfluidic device is a microfluidic disc (MD), which enables a controlled approach to microfluidic flow by exploiting the centrifugal forces involved in high-speed rotation. A MD is typically composed of stacked interchanging layers

of polymethylmethacrylate (PMMA) and pressure-sensitive adhesive (PSA). Given that PMMA and PSA are widely available and cost-effective materials, combined with the relatively simple manufacturing processes used to fabricate MDs, centrifugal microfluidic devices are well suited to large-scale production. The manufacturing processes involved with the fabrication of microfluidic discs are also compatible with rapid prototyping processes, which leads to efficient and inexpensive development of novel ideas.

While the design of microfluidic devices varies greatly and researchers continue to develop innovative methods of miniaturizing laboratory processes, the fundamental structural components of microfluidic discs remain consistent. Discs commonly contain reservoirs for sample storage and channels to facilitate the flow of liquid between reservoirs. Complex processes are facilitated by a multi-layer design, like that of a printed circuit board. Inter-layer liquid transfer is facilitated by through-holes, known as vias. Certain microfluidic discs require advanced sample processing, incorporating mechanisms for metering, mixing, and valving. Additionally, the disc format supports multiplexing, enabling simultaneous analysis of multiple samples on a single disc.

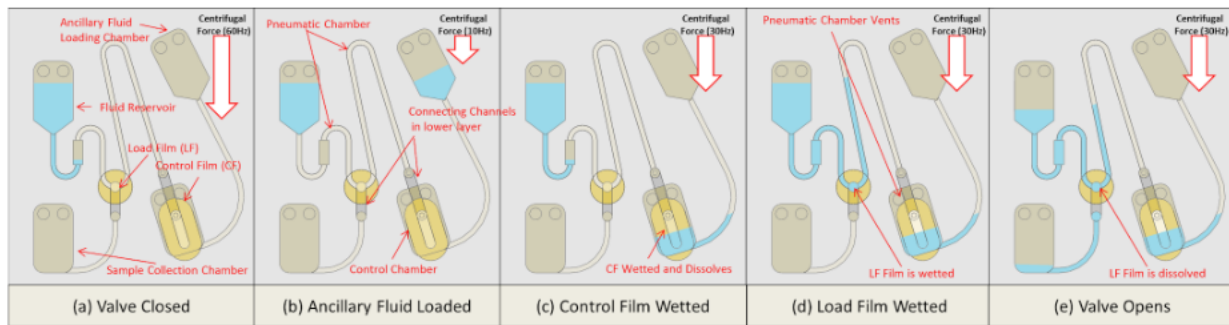


Figure 9 Operation of a dissolvable film valve[21]

Perhaps one of the most interesting mechanisms implemented in microfluidic devices is flow control through bulk-flow valving. Capillary action, hydrophobic coatings, and siphon mechanisms have been utilized to implement passive valving, while magnetic, impact, and pneumatic forces have been utilized to implement active valving[9]. In centrifugal microfluidic platforms, dissolvable films have been developed to enable timed-release, process-dependent valving[22]. The methods listed provide insight into the novel and innovative contributions made to microfluidic process development.

Nucleic Acid Testing

Nucleic acid testing (NAT) is a diagnostic technique used to detect and analyze genetic material derived from biological sources. The practice is commonly used in medical and research settings in genetic sequencing, pathogen identification, and identification of genetic disorders.

Background

In order to properly describe the intricacies of NAT and its applications in microfluidics, some foundational information is required. As such, the following subsections will detail DNA and DNA replication in-vivo.

DNA

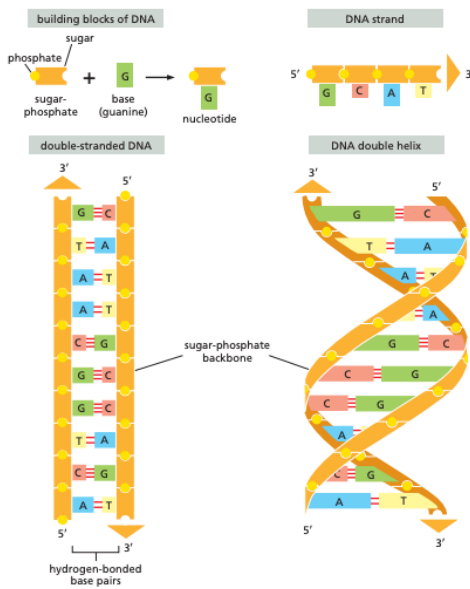


Figure 10 Structure of a DNA molecule [23]

Deoxyribonucleic acid (DNA) is a molecule that is used to carry genetic information in living organisms. DNA is a long-chain polymer, containing antiparallel single-stranded DNA (ssDNA) molecules in a double helix format. Each ssDNA molecule is composed of four types of nucleotide. Two ssDNA molecules are bonded together through hydrogen bonds between opposing nucleotides, forming a double-stranded (dsDNA) molecule. Nucleotides are composed of a five-carbon sugar attached to one or more phosphate group and a nitrogenous base. In DNA, the five-carbon sugar is deoxyribose, while the nitrogenous base can be one of adenine, guanine, cytosine, or thymine. When described diagrammatically, one of the ssDNA molecules composing a dsDNA molecule is labeled as the S strand, while the other is labelled as the S' strand. The start of the S strand is labelled as the 5' end, while the end of the strand is labelled as the 3' end[23].

DNA Replication

In-vivo, DNA is required to be replicated and repaired as part of the lifecycle of the cell. DNA replication takes place over three stages: initiation, elongation, and termination.

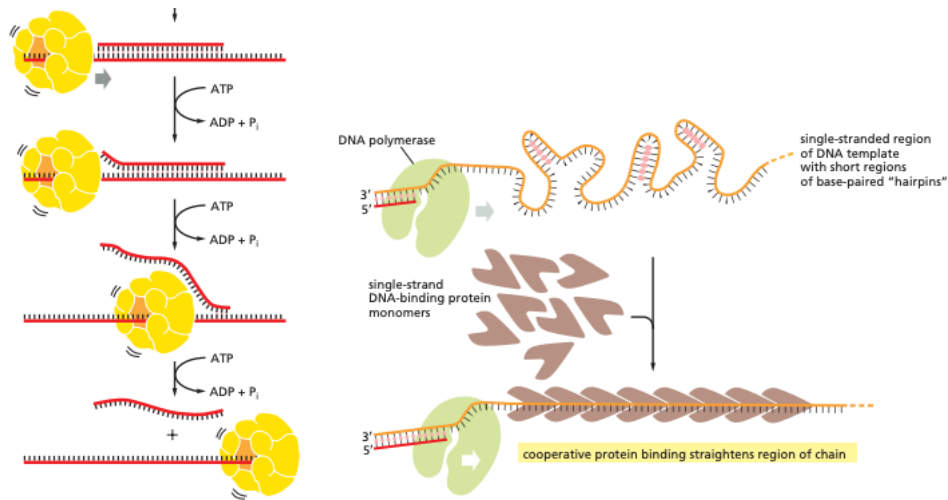


Figure 11 Action of helicase (left) and DNA Polymerase (right) [23]

Initiation involves the preparation of the DNA for replication. The enzyme Helicase breaks the hydrogen bonds between the nucleotide bases, resulting in a dsDNA molecule with the helical-structure split at one end in a fork-like format. Single-stranded binding proteins protect the open strands to prevent free-floating nucleotides from attaching to the strand in an uncontrolled manner (known as re-annealing). The enzyme Primase synthesizes as short ribonucleic acid (RNA) primer to provide a starting point for elongation[23].

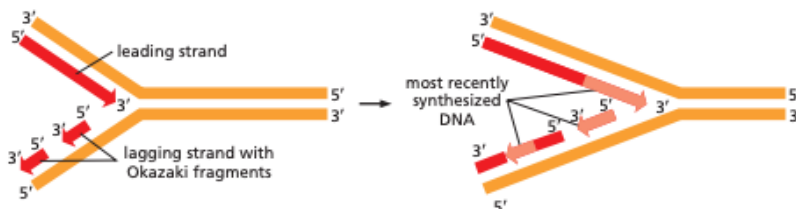


Figure 12 Formation and sealing of Okazaki fragments [23]

Elongation involves the construction of a new dsDNA molecule from a single ssDNA molecule. DNA Polymerase II (prokaryotes) or DNA Polymerase I (eukaryotes) adds nucleotides to the 3' end of the primer, extending the new strand in the 5' to 3' direction. DNA Polymerase can only add nucleotides in the 5' to 3' directions. Therefore, given that the strands run antiparallel, the leading strand (strand with a free 5' end) is elongated continuously, while the lagging strand (strand with free 3' end) is elongated in a fragmented

manner from the 5' to 3' direction. The fragmented elongations on the lagging strand are known as Okazaki fragments. The enzyme DNA Ligase traverses the lagging strand and seals the gaps between Okazaki fragments, resulting in a uniform, continuous strand[23].

Termination involves the conclusion of DNA replication. In prokaryotic organisms, elongation is concluded by a specific sequence of nucleotide bases in an arrangement known as a termination sequence. In eukaryotic organisms, replication ends when the fork in the two free strands converges. The RNA primers are removed from the strands by DNA Polymerase I. At the end of the lagging strand, DNA Polymerase fails to fully replicate the end of the strand, known as the telomere. Consequently, another enzyme, Telomerase, extends the telomere to prevent the loss of genetic material[23].

DNA Amplification

In diagnostic terms, a cell contains a minuscule amount of DNA. DNA amplification is a process of exploiting the mechanics of the natural DNA replication process described above to artificially replicate DNA in-vitro for diagnostic purposes.

Thymidine monophosphate (dTTP) denotes a nucleotide with the nucleobase thymine, bonded glycosidically with deoxyribose and a monophosphate group. DNA polymerase I requires dTTP to extend DNA where a thymidic base is required. F. Sanger, S. Nicklen, and A. R. Coulson proposed an exploit to this mechanic by using Thymidine Triphosphate (dTTP), a terminating triphosphate readily used by DNA Polymerase I in place of dTMP[24]. dTTP lacks the 3'-hydroxyl group that permits a subsequent nucleotide to append to the it's 3' end, thus immediately terminating any further DNA extension.

When used in conjunction with 3 other terminating triphosphates, each corresponding to a nucleobase, this process allows the synthesis of DNA fragments with an increasing quantity of nucleotides, permitting DNA sequencing in-vitro via natural methods. More importantly, the paper cites methodology that would later become fundamental to DNA amplification and sequencing: thermal denaturation of DNA and synthetic extension via immersion in nucleotide solution

Until 1986, the most promising method for DNA synthesis and amplification was de novo synthesis, taking inspiration from genetic engineering principles to synthesize DNA via the recombination of existing fragments using oligonucleotide kinase and DNA ligase. Mullis et al. cited an issue with de novo synthesis wherein an accurate sequence of DNA could not be synthesized unless the template was already sequenced and understood[25].

PCR

It was in the aforementioned paper that Mullis et al. would go on to propose a solution to this problem: the Polymerase Chain Reaction (PCR). The technique, referred to as end-point PCR (EP-PCR) in modern literature, involved the use of a DNA template and a primer, an oligonucleotide complementary to that of a specific sequence of interest in the template. EP-PCR was defined by the authors to take place over three distinct stages[25].

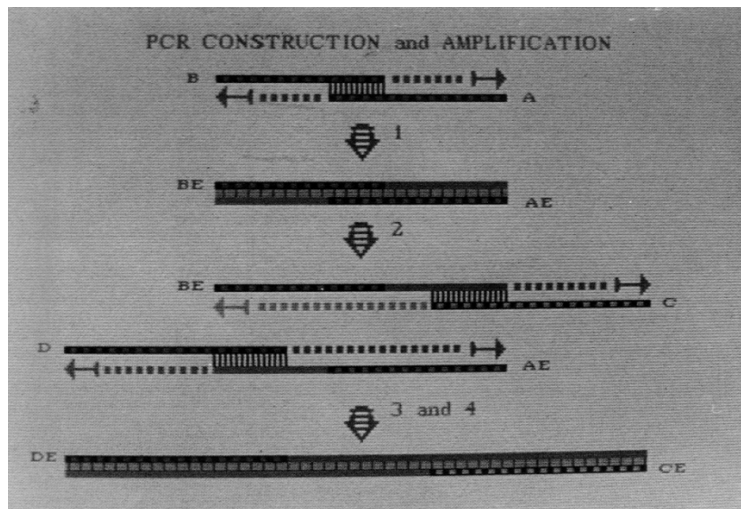


Figure 13 Original PCR mechanism proposed by Mullis et al [23]

Denaturation allows splitting of a DNA template into two single-stranded DNA molecules (ssDNA). This involves the application of heat to break apart the hydrogen bonds that link the strands together[ref]. The enzyme helicase is responsible for this action in a biological environment[ref]. This stage typically occurs over 2 minutes with the sample heated to 90°C[25].

Annealing describes a process wherein a primer bonds to a complementary oligonucleotide sequence on an ssDNA molecule. The term is used in literature to describe PCR-specific hybridization[ref]. This stage typically takes place over 2 minutes with the sample incubated at 30°C[25].

Extension refers to a process in which the DNA polymerase enzyme transcribes a new strand of DNA from the template ssDNA. DNA Polymerase I attaches to the template strand at the 3' end of the primer and extends the complementary strand in the 3' direction [ref]. Extension is an inherently active reaction, requiring the presence of dATP as a source of energy. DNA polymerase also requires the four nucleotides (thymidine monophosphate, adenosine monophosphate, cytidine monophosphate, guanosine monophosphate) as cofactors to support this reaction. This stage typically takes place over 2 minutes with the sample incubated at 30°C[25].

The aforementioned stages composed a PCR "cycle". In total, 20-27 cycles were conducted by the authors on human DNA. In practice, the number of cycles required varies greatly depending on amplification requirements[26].

Advancements in PCR

Since its discovery, PCR has become the most commonly used technique for DNA amplification in-vitro. However, the method proposed by Mullis et al is quite primitive by today's standards. The PCR process has progressed significantly since it's discovery, in no small part a result of the multitude of contributions made by the research community. These improvements include thermostability, fluorescence, and procedural advancements.

Thermostability

DNA polymerase I has a heat inactivation temperature of 30°C, resulting in denaturation during the initial stage of a PCR cycle. Consequently, fresh DNA polymerase I was required to be added prior to each cycle. Saiki et al. proposed a resolution to this issue in a 1988 paper proposing the use of thermostable Taq polymerase[27].



Figure 14 *Thermus aquaticus* [28]

Chien et al. discovered Taq polymerase a decade previously in the thermophilic bacteria *Thermus aquaticus*[29]. This enzyme has an active temperature range of 70-75°C, with a heat inactivation temperature of 95°C, affording it the ability to survive exposure to high temperatures at the denaturation stage of a PCR cycle. As a result, the enzyme was added at the beginning of the assay, rather than at the beginning of each cycle, increasing efficiency and reducing the risk of contamination.

Fluorescence

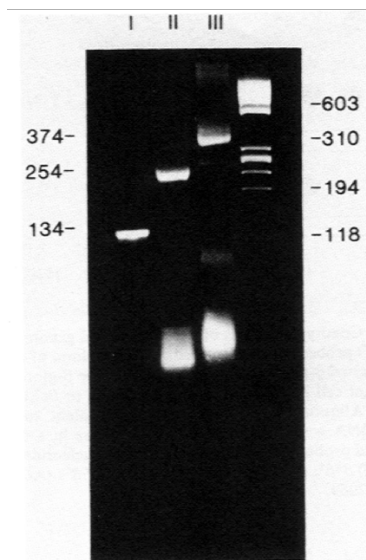


Figure 15 Gel-electrophoresis result from the PCR experiment carried out by Mullis et al [23]

The use of ethidium bromide (EtBr), a fluorescent intercalating dye, for qualifying the result of a PCR assay, as opposed to a radioactive compound or gel electrophoresis, marked a significant initial step forward for the technique[27].

Fluorescence is a type of photoluminescence in which a substance absorbs electromagnetic radiation at one wavelength, subsequently emitting at another wavelength. The phenomenon involves the absorption of photonic energy by a molecule, causing it to excite. When the molecule returns to a ground state, electromagnetic energy is released. Fluorescence ceases emission immediately after the excitation source is removed, distinguishing it from phosphorescence[30].

Fluorescence is used to modern PCR as a means of obtaining qualitative and quantitative results[31]. The specific type of fluorescent molecule used is referred to as an intercalating dye[32]. When included in solution during DNA synthesis, DNA polymerase integrates these molecules between the base pairs in a dsDNA molecule. The resulting bond significantly increases the intensity of fluorescence. Therefore, intensity of fluorescence is directly correlated to the magnitude of DNA synthesis, enabling qualitative and quantitative measurement.

In modern practical diagnostic applications, PCR analysis is conducted using a relatively straightforward procedure. The sample is loaded into an optical-grade container, such as an Eppendorf, and the PCR process is performed with the intercalating dye in solution. Upon completion of the PCR process, light from a monochromatic light source, typically a laser, is

passed through an optical filter designed to transmit only light at the peak absorption wavelength. This light is used to illuminate the sample, therefore exciting the fluorophore. The resulting fluorescence emission, combined with residual excitation light, is passed through a secondary filter, designed to selectively transmit only the fluorescence emission. A spectrophotometer is then used to quantify the level of emission from the sample.

Therefore, the fundamental properties of interest in intercalating dyes are their respective absorbance and emission spectra. The difference between the peak absorption and emission wavelengths of a fluorescent compound is known as Stokes shift[33], discovered by George Gabriel Stokes in the mid 19th century. Most intercalating dyes have a small Stokes shift, meaning that their peak absorption and emission spectra are in close proximity on the electromagnetic spectrum. This small Stokes shift mandates expensive optical filtering hardware to differentiate the excitation light source from the fluorescence output in measurement.



Figure 16 SYBR Green (left)[34], EVARuby (right)[35]

There is a wide variety of intercalating dyes used in PCR analysis. One of the most common dyes used in modern PCR is SYBR Green[36]. SYBR Green has a small Stokes shift with peak absorption wavelength of 497nm and emission at 520nm. As mentioned previously, this small Stokes shift requires specialized optical filtering hardware, which would be prohibitively expensive for this project. EvaRuby[37], in contrast, has quite a large stokes shift, with peak absorbance at 480nm and peak emission at 613nm. These spectral peaks are virtually at opposite ends of the visible electromagnetic spectrum, enabling the usage of cost-effective gel filters and optical measurement sensors.

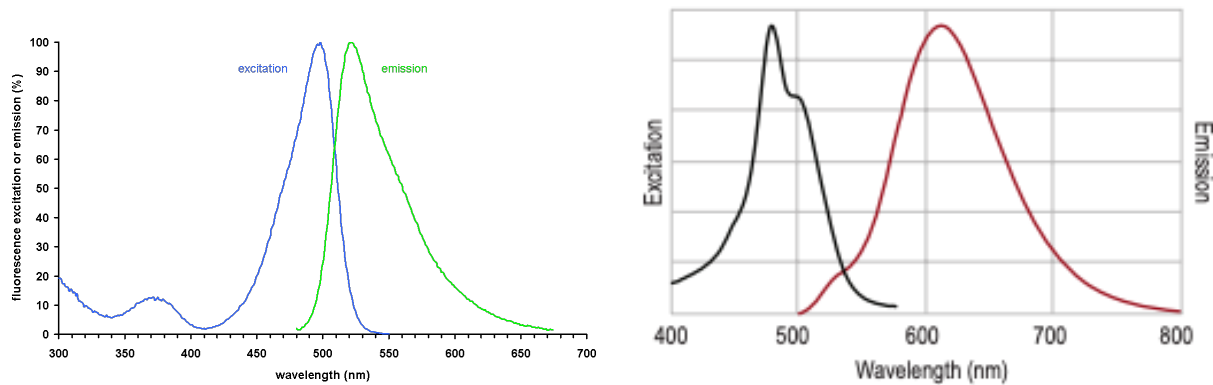


Figure 17 Absorption and emission spectral for SYBR Green (left)[38] and EVARuby (right)[39]

Types of PCR

Quantitative PCR

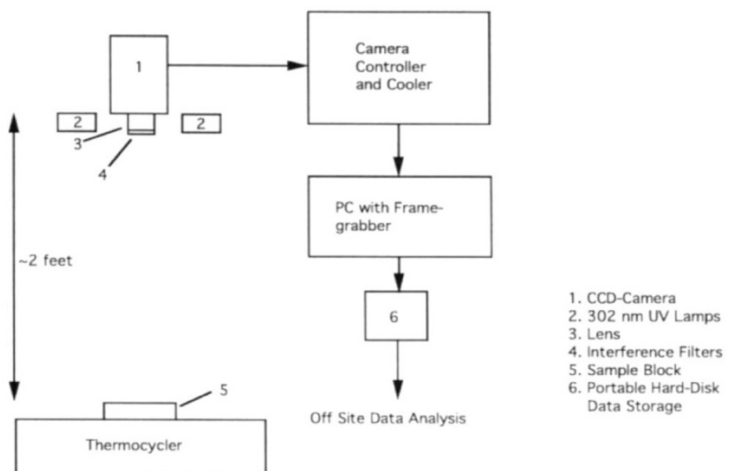


Figure 18 The experimental protocol used by Higuchi et al[31]

As mentioned previously, the PCR method proposed by Mullis et al. is inherently qualitative. On conclusion of the assay, a boolean result is acquired: the product is either positive for amplification, or it is not. Consequently, in the early 1990s, academics began work identifying a quantitative PCR technique. Higuchi et al. would devise a separate, primarily quantitative method in 1993[31]. Termed as “Kinetic PCR”, although later named qPCR or real-time (RT) PCR, the paper details the use of a video camera to discreetly monitor the fluorescence of the reactants after each PCR cycle. In samples with positive amplification, the level light emission via fluorescence is directly proportional to the quantity of target DNA in the solution. Since the quantity of target DNA doubles with each cycle, the original quantity of target DNA can be accurately inferred.

Digital PCR

While quantitative PCR proved effective for the detection and quantification of pathogenic genetic material, another biomolecular domain began to take interest in PCR. A technique termed as digital PCR began to surface, again in the 1990s, focusing particularly on quantifying genetic mutations. The technique was most commonly applied to carcinogenic mutations in early research.

A paper composed by Sykes et al. in 1992 demonstrates precursory digital PCR assay[40]. A sample of target DNA is diluted and metered into 10 distinct containers. After reaction, the ratio of positive to negative samples could be used to infer the quantity of target DNA in the original sample according to a Poisson distribution.

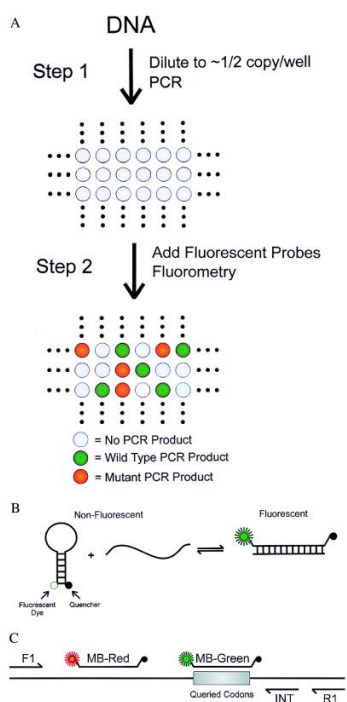


Figure 19 The experimental protocol used by Sykes et al[40]

Vogelstein and Kinzler would later propose an advancement to the previous technique in 1999[41], simultaneously coining the term "Digital PCR". Their technique involved serially diluting and metering genetic material into 96 distinct wells. The primary enhancement on the technique proposed by Sykes et al., however, was the introduction of two distinct fluorophores, each with separate emission wavelengths (485/530nm, green; 540/590nm, red). These fluorophores were oligonucleotides with stem-loop structures, with a fluorescing agent at the 5' end and a quenching agent at the 3' end. This stem-loop would "flatten" during the denaturation stage, allowing a complementary ssDNA to anneal, increasing the distance between the fluorescing agent and quenching agent upon cooling, resulting in increased fluorescence. Each fluorophore was complimentary to a DNA target

of interest: either mutant or normal DNA. The ratio of light emission at each wavelength could infer the ratio of mutant to normal genetic material. When the technique was applied over 96 distinct samples, detection of 0.1% mutant genetic material could be achieved.

Continuous-Flow Microfluidic PCR

Continuous-flow microfluidic (CFM) PCR is a microfluidic-specific PCR process in which the sample continuously moves through different temperature zones, rather than being heated and cooled in cycles, as seen in conventional PCR instruments. Microfluidic channels are typically arranged in a serpentine or spiral pattern such that the sample is repeatedly cycled through the required temperature zones over the course of the reaction. CFM PCR typically allows for faster processing due to near instant temperature ramp rates and low energy consumption as temperature modulation is not required. CFM PCR devices are also quite compact, which is ideal for point-of-care applications.

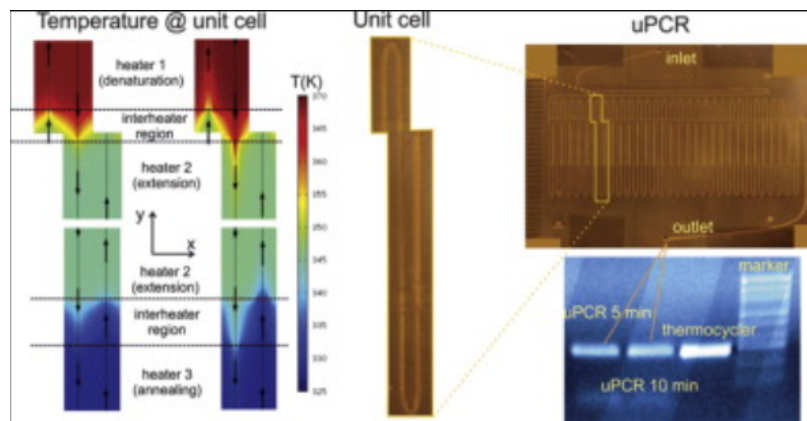


Figure 20 The experimental protocol used by Moschou et al[40]

In a method proposed by Moschou et al, a CFM quantitative PCR reaction is achieved using a microfluidic chip[42]. The sample was exposed to 30 temperature cycles, each composed of three distinct steps. Each temperature zone is controlled by an individual resistive microheater. The sample was pumped through 1.45m of microchannels by a laboratory syringe pump. The resulting instrument exhibited a total power consumption of only 2.4W, while successful DNA amplification was demonstrated after only 5 minutes.

Methods of Temperature Control in PCR

One of the core elements of the PCR process is the thermo-cycling process. Traditionally, a PCR cycle is composed of two distinct temperature stages, denaturation at 94 degrees and annealing and extension at 74 degrees, although the number of stages and the precise temperature set-points for each stage vary depending on the author's method. However, poor thermal management may allow any of the stages to fall out of operating range, resulting in the production of unwanted byproducts. It can then be inferred that the selection

of an appropriate heating element is paramount to the successful creation of a PCR instrument. In traditional thermo-cyclers, the heating and cooling is permitted though a conventional heating block.

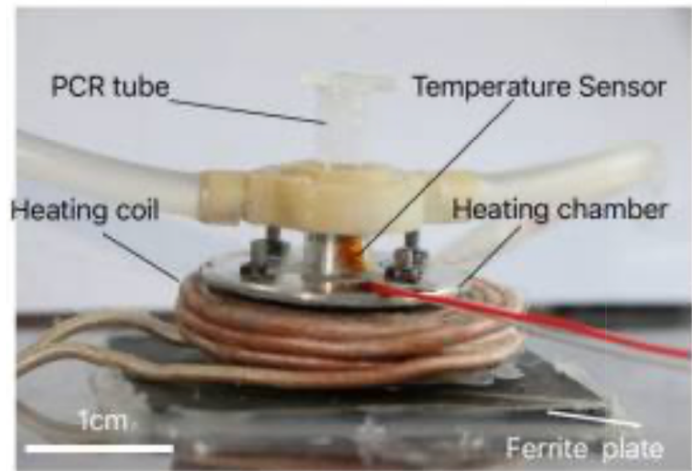


Figure 21 Experimental assembly used by Xie et al [41]

A thermocycler proposed by Xie et al introduced a method utilizing magnetic induction heating[43]. The sample was placed in the centre of a metal heating chamber, which itself was enclosed by an electromagnetic coil. When a current was passed through the coil, the resulting inductance caused the temperature of the heating chamber to increase. To cool the heating chamber, low temperature water could be pumped through the assembly. To reach a steady state temperature, heating and cooling was controlled though feedback from a temperature sensor. The result was a 100-150% increase in heating and cooling rates, with a temperature gradient reaching up to 14.92 °C/s. The proposed heating method, however, depends on a constant cold-water supply, which is unsuitable for centrifugal microfluidic platforms.

Other researchers have proposed the use of Peltier plates to both heat and cool the sample. In a method proposed by Nasser et al[44], a 50W Peltier element is integrated to heat and cool a PMMA chip. The heating and cooling of the element was controlled via Fuzzy and Bang-Bang control. The resulting thermo-cycler could achieve a temperature ramp rate of 8-8.3°C/s, however, the Peltier element mandated the requirement for a heat-sink and fan, which would again not be compatible with centrifugal platforms.

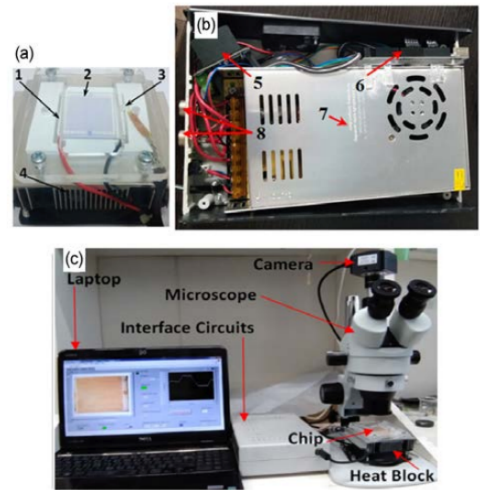


Figure 22 Experimental assembly used by Nasser et al [42]

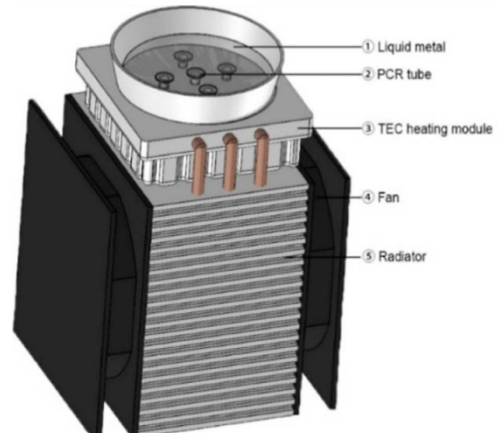


Figure 23 Experimental assembly used by Wang et al [3]

Wang et al proposed a novel heating method using liquid metal as a medium for heat exchange[3]. A liquid metal and oil bath was prepared using liquid metal with melting points of 11, 16, 30, and 47°C and dimethyl silicone oil. Sample tubes are then immersed in the liquid metal to modulate temperature. While the author does not detail specific temperature gradients, it is stated that the resulting thermo-cycler can achieve an efficiency three times greater than traditional methods. Although an interesting and innovative solution to thermo-cycling, the reason for which this is unsuitable for centrifugal microfluidic platforms is self-evident: safety.

In a paper published by Talebi et al[45], a PCB-based heater was proposed as a heating element for a continuous-flow PCR chip. The chip was fabricated from PMMA, containing microfluidic channels in a serpentine pattern. A PCB with integrated heating elements was then placed over the chip, such that half of each channel was covered by the high-temperature heating element, and the other was covered by the low-temperature heating element. The result was a heater capable of transitioning the sample between two temperature zones at a near-instant rate, without the requirement for pumping or active cooling.

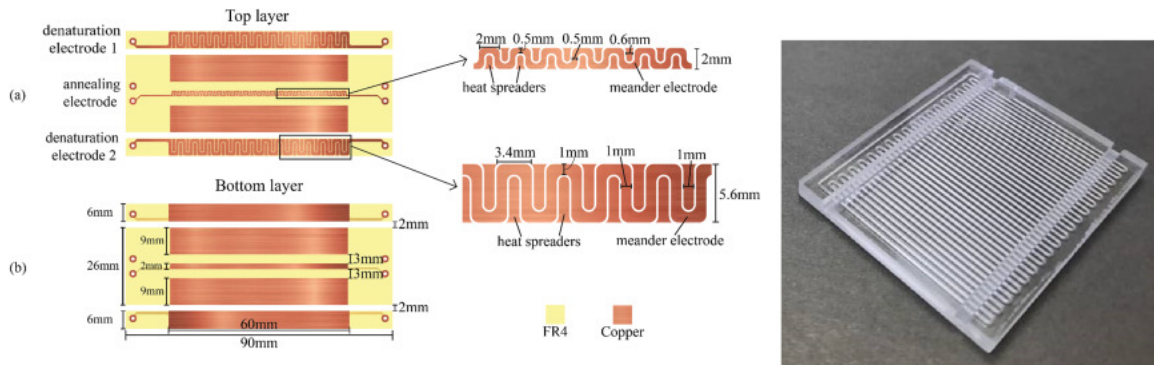


Figure 24 Experimental designs used by Talebi et al: left: PCB-based heater, right: PMMA chip[43]

Technical Background

Given the multi-disciplinary nature of this project, a vast breadth of background information is required to understand how each concept links to the next. This section provides critical information on the hardware, software, and communications architectures that permit the creation of this project's instrument. This section contains a vast amount of information required to understand the implementations detailed in the **Design** section.

Mechanics

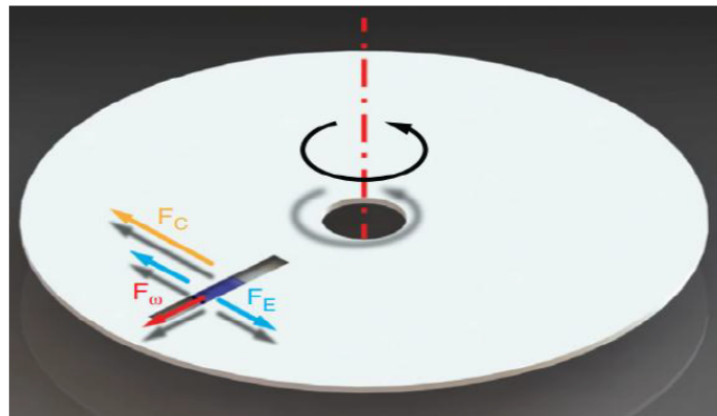


Figure 25 Forces on a microfluidic disc [19]

As mentioned previously, microfluidic discs exploit centrifugal forces to propel fluids through channels. The specific forces involved are centrifugal force (F_ω), Coriolis force (F_C), and Euler force (F_E). For most applications, the effect of F_C and F_E can be disregarded due to their relatively low magnitudes. Therefore, the effect of F_ω on the fluid in a channel is characterized by centrifugal pressure (p_{cent}). An expression can be derived to draw a relationship between p_{cent} and F_ω by modifying the expression for the hydrostatic fluid pressure imposed by gravity[21].

$$p = \rho gh$$

Where p is hydrostatic fluid pressure, ρ is fluid density, g is acceleration due to gravity, h is fluid column height. If the gh term is replaced with $\omega^2(r\Delta r)$, an expression for rotationally induced pressure can be derived[21].

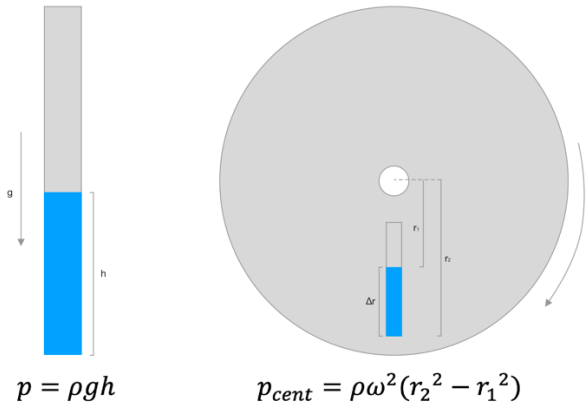


Figure 26 Visual representation of centrifugal pressure

$$p_{cent} = \rho\omega^2(r_2^2 - r_1^2)$$

In some applications, it is important to consider the rate at which the fluid flows through the channels in the disc, such as in this thesis. The pressure-driven, steady-state flow of liquid in microfluidic channels is known as Poiseuille flow, which itself is an analytical representation of the Navier-Stokes equations. Poiseuille flow was originally studied by Jean Léonard Marie Poiseuille, in channels with circular cross-sections. However, the channels used in centrifugal microfluidic devices typically have rectangular cross-sections due to the manufacturing processes involved. Unfortunately, there remains no analytical solution to Poiseuille flow in channels with rectangular cross-sections. In conditions where the width of the channels is significantly greater than the height, an approximation can be made via a Fourier sum, resulting in the following expression[46].

$$Q = \frac{h^3 \omega \Delta p}{12\eta L} \left[1 - 0.630 \frac{h}{w} \right], h < w$$

Where Q is volumetric flow rate, h is channel height, ω is angular velocity, Δp is the difference in rotationally induced pressure between the two ends of the channel, η is the dynamic viscosity of the fluid, L is channel length, and w is channel width.

Fabrication

A recurring theme in the discussion of microfluidic disc fabrication is the innovative adaptation of established "macro" processes to produce "micro" devices. As previously noted, microfluidic discs are composed of a stacked arrangement of interchanging layers of PMMA and PSA.

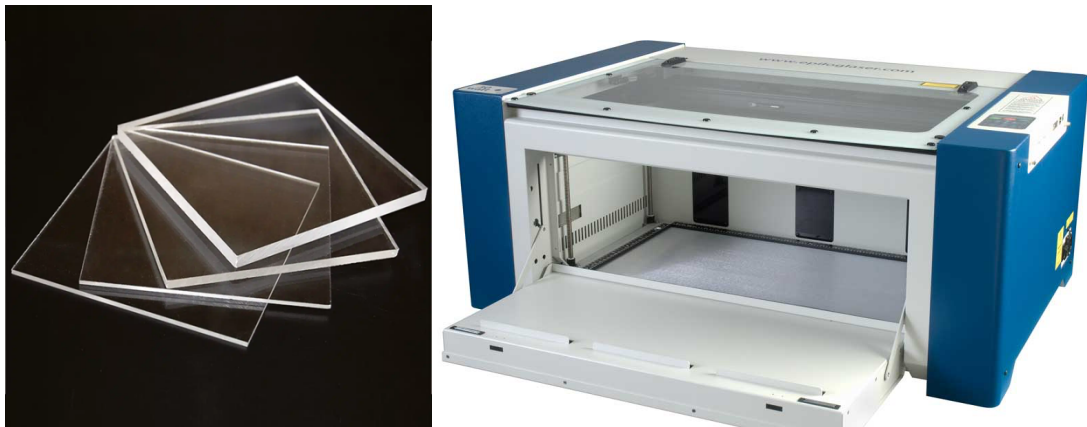


Figure 27 Left: PMMA sheets[47], right: laser cutter[48]

The layers composed of PMMA are typically fabricated using a CO₂ laser cutter. PMMA, also known as acrylic, is considered an excellent candidate for laser cutting[49]. While PMMA may appear transparent in the visible spectrum, it is opaque in the infrared spectrum. When exposed to a focused beam of infrared light at a precise wavelength, such as the 10.6 μm wavelength emitted by a CO₂ laser, localized heating occurs which results in precise cutting[50].



Figure 28 Left: roll of PSA[51], right: plotter cutter[52]

In contrast, the layers composed of PSA are not suitable for laser cutting due to their material properties and thickness. PSA is typically cut with a plotter cutter, a machine which uses a computer-controlled blade to precisely cut the material. Plotter cutters are commonly utilized in the fabrication of vinyl, fabric, and paper products.



Figure 29 Hot-roller laminator [53]

Unlike common adhesives which typically require the application of heat or a chemical activator, PSA is a viscoelastic polymer that activates with the application of pressure. When a layer of PSA is placed over a layer of PMMA, the two layers are then compressed between high-pressure rollers, activating the adhesive. Another layer of PMMA can then be placed on top of the PSA and subsequently compressed, forming a strong bond between the two PMMA layers. In addition to its strength, the resulting bond is also watertight.

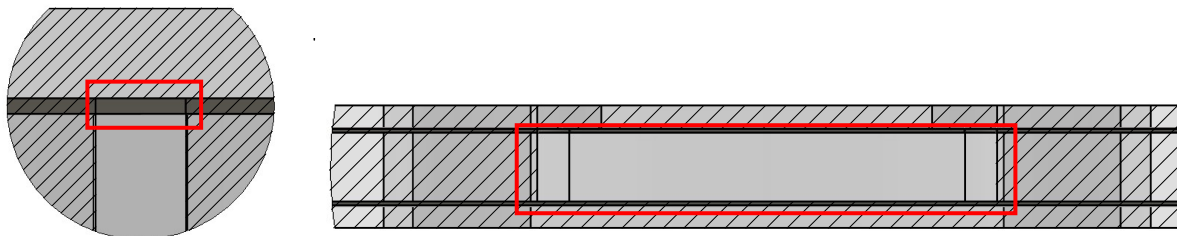


Figure 30 Left: channel in microfluidic disc, right: reservoir in microfluidic disc

A channel between the two layers of PMMA is formed by a narrow rectangular section cut from the PSA through this process. A reservoir is created by repeating this process to form a five-layer stack with a relatively thick sheet of PMMA in the center and a rhomboidal shape cut from the PMMA.

Heating

Heating refers to the process of increasing the temperature of an object through the transfer of energy. Resistive Heating, referred to as Joule or Ohmic heating, is a process in which a current is passed through a conductive material. The resistance of most conductive materials results in the conversion of a proportion of the electrical energy to thermal energy due to electron collisions, resulting in the generation of heat. This heat is subsequently distributed throughout the conducted and to the surrounding area by conduction, convection, and radiation. The principle that governs resistive heating is known as Joules law[54], described by the equation below.

$$P = I^2R$$

Where P is power in watts, I is current in amps, and R is resistance in ohms. Resistive heating is typically regarded as undesirable in most applications, particularly in circuit design. Recently, however, a novel and innovative application of resistive heating in printed circuit boards (PCBs) has arisen. This section will explore the foundations of PCB heater design.

PCB Heaters

A PCB consists of a non-conductive substrate with conductive traces etched onto its surface. The most common substrate in PCBs is FR-4, a fiberglass-reinforced epoxy resin, while the traces are typically composed of copper. PCBs are widely used in modern electronics to connect electronic components without the need for discrete conductors [55].

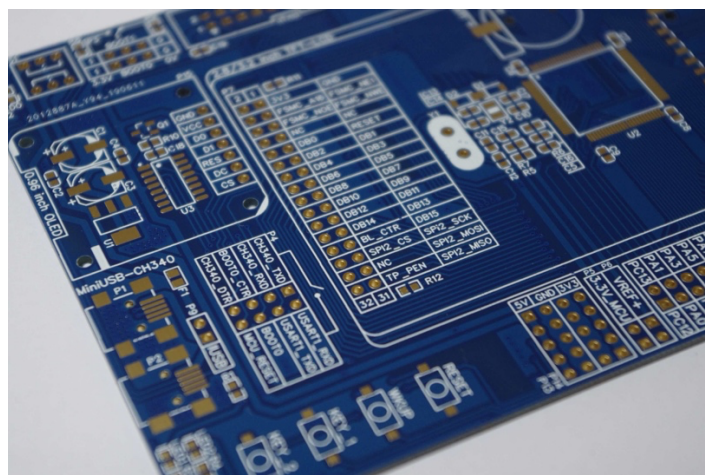


Figure 31 A printed-circuit board [56]

Due to the inherent resistance of the copper traces, resistive heating occurs as a byproduct of PCB operation. While the effect is generally undesirable in most applications, the phenomenon is leveraged in the innovative usage of PCBs as heating elements.

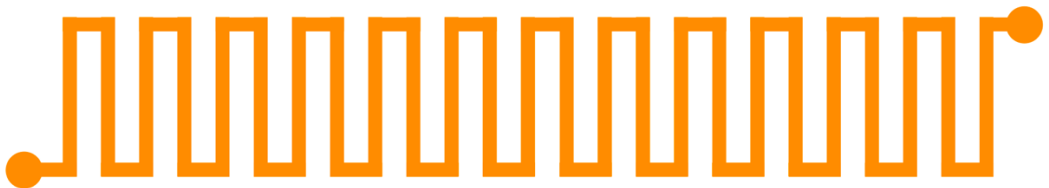
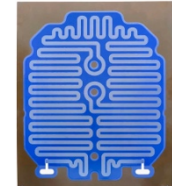


Figure 32 Example of a serpentine PCB heater trace

In PCB-based heating applications, a long, narrow trace is typically arranged in a serpentine pattern to maximize resistance. When a current flows through these traces, the resulting heat is uniformly dispersed across the surface of the PCB, allowing for controlled thermal output [57]. PCB heaters are available in many formats, as described in Table 1.

Table 1 A table describing different PCB heaters

Heater	Description
Etched Foil Heaters	<p>Etched foil heaters use a thin metal foil in a chemically etched pattern. The metal foil is then laminated between two sheets of insulating material for electrical insulation and mechanical stability.</p> <p>Nichrome is commonly used as a conductor, while polyimide or silicone is used as an insulator[57].</p>
Thick Film Heaters	<p>Thick film heaters use a resistive paste baked onto a rigid substrate to form a thin, durable heater.</p> <p>The resistive paste is typically composed of a blend of ceramic and conductive materials, while the rigid substrate composed of ceramic or glass[57].</p>
Flexible PCB Heaters	<p>Similar to etched foil heaters, flexible PCB heaters use a thin conductor insulated between two layers of insulative material, however, a traditional copper trace is used a conductor instead of nichrome[58].</p>
Rigid PCB Heaters	<p>Rigid PCB heaters use traditional PCB materials, resulting in a cost-effective thick-film heater. Instead of resistive paste, the conductor is composed of a traditional copper trace.</p> <p>Image from [59]</p>



Control Systems

As mentioned previously, Joule's law dictates that when a current flows through a conductor with resistance, the electrical energy is converted into heat energy. If the current is continuously supplied, power is steadily dissipated as heat, leading to sustained heating of the conductor. This mechanic will eventually lead to overheating. To prevent this, a control system will be implemented. This section will detail background information on the various control strategies considered for this project.

Bang-Bang Control

A Bang-bang controller is a type of feedback controller that switches between two states, typically fully on or fully off, based on the error between the setpoint and the actual measured value. This type of controller is typically used when precise control is not required or when rapid response is of a higher priority than steady state[60].

PWM Control

Similar to a Bang-Bang controller, a PWM controller is a type of feedback controller that rapidly toggles between two states. However, a PWM controller adjusts the rate at which it toggles the output on and off, such that the on-time is some fraction of the total cycle time, otherwise known as duty cycle. PWM controllers are typically used to simulate analog signals in DC devices[61].

PID Control

One of the most common and well-documented approaches to control is the proportional-integral-derivative (PID) controller.

$$u(t) = K_{pe}e(t) + K_{de}\frac{de(t)}{dt} + K_{ie}\int e(t) dt$$

A PID controller is a type of feedback controller that calculates the difference between the actual and desired value of a system (error, $e(t)$) and adjusts its output ($u(t)$) to maintain the desired value set-point. A PID controller has three fundamental components, each with a corresponding control parameter: a proportional controller, an integrate controller, and a derivative controller[62]. The mathematical expression for a PID controller is described above, while the functionality of each element is described in Table 2.

Table 2 A table describing the components of a PID controller

Controller	Description
Proportional Controller	<p>The proportional control output depends solely on the system's raw error. A proportional gain is applied to the error to generate a response. This gain influences the rate at which the controller responds to changes in input. If the proportional gain is too high, the system may oscillate, leading to instability [62].</p> <p>The corresponding control parameter is P_p.</p>
Integral Controller	<p>The integral control output depends on the accumulated past error of the system, generating a response based on the historical error over time. It helps to eliminate steady-state error by adjusting the output until the error reaches zero, allowing the system to reach steady-state [62].</p> <p>The corresponding control parameter is P_i.</p>
Derivative Controller	<p>The derivative controller depends on the rate of change in error values, allowing it to roughly predict the system's future behavior. If the error increases rapidly, the derivative controller reduces its output to counteract this change. The control parameter, derivative time, determines the controller's sensitivity to the rate of change of the input. Large values for derivative time may cause system instability as a result of overreaction to small changes [62].</p> <p>The corresponding control parameter is P_d.</p>

Spectrometry

Spectrometry is the study of the interactions between matter and electromagnetic radiation, typically in terms of absorption and emission. The techniques involved in spectrometry may be used to derive information about materials, including molecular and atomic behavior in response to light.

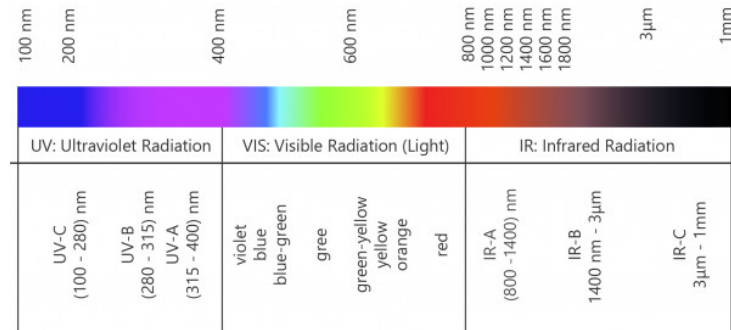


Figure 33 Optical electromagnetic spectrum [63]

Optical spectrometry is a sub-discipline within spectrometry, focusing specifically on the interaction between matter and light. Optical spectrometry techniques are used to identify the emission, absorption, and diffraction of light in the ultraviolet (UV), visible, and infrared (IR) spectra. The data derived from optical spectrometry analysis is exceptionally useful in research and industrial settings.

This section will explore optical spectrometry techniques, fluorescence, and measurement apparatus.

Optical Filtering

Optical filtering involves the selective transmission of light through a material based on the light's wavelength. There are many types of optical filters available, with each type having distinct optical properties, as outlined in Table 3[64].

Table 3 A table describing the different methods of optical filtering

Filtering Type	Description
Absorbance Filtering	Absorption filters <i>absorb</i> certain wavelengths of light, while allowing others to pass[64].
Interference Filtering	Interference filters <i>reflect</i> certain wavelengths of light, while allowing others to pass[64].
Diffraction Filtering	Diffraction filters bear etched patterns that diffract light, allowing the transmission of only a very specific range of wavelengths[64].

Additionally, optical filters can be composed to perform a range of different functions, as outlined in Table 4.

Table 4 A table describing the different types of optical filters.

Filter Type	Description
Shortpass Filters	A shortpass filter allows light with a wavelength shorter than a specified cutoff wavelength to pass, while blocking others[64].
Longpass Filters	A longpass filter allows light with a wavelength longer than a specified cutoff wavelength to pass, while blocking others[64].
Bandpass Filters	A bandpass filter is a composition of both shortpass and longpass filters, allowing light with a wavelength within a specified wavelength range to pass. A special type of bandpass filter with a narrow wavelength range is known as a notch filter[64].
Dichroic Filters	Dichroic filters operate on the principle of interference filtering, using thin layers of a dielectric material, each with different refractive indices, to selectively transmit certain wavelengths of light, while reflecting others. Unlike the traditional filters mentioned previously, dichroic filters tend to have sharp transitions between transmitted and blocked wavelengths[64].
Gel Filters	Gel filters are a widely available form of optical filter typically used to adjust lighting conditions for photography and film. These filters consist of a pigmented gel or plastic material, resulting in a specific light transmission over a wide passband. Therefore, optical filtering with gel filters is typically limited to <i>colors</i> of light, rather than specific wavelengths. Academics have proposed the usage of gel filters in spectrometry to their low cost in contrast to optical filters designed specifically for spectrometry[64].



Figure 34 Left: laboratory-grade optical filters, right: gel filters[65]

Electronics

This section will discuss the background information pertaining to the electronic components of the instrument.

Brushless Direct Current Motor

For the purpose of this thesis, a brushless direct current (BLDC) motor was selected. A BLDC motor is composed of several components, including a stator, rotor, and commutator. Some BLDC motors incorporate sensors for position or speed control. The role of each component is detailed in Table 5. Image from [66].



Table 5 A table outlining the parts of a BLDC motor

Part	Description
Stator	The stator contains windings of enameled copper wire. When current is passed through the windings, they generate a magnetic field. The windings are typically wound around a laminated steel core to minimize eddy currents, similar to transformer construction[67].
Rotor	The rotor contains permanent magnets attached circumferentially around a shaft. These magnets interact with the electromagnetic fields generated by the stator, producing torque and thus inducing rotation. The shaft transmits rotational energy from the motor to the load[67].
Commutator	The commutator is a device that switches the direction of current flow through the stator windings. Traditional DC motors use a mechanical commutator and carbon brushes that switch the current in the windings as the motor rotates, hence the term brushed DC motor. BLDC motors replace mechanical commutation with digital commutation, using sensors to detect the location of the rotor and switch current direction accordingly. In contrast to their brushed counterparts, BLDC motors offer greater reliability and extended service life[67].
Sensor	A BLDC motor may contain a hall sensor that monitors the presence and polarity of magnetic fields. This sensor analyzes the magnetic stator-rotor interaction, allowing the digital commutator to operate as mentioned previously. Hall sensors may also be used as encoders, allowing for closed-loop shaft position or angular velocity control[67].

This type of (A BLDC) motor was selected over a brushed DC motor due to advantages in performance and reliability, as detailed above. It was also determined that a stepper motor would not be able to sufficiently maintain the balance of torque, angular velocity, and angular acceleration, without sacrificing accuracy. Servo motors were also excluded, as typical servos exhibit a limited range of motion. This left only some specialized industrial motors, such as AC motors, which would require excessively complex power and control systems. Therefore, they were excluded in recognition of safety and costs.

BLDC Motor Driver

A closed-loop speed controller was selected for this project. Motor drivers vary in construction depending on their application and manufacturer, complicating detailed analysis. However, for the purposes of this thesis, a high-level overview is sufficient. The driver connects to the phase windings of the motor and the data lines of the hall sensor. The driver receives feedback from the hall sensor and adjusts the current through the phase windings, thereby facilitating rotation and maintaining a set angular velocity[68]. Image from [64].



The driver selected for this project contains a built-in closed-loop control system. The control system operates on the principle of proportional-integral-derivative (PID) control; however, the specific control parameters are not detailed by the manufacturer. As such, no detailed control system analysis was conducted. To communicate with the microcontroller, the driver supports either an analog or digital control signal, the latter utilizing Modbus. Modbus communication was selected for this project, since the analog control signal requires a maximum amplitude of 5V, while the microcontroller's general-purpose input/output (GPIO) operates at 3.3V.

Microcontroller

The heart of this instrument is the ESP32-S3-WROOM1, an internet-of-things (IoT) oriented microcontroller developed by Espressif. The ESP32 is a series of low-cost, low-power system-on-chip (SoC) microcontrollers, designed specifically for IoT and embedded applications. All microcontrollers in the ESP32 product line are dual-core 32-bit devices, containing integrated Bluetooth low-energy (BLE) and Wi-Fi functionality. These microcontrollers are widely appreciated for their low energy consumption, vast array of GPIO functionality, and ease of programming [69]. Image from [70]



Communications Protocols

This section provides information on the communication protocols used in this project, including Modbus, TTL, ESPNow, I2C, and WebSockets.

Modbus[71]

The Modbus protocol is an industrial communication protocol used to facilitate inter-device communication, particularly in industrial automation. Developed by Modicon, now Schneider Electric, in the late 1970s, Modbus operates on a ‘master-slave’ architecture using a bus topology, in which one device acts as a master and at least one device serves as a slave. It is typically implemented in two forms: Modbus RTU, which operates over RS232 or RS485 serial, or Modbus TCP, over Ethernet. Modbus RTU is used for this project as it is directly supported by the driver and easily integrates with the selected microcontroller.

As mentioned previously Modbus RTU protocol operates under a master-slave paradigm. Communication between the master and slave is typically managed through registers and coils, each of which are allocated designated memory addresses on the slave device. Registers are used to hold byte-oriented (hexadecimal) data, whereas coils are used to hold bit-oriented (binary) data. The master can write to a coil or register as an input to the slave, or the slave can write data to a coil or register as an output to the master. Devices usually support up to 255 register addresses, each with a unique function. These functions vary by device, and detailed functionality is typically described in the manufacturer’s product datasheet.

Data is transmitted between the master and slave in a format known as a frame. A typical frame consists of eight bytes, where one byte equals eight bits, or two characters of hexadecimal. The structure of a typical frame is outlined in Table 6, followed by a description of each frame segment in Table 7.

Table 6 A table describing Modbus frame structure

Slave Address	Function Code	Target Address	Register	Payload	Error Checking
1 Byte	1 Byte	2 Bytes		2 Bytes	2 Bytes

Table 7 A table describing each segment in a Modbus frame.

Frame Property	Description
Slave Address	The address of the slave on the Modbus network.
Function Code	The action to be performed. A list of the most common actions, those which will be used within this thesis, are listed below. 0x01 – Read Coil 0x03 – Read Single Holding Register 0x06 – Write Single Holding Register 0x10 – Write Multiple Holding Registers
Target Register Address	The address of the register on the slave where the data should be read from or written to.
Payload	The payload, which is only used in a <i>write</i> action, contains the data that should be written to the target register.
Error Checking (CRC)	To ensure data integrity, a cyclic redundancy check (CRC) is used as a checksum for verification purposes. The CRC checksum is calculated based on the content of the message and a predetermined CRC start value (for example 0xFFFF). This checksum is appended to the end of a frame by the sender. Upon receiving the frame, the receiver recalculates the checksum using the same start word. If the checksums match, the transmission is considered successful and free of corruption.

RS485, in common voltage mode, uses differential signals in the range of -7V to +12V, which is not directly compatible with many microcontrollers, including the one selected for this project. Therefore, the RS485 signal must be converted to Transistor-Transistor Logic (TTL) serial, which operates in a range of 0V to 3.3V, to interface with the microcontroller.

Transistor-Transistor Logic (TTL) Serial[72]

TTL Serial uses the Universal Asynchronous Receiver-Transmitter (UART) protocol and operates with TTL logic voltage levels. Data is also transmitted using frames, though the structure of the frame is different, as shown in Table 8. Additionally, TTL transmissions operate at a variety of frequencies, known as a baud rate. Transmission frequency must be synchronized between the two devices or data corruption will occur.

Table 8 A table describing TTL frame structure

Start Bit	Data Byte	Parity Bit	Stop Bit
1 Bit	1 Byte (8 Bits)	None	1 Bit

To facilitate communication, the RS485 signal from the driver must be translated into a TTL signal for the microcontroller, and vice versa. To meet this requirement, an RS485-to-TTL converter is used. These converters are typically available in SMD packages, such as the MAX485. The MAX485 is manufactured by Analog Devices, Inc. specifically for this purpose.

ESPNow[73]

ESPNow is a low-energy communication method developed by Espressif to permit communication between ESP32 modules without the need for a Wi-Fi network. The protocol is highly energy-efficient and low latency.

I2C [74]

I2C is a synchronous, multi-slave serial communication protocol developed by NXP Semiconductors (previously Phillips). I2C uses two connections, a data line and a clock line, to offer high-speed hardware communication (100kbits/s to 5Mbits/s). I2C is directly supported by all ESP32 modules in hardware.

HTTP[75]

Hypertext transfer protocol (HTTP) is a data-transfer protocol used for internet communications, invented by Tim Berners-Lee in 1991. The protocol allows devices to communicate over the internet by transmitting structure data packets. Operating on a request-response model, each transmission is independent, and the server does not maintain any data between requests. Each transmission is labelled with a specific action, referred to as a method, including GET, POST, PUT, DELETE. These methods are loosely standardized per the representational state transfer (REST) application programming interface (API) paradigm.

HTTPS [75], [76]

Security concerns in HTTP led to the development of HTTP Secure (HTTPS) shortly after the initial release of HTTP. HTTPS achieved encrypted communication using security layers, including the transport layer security (TLS) and secure sockets layer (SSL). HTTPS began development in the early 1990s, with its first implementation by Netscape in 1995.

WebSockets[77]

Until the late 2000s, communication between client and server was handled on a request-response basis. With internet applications growing in complexity, this inevitably led to increased overhead and latency and high bandwidth usage. Recognizing this problem, Ian Hickson and Michael Carter proposed the WebSocket protocol in 2008.

The WebSocket protocol is a full-duplex, real-time communications protocol allowing the client and server to communicate on-demand, without the requirement for a new request for each message. The protocol was standardized in 2011 by the Internet Engineering Task Force (IETF) under RFC 6455. An API for WebSocket communication is directly available in all modern browsers.

Software

This section provides background information on some of the languages and frameworks used in this project.

Javascript [78]

JavaScript (JS) is a high-level interpreted programming language invented by Netscape in 1995. To ensure consistency in implementation across platforms, the language was standardized as ECMAScript (ES) by Ecma International in 1997 under ECMA-262. While JS is predominantly used in front-end web development, frameworks like NodeJS expanded its usage as a server-side and scripting applications. The language supports object-oriented and functional programming. A statically typed version of the language, known as TypeScript, was later developed by Microsoft in 2012, due to programming inefficiencies caused by the JS dynamic type system.

ReactJS [79]

The widespread adoption of JS for front-end development led to the creation of ReactJS (referred to as React), an open-source library developed by Facebook in 2013. React addresses many of the drawbacks in JS front-end development, such as challenges in document object model (DOM) manipulation and state management. The library introduced the concept of components, allowing developers to compartmentalize webpage elements in dedicated containers. Data to be passed between these components a property, known as “props”, allowing for the creation of interactive and dynamic user interfaces.

Next.js [80]

Building on the evolution of the web-technology ecosystem, NextJS (referred to as Next) was introduced by Vercel in 2016. Next is an extension of React, offering additional functionality including server-side rendering and enhanced filesystem-based application routing. One of its most significant features is the ability to merge client and server applications into a single codebase, allowing seamless code-sharing and communication between the pair. This functionality makes Next an extremely powerful tool for developing full-stack web applications.

Design and Implementation

Central Control System

The central control system (CCS) is responsible for governing the function of the instrument and reporting vital information to the user. In essence, the CCS manages the control of peripheral control systems (PCSs), including the centrifuge and the heater, and also acquisition of data from sensors such as the spectral sensor.

Software Implementation

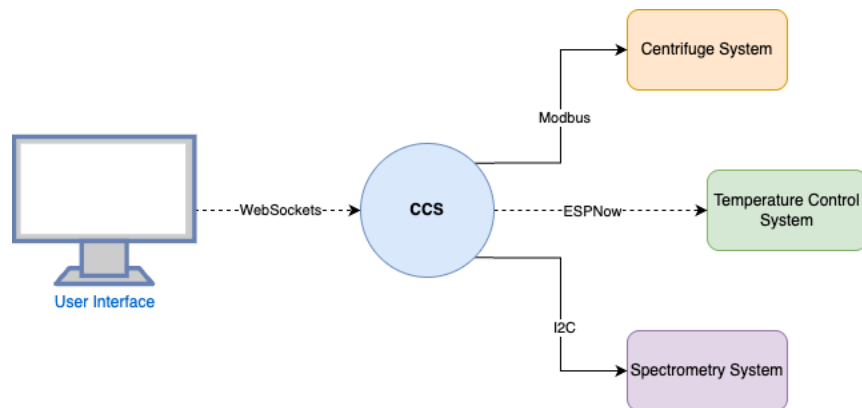


Figure 35 CCS communications architecture

The CCS is connected to all peripheral devices in the instrument, including the centrifuge system, heating system, and spectrometry system. Interfacing with these devices requires an array of communication methods to be used, including Modbus, ESPNow, I2C, and one-wire GPIO. The CCS also connects to the user interface via WebSockets, allowing the user to communicate with the instrument. This connection is managed through WebSockets. A network diagram of the interconnection between instrument components and the CCS is shown in Figure X. The specific implementation for communications and control for the PCSs will be discussed in their own respective sections.

Instrument-Side Websocket Implementation

To facilitate communications between the CCS and the user interface, the CCS broadcasts a websocket server over Wi-Fi. As such, the first requirement is to connect the CCS to a Wi-Fi network.

```

1. const char* ssid = "";
2. const char* password = "";
3.
4. // Connect to WiFi
5. void setup_wifi() {
6.     WiFi.mode(WIFI_STA);
7.     WiFi.begin(ssid, password);
8.     Serial.print("Connecting to WiFi ..");
9.     while (WiFi.status() != WL_CONNECTED) {
10.         Serial.print('.');
11.         delay(1000);
12.     }
13.     Serial.println(WiFi.localIP());
14. }
```

Subsequently, the WebSocket server can be initialized.

```

1. // Create server object on port 80, then websocket
2. static AsyncWebServer server(80);
3. static AsyncWebSocket ws("/ws");
4.
5. void setup_websocket() {
6.     ws.onEvent(onEvent);
7.     server.addHandler(&ws);
8. }
```

To handle messages from the user interface, a handler function must be established to parse incoming data. For brevity, functions are shortened to only include necessary information. Omissions are marked by an ellipsis.

```

1. void onEvent(..) {
2.     switch (type) {
3.         ...
4.         case WS_EVT_DATA:
5.             handleWebSocketMessage(arg, data, len);
6.             break;
7.         ...
8.     }
9. }
10.
11. void handleWebSocketMessage(void *arg, uint8_t *data, size_t len) {
12.     ...
13.     handle_command((char*)data);
14. }
15.
16. void handle_command(char* buffer) {
17.     parse_command(buffer);
18.     if (strcmp(action, "<ACTION>") == 0) {
19.         dispatch_action(<ACTION>)
20.     }
21. }
```

Finally, a method is established for the CCS to send a message to the user interface.

```
1. void notify_clients(String sensorReadings) {  
2.     ws.textAll(sensorReadings);  
3. }
```

Power System Implementation

The CCS also encompasses the power system for the instrument. The instrument is powered by both 24V/14A and 5V/7A power supplies. The 24V power supply was salvaged from a broken Ender3 3D printer, while the 5V supply (Meanwell LRS-35-5) was purchased new from StepperOnline. The power supplies are powered via a fused 240V mains connection. All 240V lines are properly color coded per IEC standards. If a mains voltage line is required to be spliced between two or more locations, WAGO 221-series lever connectors are used for secure connection. All current carrying conductors are specified to the correct gauge to prevent voltage drops and potential overheating.

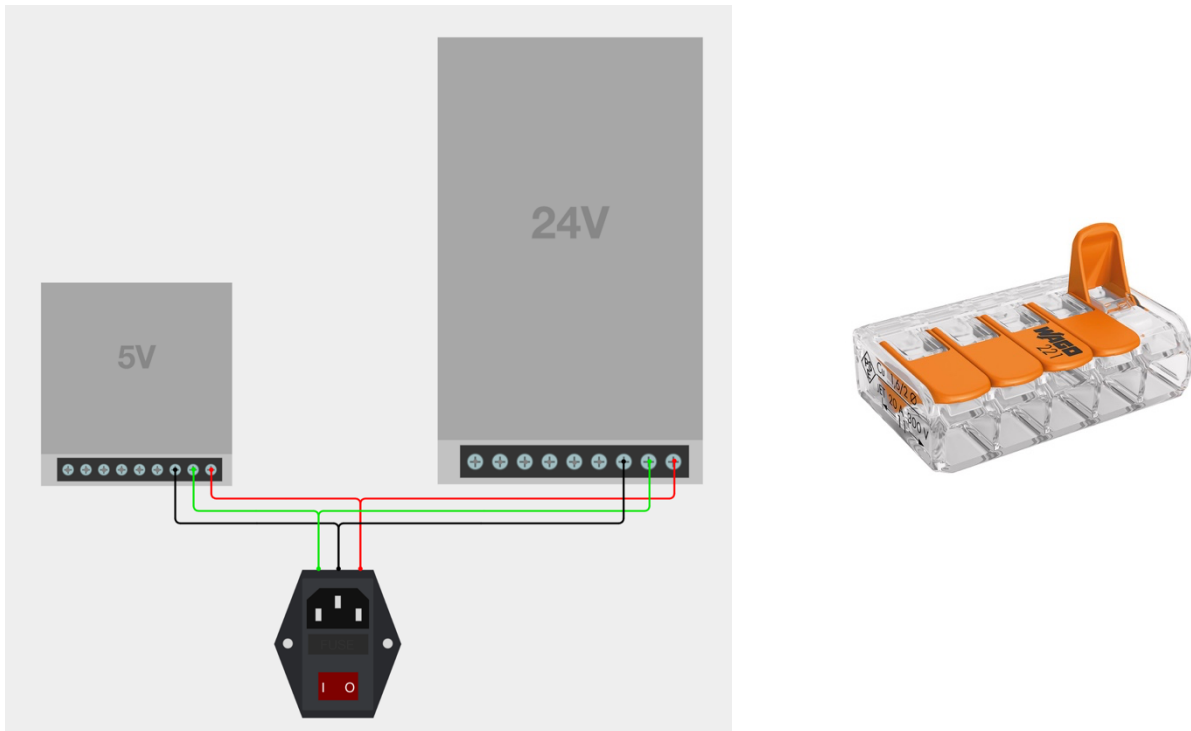


Figure 36 Left: power supply circuit diagram, right: WAGO 221 lever connector [79]

Microfluidic Disc

The primary objective of this project is to create an instrument capable of supporting a PCR assay. As such, the determination was made that a disc capable of supporting the simplest form of PCR, end-point PCR, should be designed first. In order to support an end-point PCR reaction, the disc must contain reservoirs to hold the sample before and after the reaction and channels to perform the reaction in. This section will detail the design of a microfluidic disc capable of sustaining an end-point PCR reaction.

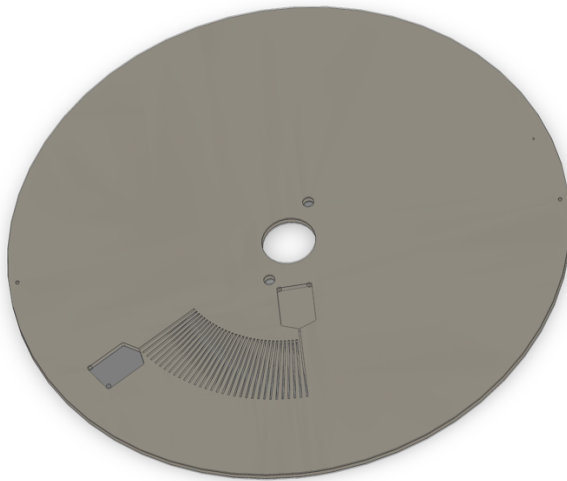


Figure 37 The microfluidic disc designed for this project

Channel Dimensions

Regardless of the type of PCR undertaken, the reaction requires the sample to be exposed repeatedly to heating and cooling cycles, between the temperatures of 74°C and 94°C. While heating a liquid between the two temperatures listed previously in itself is not a difficult task, cooling presents a unique challenge. Other academics have tackled this issue using Peltier elements as described in this documents Literature Review, however, these elements do not align well with a centrifugal designed, given the requirement for cooling fans.

To circumvent this issue, a unique solution is proposed. If the volume of the channels is reduced, the thermal mass for the fluid is reduced, consequently reducing the energy required to heat the fluid and the energy loss required to cool the fluid. To achieve this reduction in volume, the channels are cut from PSA rather than PMMA, permitting a channel height of only 0.086mm. Given a channel width of 0.5mm, the resulting cross-sectional area of only 0.043mm².

$$5 \times 10^{-4} \cdot 8.6 \times 10^{-5} = 4.3 \times 10^{-8} m^2 = 0.043 mm^2$$

To demonstrate the effectivity of the small cross-sectional area, the thermal diffusion time can be calculated per the following equation.

$$t_d \approx \frac{d_h^2}{\alpha}$$

Where t_d is thermal diffusion time, d is hydraulic diameter, and α is the thermal diffusivity of the liquid. The hydraulic diameter of the channel can be roughly obtained using the following equation.

$$d_h = \frac{4A}{P}$$

Where d_h is hydraulic diameter, A is cross sectional area, and P is the wetted perimeter of the channel. A is given above, while P is given by:

$$P = 2 \cdot (w + h) = 2 \cdot (5 \times 10^{-4} + 8.6 \times 10^{-5}) = 1.172 \times 10^{-3} m$$

Using these values to solve the hydraulic diameter equation above:

$$d_h = \frac{4 \cdot 4.3 \times 10^{-8}}{1.172 \times 10^{-3}} = 1.47 \times 10^{-4} m$$

Assuming the liquid in the channels is water, the thermal diffusivity is $1.43 \times 10^{-7} m^2 \cdot s^{-1}$, the thermal diffusion time can be calculated as:

$$t_d \approx \frac{(1.47 \times 10^{-4})^2}{1.43 \times 10^{-7}} \approx 0.15 s \approx 150 ms$$

Given the above, it can be inferred that the time taken for heat to diffuse across the liquid is only 150ms, which is sufficiently fast for this application.

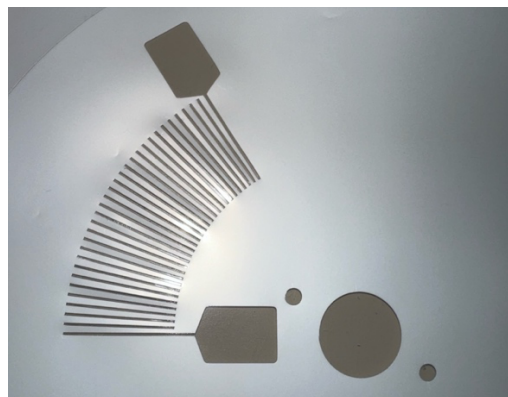


Figure 38 Example of channels and reservoir cut from PSA

Channel Pattern

In addition to temperature modulation, the rate of change in temperature is also a significant factor. The channels must be designed to physically support the modulation of temperature at a rapid rate. To achieve this, there are effectively two options: a single-sided disc with a dual-temperature heater, or a double-sided disc with a single-temperature heater on either side. To properly identify the superior pattern, both a single-sided and double-sided discs were designed.

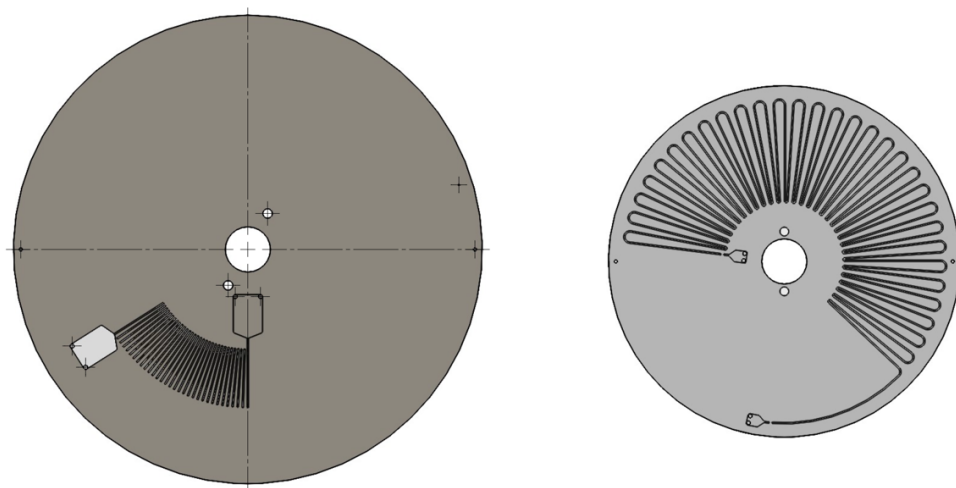


Figure 39 Left: disc revision 4 channel pattern, right: disc revision 1 channel pattern

Both designs effectively include a single channel connecting an input and output reservoir. The single-sided disc contains a single, serpentine-pattern channel, while the double-sided disc contains high temperature channels on one side of the disc, and low temperature channels on the other, connected by vias.

It was determined that the single-sided design may have issues with thermal diffusion between the two heating elements and across the top layer of the disc, causing the high-temperature heater to push the low-temperature heater outside of its operating range. Additionally, integrating two separate heaters into a single module causes increased complexity in the design of the heater circuitry. As a result, the dual-layer design was selected as the appropriate design for this project.

Reservoir Design

As mentioned previously, the disc must contain an input and an output reservoir to store the sample before and after the reaction. The mechanics of a centrifugal microfluidic disc, however, present a significant caveat. The progression of liquid through the channels is dependent on the pressure exerted on the liquid, which in turn is dependent on the

difference between the radial locations of the start of the liquid and the end of the liquid. Given that the liquid in the channels on the top layer will flow radially outward, down through a via, and return radially inward, the relative pressure on the fluid in the channels on the bottom layer will cancel that of the channels in the top layer.

If a volume of the sample is less than or equal to the total volume of the channels, the input reservoir will empty before the sample can progress to the output reservoir, the pressure on the sample will fall to zero, causing the reaction to stall. To identify whether this phenomenon will cause an issue, the volume of the sample can be compared to the total volume of the channels. An expression for the total volume of the channels (V_{total}) is shown below:

$$V_{total} = N_{cyc} \cdot (A \cdot L_t + A \cdot L_b + 2 \cdot A \cdot L_v)$$

Where N_{cyc} is the number of PCR cycles, A is the cross-sectional area of the channels, L_t is the length of a single top layer channel segment, L_b is the length of a single bottom layer channel segment, L_v is the length of a via transition between the top and bottom layers. Using values from the channel design detailed in the previous section to solve for V_{total} :

$$V_{total} = 32 \cdot (4.3 \times 10^{-5} \cdot 2 \times 10^{-2} + 4.3 \times 10^{-5} \cdot 1.9 \times 10^{-2} + 2 \cdot 4.3 \times 10^{-5} \cdot 1.69 \times 10^{-3})$$

$$V_{total} = 32 \cdot (8.6 \times 10^{-7} + 8.17 \times 10^{-7} + 1.45 \times 10^{-7})$$

$$V_{total} = 5.83 \times 10^{-5} m^3$$

Given that the intended sample volume for the reaction is $200\mu L$, the calculation above dictates that reaction will stall. To work around this, a volume equal to V_{total} of low-density, immiscible liquid such as mineral oil is added to the input reservoir, and as such, the input reservoir will require a total volume of the sample and the mineral oil.

$$V_{res} = 2 \times 10^{-7} + 5.83 \times 10^{-5} = 5.85 \times 10^{-5}$$

Centrifuge

A centrifuge is a laboratory instrument that is used to separate the contents of a mixture based on their relative densities by subjecting them to rapid rotation, generating outward acceleration on denser components. In this project, outward acceleration is required to propel the sample through microfluidic reservoirs. As such, a centrifuge mechanism is required.

Key design components of the centrifuge include a motor, motor driver, and microcontroller. This section will discuss the selection of a motor and motor driver, along with the communications implementation required for integration with the greater system.



Figure 40 The instrument's centrifuge mechanism

As mentioned previously, the instrument is designed around a chassis built as part of a previous project. As such, the specifications for the centrifuge system depend heavily on the mechanical properties of the existing chassis. This section will include detail on the derivation of centrifuge parameters, the specification of a suitable motor and motor driver, and their integration into the greater system.

Spindle

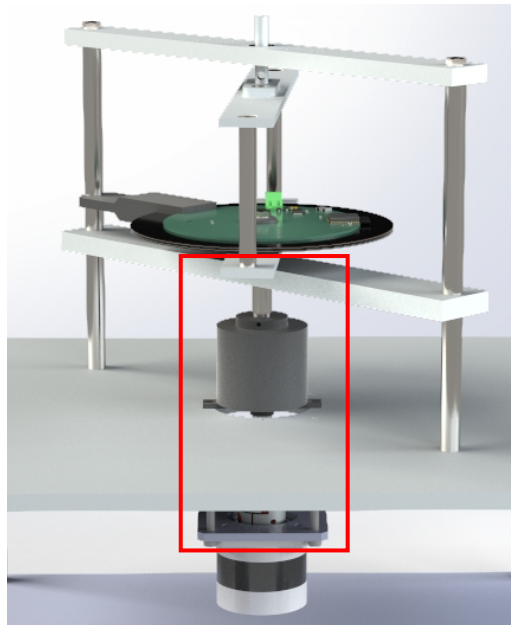


Figure 41The instrument's centrifuge mechanism with spindle highlighted

In order to couple the disc to the driver mechanism, a spindle has been adapted from existing chassis. An adapter has been designed to permit this project's disc to be mounted on the existing spindle. The spindle is mounted to the chassis using a sliring, permitting the rotation of the spindle and power transmission to the rotating body. A shaft connects the spindle to a motor through a jaw coupling.

Motor Specification

There are two significant parameters that require consideration in the selection of an appropriate motor: torque and maximum speed. The maximum speed has been predetermined at a rate of 3000RPM. The torque however requires significantly more consideration.

When identifying the torque required to accomplish a given task, the moment of inertia of the rotating body and the angular acceleration must be considered. The angular acceleration may be identified by suggesting an arbitrary time interval for the motor to accelerate from stopped to the desired maximum speed. For the purposes of this project, the period has been set at ten seconds. The required angular acceleration may then be roughly calculated as below.

$$\alpha = \frac{\omega_f - \omega_0}{t}$$

Where α is the required angular acceleration ($rad \cdot s^{-2}$), ω_f is the final angular velocity ($rad \cdot s^{-1}$), ω_0 is the initial angular velocity ($rad \cdot s^{-1}$), and t is acceleration time (s). Given that $\omega_f = 314.16 rad \cdot s^{-1}$, $\omega_0 = 0 rad \cdot s^{-1}$, the equation can be solved as follows.

$$\alpha = \frac{314.16 - 0}{10} = 31.416 rad \cdot s^{-2}$$

The required torque can then be calculated per the the following expression.

$$T = J\alpha$$

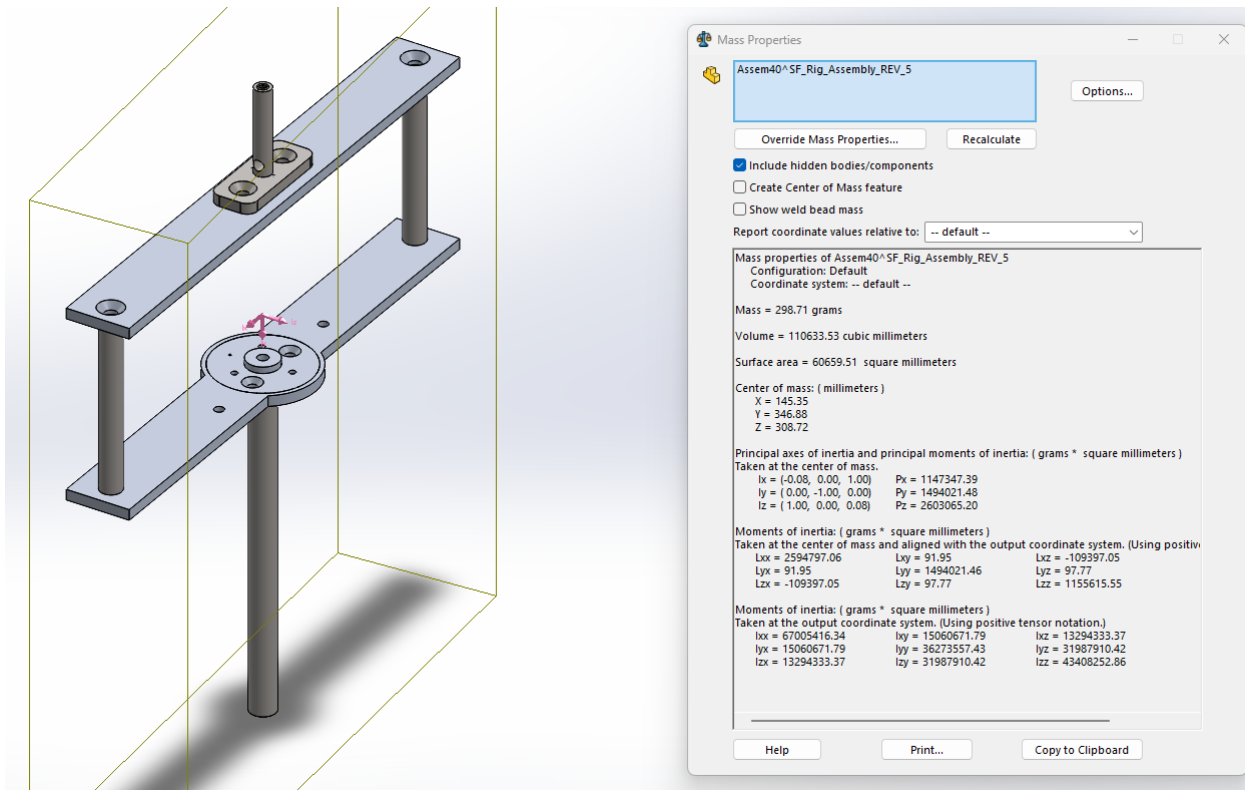


Figure 42 Measure statistics from Solidworks, showing mass moment of interial along the Y-axis

Where T is torque and J is the total moment of inertia of the spindle, evaluated using the measure tool in SolidWorks at $x kg \cdot m^2$. Evaluating the expression results in:

$$T = 0.001494021 \cdot 31.416 = 0.04398 Nm$$

Indicating that the motor will need to supply at least $0.04398 Nm$ of torque to bring the spindle to full speed within 10 seconds.

Motor and Motor Driver Selection

Per the specifications outlined in the previous section, suitable BLDC motor was selected (StepperOnline, 57BLR50-24-01). In line with the manufacturer's recommendations, a suitable motor driver (BLD-305S) was also selected. The specifications for the motor can be found in Table 9, while the specifications of the Motor Driver can be found in Table 10.

Table 9 A table showing the properties of the selected BLDC motor

Property	Value	Unit
Operating Voltage	24	V
Operating Current	5	A
Rated Speed	3500 ($\pm 10\%$)	RPM
Rated Torque	0.23	Nm

Table 10 A table showing the properties of the selected motor driver

Property	Value	Unit
Standard Input Voltage	24	V
Continuous Output Current	8	A
Speed Control Range	0 – 20000	RPM
Chopper Frequency	20	kHz

Circuit Implementation

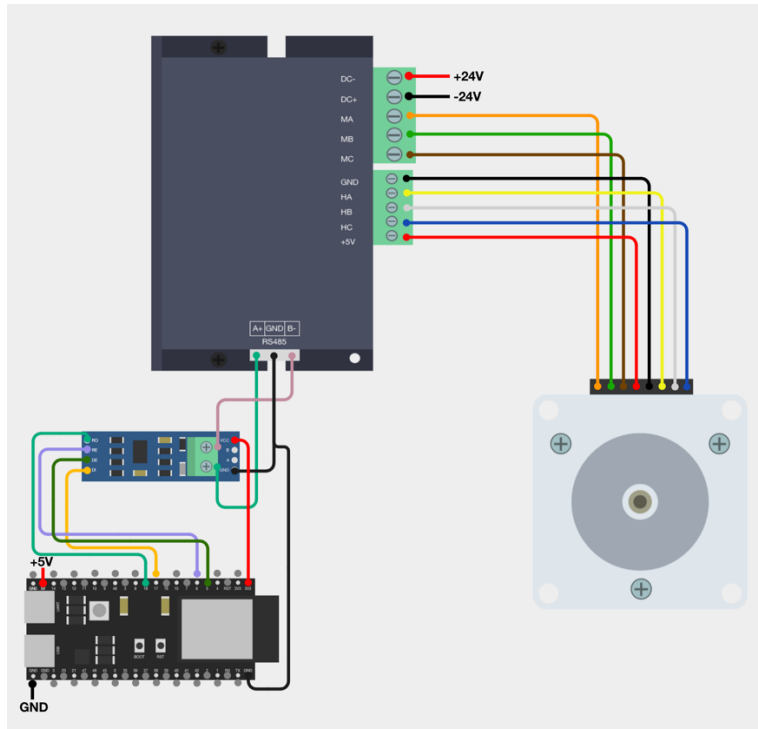


Figure 43 Wiring diagram for the motor and driver

The motor, motor driver, and RS485-to-TTL converter are connected to the ESP32-S3 (CCS) as described in Figure X. The U, V, and W phase pins and 5V, ground, A, B, and C hall sensor pins on the motor are connected to the corresponding pins on the driver. The A, B, and ground RS485 connections on the driver are connected to the corresponding pins on the RS485-to-TTL converter. The RE and DE pins on the RS485-to-TTL converter, which enable and disable receive and transmit functionality, are connected to generic GPIO pins on the ESP32, in this case pins 5 and 6.

Given that the RS485-to-TTL converter communicates with the ESP32-S3 over serial, functions like `Serial.print`, which also use serial, would corrupt Modbus communications if both were using the same serial controller. To avoid this, the second serial controller on the ESP32-S3 is used. In this case, pins 17 and 18 were selected arbitrarily, although the ESP32-S3's GPIO multiplexer permits the usage of any pins for this functionality. As such, the RO and DI pins, which receive and transmit data between the devices, are connected to pins 17 and 18 respectively.

Finally, power is connected to the devices. The ground connections for the motor driver's RS485 connection, the RS485-to-TTL converter, and the ESP32-S3 are connected together to provide a common voltage reference for all devices. The DC+ and DC- pins are connected to the V+ and V- pins on the 24V power supply respectively.

Software Implementation

Within the CCS software package, a library has been created to manage communications between the CCS and the motor driver. As mentioned previously, the two devices communicate over Modbus. The Modbus-Master library is used to establish the fundamental Modbus communication functions. A set of independent functions are built on top of the Modbus-Master library to control factors such as motor power, motor speed, and motor acceleration time are created. This section will briefly discuss the method of communication, while specific implementation with comments can be seen in the project repository.

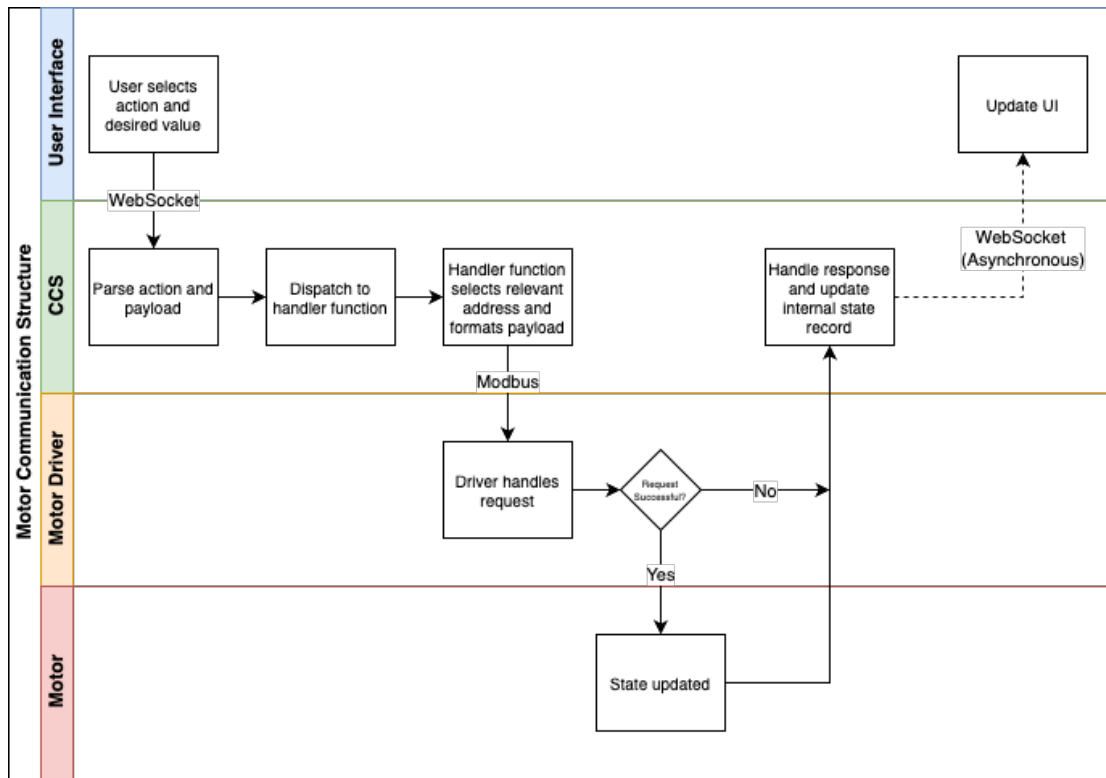


Figure 44 Communications workflow for motor control

A generalized communication workflow is described in Figure X. From the user interface, the user selects the parameter to be changed and the value it should be changed to. Subsequently, a WebSocket message is sent from the application to the CCS in action-payload format. Table 11 shows a list of actions the CCS can handle, and their respective payload data types and possible values.

Table 11 A table showing available motor functions

Action	Action Description	Payload Type	Payload Values
SET_MTR_SPEED	Set motor rotation speed	Number	0-3000
TGL_MTR_ON	Start or stop motor rotation	Boolean	0 (off) or 1(on)
TGL_MTR_MODE	Toggle between analog or Modbus motor control	Boolean	0 (analog) or 1 (Modbus)
SET_MTR_ADT	Set the motor acceleration and deceleration time	Number	Any

The action is then dispatched to a handler function that communicates the message over Modbus to the driver. Once the driver processes this function, a response is returned to the CCS as to whether the request was successful. The user interface is updated with the resulting state in the next vitals cycle, as described in the CCS section. Table 12 describes the composition of the Modbus messages corresponding to each action. Note that the slave address is always 0x01, and the payload is always encoded in hexadecimal prior to transmission.

Table 12 A table showing the registers for each function

Action	Function Type	Address
SET_MTR_SPEED	Write Single Register	0x0056
TGL_MTR_ON	Write Single Register	0x0066
TGL_MTR_MODE	Write Single Register	0x0136
SET_MTR_ADT	Write Single Register	0x00E6

Heating

Given that a regulated temperature is required for a PCR reaction, a temperature control system is required to regulate the temperature of the heating element. This section will detail the design and implementation of a temperature control system, including a PCB heater and the relevant control mechanisms.

Calculation of PCB parameters

The design of the heater is made difficult by virtue of the number of viable entry points into calculating heater parameters. Additionally, drawing a heater composed of a large number of repeating traces is quite tedious. Consequently, a solution was designed to identify the optimal design for the heater.

To effectively design the heater, a number of design parameters are set out:

- An identical heater design should be used for the heaters on the top and bottom of the disc. The temperature should be adjusted via software control rather than design differences.
- The heater should be supplied by 5V, at a maximum of 7A.
- The thickness of the copper traces should be the default thickness provided by the manufacturer, at $1 \text{ oz} \cdot \text{ft}^{-1}$.
- The ambient temperature (T_A) is defined as 20°C , while the maximum operating temperature (T_{max}) is defined as 100°C .
- The heater trace should be a single, uniform trace in a serpentine pattern, filling a radial segment of 180° . The innermost radius of the radial segment should be 35mm , while the outermost radius should be 55mm .

With these design parameters, the heater can be effectively designed from a mathematical perspective. The rate at which the heater can increase in temperature is limited by the power dissipated by the heater trace. The power dissipated by a resistive element is defined by Equation X.

$$P = I^2 R$$

Where P is the dissipated power, I is the current flowing through the resistor, and R is the resistance of the resistor. To calculate R , a separate expression in Equation X may be used.

$$R = \frac{\rho \cdot L}{A}$$

Where ρ is the resistivity of the conductor, L is the length of the conductor, and A is the cross-sectional area of the conductor. While ρ is a known value, L and A are not defined

parameters, and must be calculated. A is a product of trace width w_t and trace height h_t , the exact relationship of which is shown in Equation X.

$$A = w_t \cdot h_t$$

As such, the issue presents itself. If any of R , L , and A are set as fixed values and the others are solved algebraically, there are infinite possible combinations. The vast majority of these combinations will fail to meet the design conditions outlined above. To work around this issue, a Python script was created with inspiration from dynamic programming. The script iterates over possible design parameters and identifies the optimal solution. A set of additional initial conditions, outlined in Table 13.

Table 13 Table of design parameters for the PCB heater

Condition	Value	Unit
Inner Radius (D_i)	35	mm
Outer Radius (D_o)	55	mm
Spacing (s)	Variable	mm
Trace Width (w_t)	Variable	mm

Consider the space between D_i and D_o which the serpentine heater trace can occupy. There are a finite set of radii that can fit within this space when separated by a defined spacing s . The function described in Equation X shows a method of calculating

$$r = R(n) = D_i + (n \cdot s), \quad \text{if } D_i \leq r \leq D_o$$

Taking an iteration of this expression with $s = 1\text{mm}$, the corresponding set of radii are described in Table 14.

Table 14 A table showing the pattern in heater trace increments

Radius	R_1	R_2	R_3	...	R_{n-1}	R_n
Value	35	36	37	...	$35 + ((n - 1) \cdot 1)$	$35 + (n \cdot 1)$

If an arc of 180° is drawn for each of these radii and connecting lines are drawn to connect the start of the current arc to the beginning of the next arc, a single, uniform heater trace is obtained. The resulting length can be processed through equations X, Y, and Z to identify the cross-sectional area, resistance, and power dissipation of the trace.

Additionally, KiCad PCB schematics do not use special encoding. Therefore, the syntax that corresponds to an arc trace and connecting line in KiCad itself can be appended to a string for each iteration. This string can then be pasted into an empty schematic file directly generate the trace from the script.

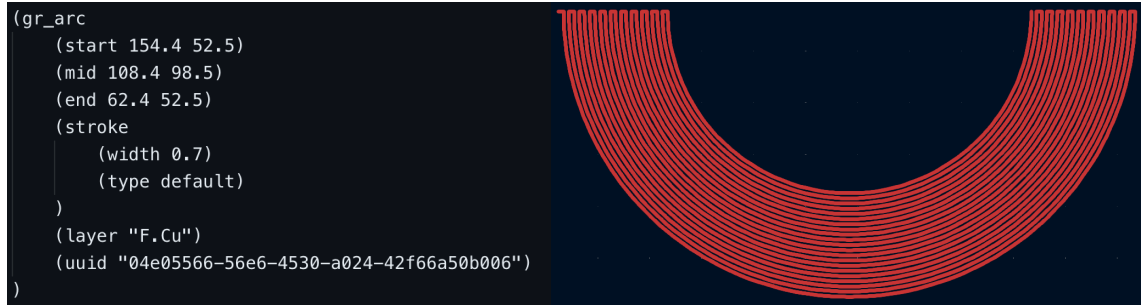


Figure 45 Left: example of how an arc is defined in KiCAD, right: the complete heater trace

Upon completion, the optimal parameters for the heater trace are determined, as shown in Table 15. The complete trace is output to a file and then converted to a component in KiCad. The full script is available in the project repository.

Table 15 A table showing final PCB parameters

Parameter	Value	Unit
Trace Width	0.7	mm
Trace Spacing	0.3	mm
Trace Length	3	m
Resistance	2.05	Ω
Operating Current	2.05	A
Power Dissipation	12.2	W

PCB Routing and Layout

The heater PCB was designed using KiCad, a software that facilitates both schematic and PCB design. A schematic was drawn to demonstrate connections between the numerous components on the board. The primary microcontroller on the board is an ESP-S3 module. A USB-micro connector, as well as reset and boot buttons, are provided for programming over the ESP32-S3's integrated USB-OTG driver. The board is supplied with a 5V connection via terminal blocks, which is stepped down to a suitable voltage for the ESP32-S3 by a 3V3 regulator. A MOSFET is used to switch power to the heater trace to control heating. The temperature of the heater is acquired via a digital temperature sensor.

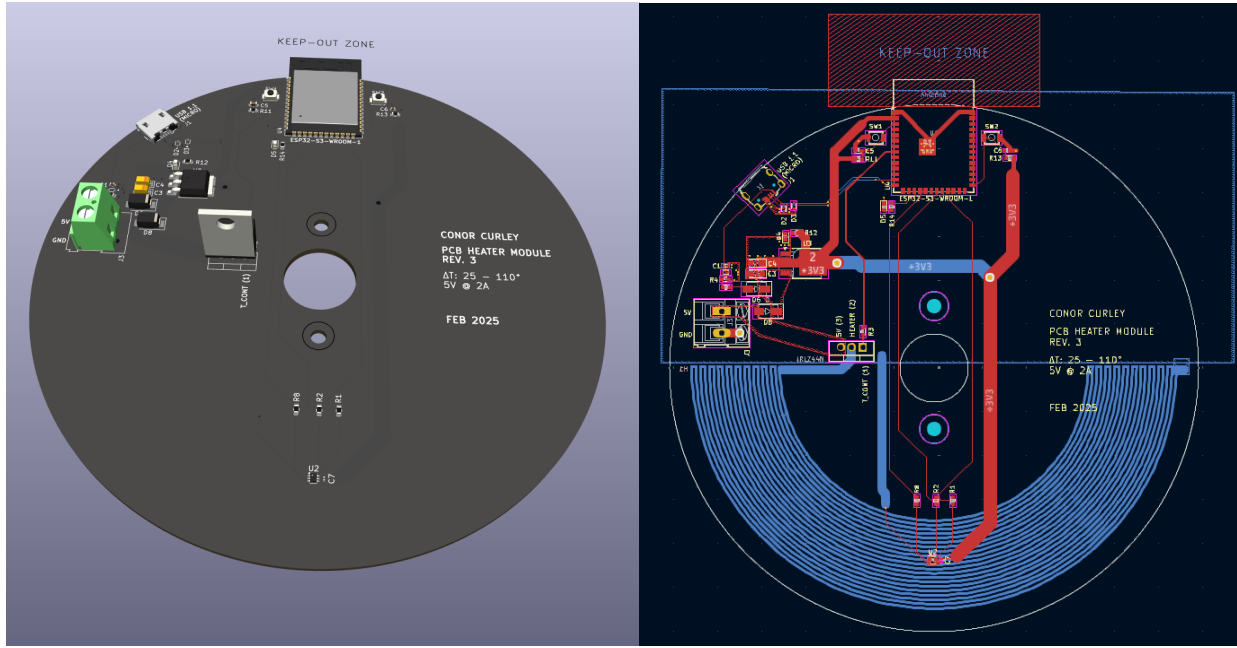


Figure 46 Left: a render of the completed PCB, right: a PCB layout schematic of the PCB

A PCB layout was then created to position each of these components on the board. The board is modelled as two layers. The top layer of the board is used for component placement and power and signal routing. The bottom layer of the board is split in half, with the top half an uninterrupted ground pour to offer a good ground return path, while the bottom is occupied by the heater traces. The board also contains two M3 mounting points. A complete list of components used on the Heater PCB is available in the bill of materials in the project repository.

Control System

In order to design an appropriate temperature control system using PID control, a dynamic model for the system must first be derived. The derivation may be made by means of the first law of thermodynamics.

$$\frac{dQ}{dt} = Q_i - Q_{loss}$$

Where $\frac{dU}{dt}$ is the rate of change of energy in the system, Q_i is the internal energy in the system, and Q_{loss} is the loss of the energy from the system. Q may be described by:

$$Q = mC(T - T_a)$$

Where m is the mass of the system, C is the specific heat capacity of the system, T is the temperature of the system, and T_a is the ambient temperature. By differentiating both sides with respect to time:

$$\frac{dQ}{dt} = mC \left(\frac{dT}{dt} - 0 \right) = mC \frac{dT}{dt}$$

Assuming ambient temperature doesn't change, so $\frac{dT_a}{dt} = 0$. Assuming the heater is exposed to air, an expression for U_{loss} may also be derived by means of convective cooling:

$$Q_{loss} = hA(T - T_a)$$

Where h is the coefficient of convective heat transfer and A is the convective surface area. By substituting Equation X and Y into Equation Z, a dynamic equation for the heater can be obtained.

$$mC \frac{dT}{dt} = Q_i - hA(T - T_a)$$

Given $C = 1100 J \cdot (kg \cdot ^\circ C)^{-1}$ and $h = 10 W \cdot (m^2 K)^{-1}$. Assuming A to be only the surface area directly above the heating element:

$$A = \frac{(\pi r_o^2 - \pi r_i^2)}{2} = \frac{(\pi 0.055^2 - \pi 0.035^2)}{2} = \frac{(0.0095 - 0.00385)}{2} = 0.002825 m^2$$

m may also be derived as a product of the area, the thickness of the PCB, and the density of FR-4:

$$m = A \cdot t_{PCB} \cdot \rho = 0.002825 \cdot 0.0016 \cdot 1850 = 8.36 \times 10^{-3} kg$$

Where t_{PCB} is the PCB thickness and ρ is the density of FR-4 ($kg \cdot m^{-3}$). The dynamic equation given in equation Y can be expanded, assuming the ambient temperatures is $0^\circ C$ to simplify derivations:

$$8.36 \times 10^{-3} \cdot 1100 \frac{dT}{dt} = Q_i - 10 \cdot 0.002825 \cdot T$$

$$9.20 \frac{dT}{dt} = Q_i - 0.02825T$$

Replacing time dependent variables as functions of time:

$$9.20 \frac{dT(t)}{dt} = Q_i(t) - 0.02825T(t)$$

Then applying the Laplace transform:

$$9.20sT(s) = Q_i(s) - 0.02825T(s)$$

The resulting function can be reordered as a stable, first-order transfer function:

$$9.20sT(s) + 0.02825T(s) = Q_i(s)$$

$$(9.20s + 0.02825)T(s) = Q_i(s)$$

$$T_F(s) = \frac{T(s)}{Q_i(s)} = \frac{1}{(9.20s + 0.02825)}$$

However, the derivation presented above reveals a significant problem. If this system is to be controlled using this model, $Q_i(t)$ needs to be controllable. Given that in this case $Q_i(t) = I(t)^2R$, $I(t)$ must be modulated to control the temperature of the system. As mentioned previously, the current supplied to the heater is constant, inferring that this model of temperature control is not applicable.

Due to time constraints imposed on the project, rather than attempting to resolve the issues presented with the control system above, it was decided to instead use a combination of Bang-Bang control and Pulse-Width Modulation (PWM) control. The Bang-Bang controller will turn the heater fully on until the target temperature is reached, at which point, the PWM controller will take over, turning the heater on and off in cycles to maintain the set-point. While likely not as accurate, this type of control will be able to maintain the temperatures required of this heater. In both cases, feedback from the temperature sensor is used the reference for the temperature of the heater.

Fabrication

The relevant manufacturing files were compiled for production by JLCPCB. The types of files required for PCB production are shown in Table 16, while the actual manufacturing files are available in the project repository.

Table 16 A table detailing the files sent to the manufacturer

File	Description	Extension
Bill of Materials	A file containing the list of components required during PCB assembly.	.csv
Gerber Files	Files containing information on the locations of edge cuts, traces, and solder points.	.gbr (individual) .zip (multiple)
Drill Files	Files containing information locations of drill holes for vias and mounting holes.	.drl
Placement Files	Files containing information on component placement for pick-and-place robot assembly.	.pos

The manufacturing parameters selected when ordering the PCBs for this project are shown in Table 17.

Table 17 A table showing the fabrication parameters used for the PCB

Parameter	Description
Material	FR-4
Layers	2
Product Type	Industrial/consumer electronics
PCB Thickness	1.6mm
Outer Copper Weight	1oz

Spectrometry

A fluorophore will be used to qualify the result of the PCR reactions undertaken by the instrument. This section will detail the creation of a spectrometry system which will have the capacity to measure the magnitude of fluorescence in the sample after a PCR reaction has taken place.

Spectral Sensor Selection

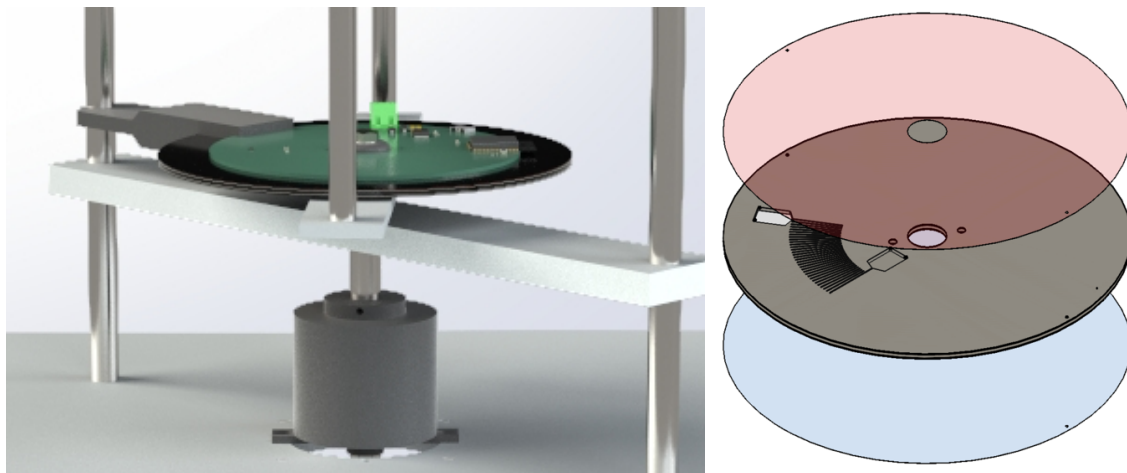


Figure 47 Left: spectrometry system assembly, right: stacked gel filters over disc

The spectrometry system is designed as a C-shaped assembly, to be attached to the spindle support. The assembly may be rotated over the disc once the PCR reaction is complete. The system is designed such that the C-shaped assembly covers the sample reservoir, preventing extraneous light from entering the reservoir while analysis is underway. A blue LED (C503B-BCN-CV0Z0461) with a peak emission wavelength of 470nm projects light onto the sample from the bottom of the disc through a blue gel filter. This light illuminates the sample, causing fluorescence. The fluorescent emission projects upwards towards the top of the disc, through a red gel filter, and into a spectral sensor. When designing the spectrometry system, numerous spectral sensors were considered, including the Hamamatsu C12666MA, the ams AS72651, and the ams AS7341.



Figure 48 Hamamatsu C12666MA micro-spectrometer[82]

As a micro-spectrometer, the Hamamatsu C12666MA is the most accurate sensor of those reviewed, with a spectral response range of 380-780nm and a spectral resolution of 15nm (max). However, the sensor was disqualified due to its cost, at €494.63 per unit.

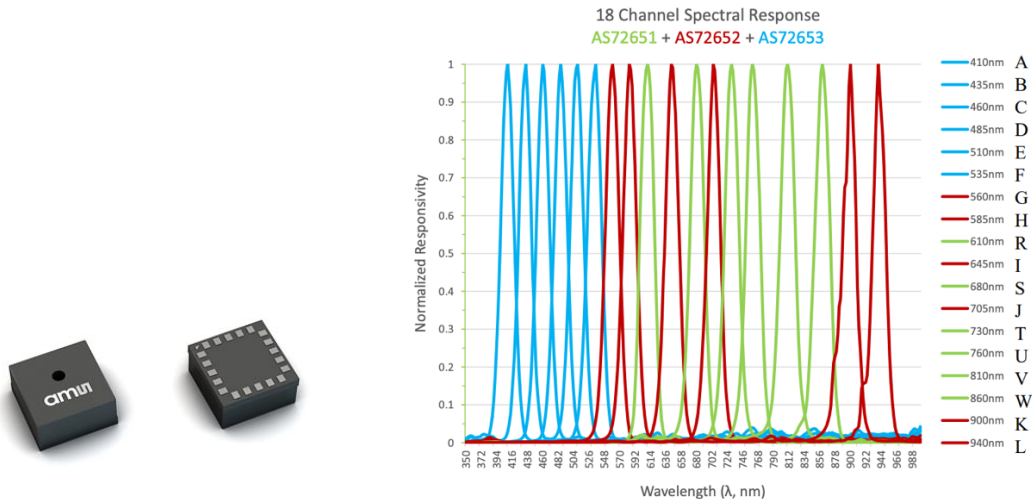


Figure 49 Left: AS72651 spectral sensor[83], right: optical response of the AS72651[84]

The ams AS72651 is a 6-channel spectral sensor, with a peak spectral response in channel R of 610nm. This aligns well with the peak emission wavelength of EvaRuby, however, there are no breakout boards available for only the AS72651, mandating the requirement for another custom PCB.

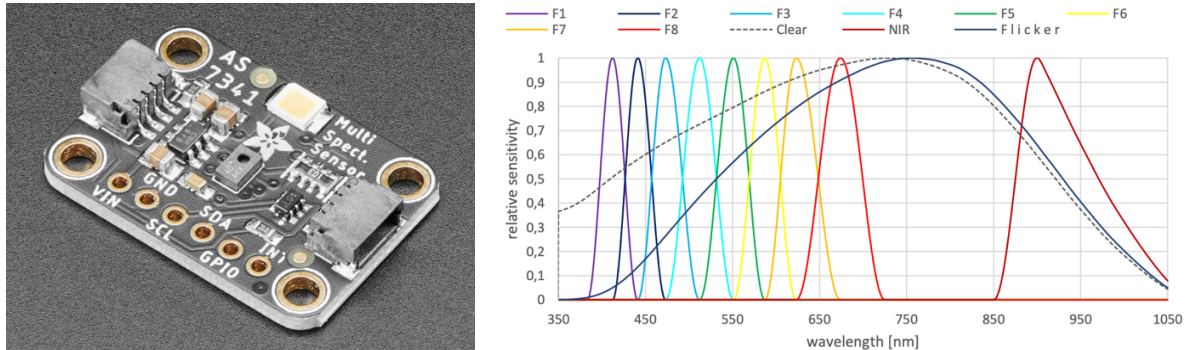


Figure 50 Left: AS7341 spectral sensor[85], right: frequency response of the AS7341[86]

To avoid the design and fabrication of another PCB, the AS7341 is selected instead. The AS7341 is a 10-channel spectral sensor, integrating high-precision CMOS optical filters to achieve a peak spectral response between 620-640nm and a full half-width maximum response between 580-680nm in channel F7, encompassing the full emission spectrum of EvaRuby. The sensor communicates with the controller over I2C and is capable of transmitting data on all channels at once. The sensor is available in a breakout board produced by Adafruit (Adafruit AS7341) at a price of €15.95.

Fabrication

Mechanical Assembly

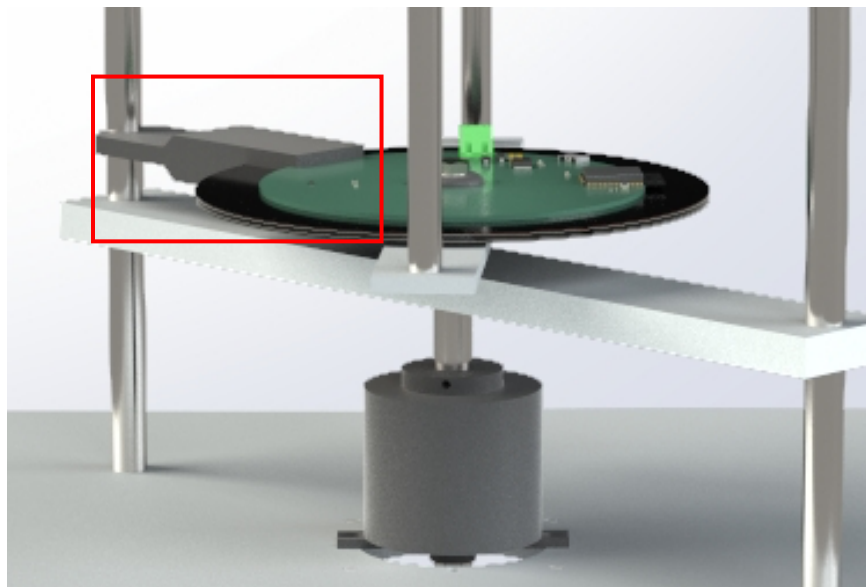


Figure 51 An image of the spectrometry system with the spectrometer head highlighted

The spectral sensor and LED are contained in a 3D printed C-shaped enclosure. The enclosure features a protruding arm that clips onto the spindle support. The gel filters are

laminated onto the disc itself using PMMA. The sensor and LED are then connected directly to the CCS via jumper cable

Circuit Implementation

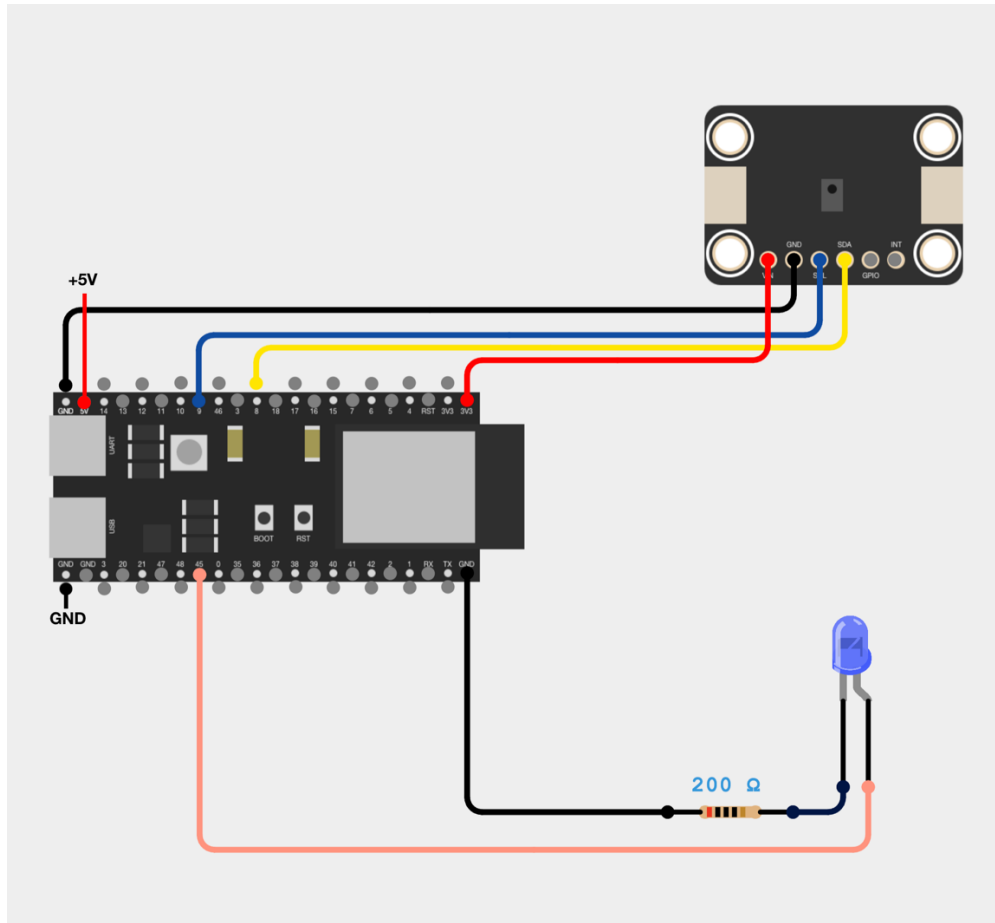


Figure 52 Circuit diagram for the spectrometry system

The circuit diagram for the spectrometry system is outlined in Figure 52. The VIN and GND pins of the AS7341 are connected to the 3V3 and GND pins on the ESP32-S3. The SCL and SDA pins are connected to GPIO 9 and 8 on the ESP32-S3 respectively. The GPIO and INT pins on the are left floating. GPIO45 is connected to ground via the LED in series with a 200Ω resistor.

Software Implementation

The software implementation for the spectrometry system addresses two primary objectives: control of the AS7341 and LED via the user interface and acquisition of sensor data via the CCS. Both of the objectives listed are addressed over WebSockets.

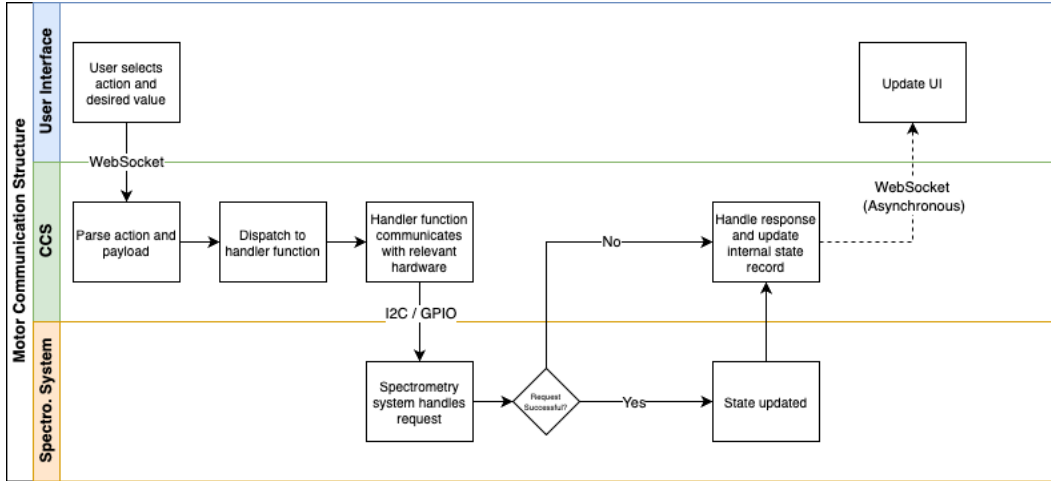


Figure 53 Communications architecture for the spectrometry system

Similar to the communications method for the centrifuge, the user interface communicates with the spectrometry system over WebSockets as shown in Figure 53. The AS7341 has a number of configurable parameters, including integration step and time and gain. To interface with the AS7341, the Adafruit_AS7341 library is used. To control these parameters, as well as the state of the LED, the same action-payload message format is used. A list of actions the CCS can handle with regards to the spectrometry system is shown in Table 18.

Table 18 A table showing available spectrometry functions

Action	Action Description	Payload Type	Payload Values
FLR_SET_GAIN	Set the gain value applied to the spectral response	Number	1-512
FLR_SET_ATIME	Set the integration time of the spectral response	Number	Any
FLR_SET_ASTEP	Set the integration step of the spectral response	Number	Any
FLR_TGL_LED	Toggle the LED on and off	Boolean	0 (off) or 1 (on)

The action and payload are parsed by the CCS and dispatched to the relevant handler function. Actions relating to the AS7341 are handled by functions exposed by the Adafruit_AS7341 library, while LED actions are handled by custom handlers.

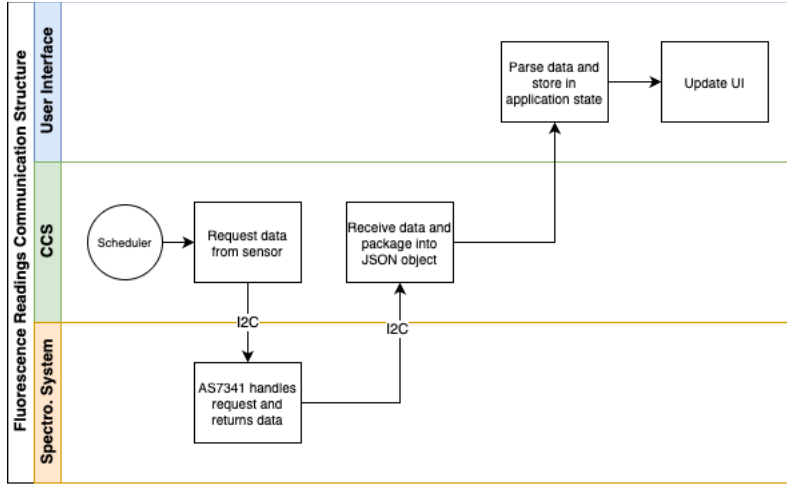


Figure 54 Communications architecture to send data from the spectrometry system to the user interface

Unlike the communications methods outlined previously, a separate communications method used by the UI and CCS for acquiring sensor data as shown in Figure 54. On a scheduled basis, for example once per second, the CCS reads the output of each of the sensor channels via a function exposed by the Adafruit_AS7341 library. The sensor readings are then packaged into a JSON object and labelled as fluorescence readings. The JSON object is then converted into a string and communicated to the UI over the WebSocket connection. Upon receiving the data, the UI parses the JSON object and stores it in application state, updating the interface accordingly.

User Interface

A fundamental objective of this project is to provide a professional, usable interface for interacting with and receiving data from the instrument. This objective is fulfilled with a web-based user interface, which communicates with the instrument in real-time wirelessly over the WebSocket protocol. This section will describe the communications protocols, languages, and frameworks used in the development of the instrument's user interface.

Design

The user interface is built upon Next.js, operating in a NodeJS runtime. The application is hosted locally on localhost using Node Package Manager (npm).

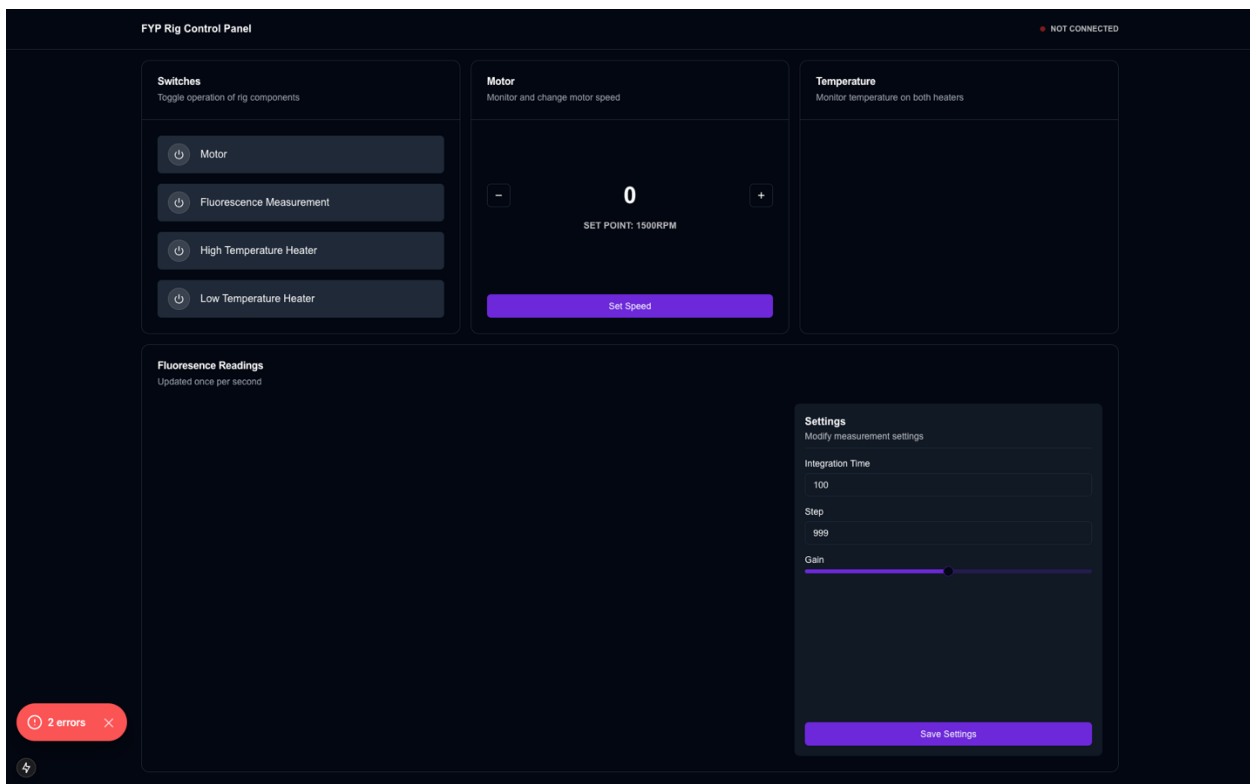


Figure 55 An image of the user interface

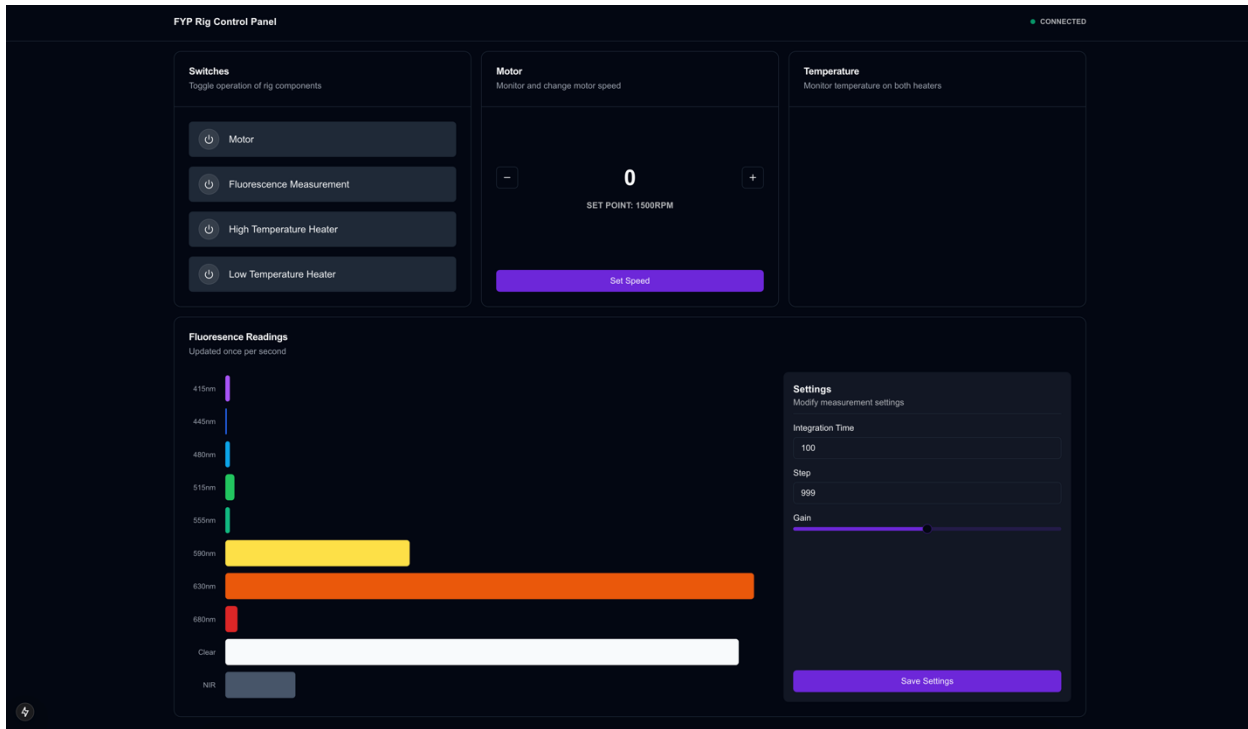


Figure 56 An image of the user interface in operation

The user interface is built as a single-page application. The home page contains a range of cards, each with unique functions. An indicator in the top right of the screen shows whether there is an active WebSocket connection to the instrument. An image of the interface on startup is shown in Figure 55. An image of the interface while the instrument is running is shown in Figure 56.

Switches allows the user to control boolean actions, such as turning on the motor or activating the heaters.

Motor allows the user to view the actual speed of the motor and adjust the speed set-point.

Temperature allows the user to view the actual temperature of both heaters.

Fluorescence Readings allows the user to view a plot of the most recent readings from the spectral sensor. The user can also adjust spectral sensor parameters in the menu to the right of the card.

Communications Implementation

As mentioned previously, the user interface uses WebSockets to communicate with the CCS. Until this point, however, the application side WebSocket implementation has not been discussed.

Within the application, the built-in `WebSocket` object is used to initialize a Websocket connection. As outlined previously, the CCS hosts the `WebSocket` server. As such, the first task on the application side is to connect to the CCS.

```
1. const socket = new WebSocket("ws://192.168.68.140/ws");
```

Subsequently, it is necessary to establish a set of callback functions. When a connection is established, for example, an `isConnected` variable is toggled to true, such that the connection can be reflected in the user interface.

```
1. socket.addEventListener("open", (event) => {
2.   console.log("connected")
3.   setIsConnected(true);
4.});
```

In the cases of the centrifuge and heating systems, the CCS automatically reports hardware state data on a scheduled basis. As such, a message handler must be established to handle CCS messages. This handler parses the message and stores it in the relevant application state variable.

```
1. socket.addEventListener("message", (event) => {
2.   let data = JSON.parse(event.data);
3.
4.   switch (data.type) {
5.     case "MOTOR_VITALS":
6.       setMotorVitals(data);
7.       break;
8.     case "FLUORESCENCE_READINGS":
9.       setFluorescenceReadings(data);
10.      break;
11.    }
12.  });
```

The application must also be able to communicate data to the CCS in the action-payload format mentioned earlier. This functionality is provided through a `sendMessage` function.

```
1. const sendMessage = (message) => {
2.   if (ws) {
3.     console.log("sending command: ", message)
4.     ws.send(message);
5.   }
6.};
```

An example of how this method could be used is shown in the motor toggle switch.

```
1. <Switch
2.   state={motorOn}
3.   action={() => {
4.     sendMessage(motorOn ? "TGL_MTR_ON=0" : "TGL_MTR_ON=1")
5.   }
6.   setMotorOn(!motorOn)
7.   text={"Motor"}
8. />
9.
```

The full user interface application source code is available with comments in the project repository.

Experimental Procedure

The experimental procedure for this project is composed of two components. First, each of the components of the instrument must be validated to ensure they meet the requirements of the project. After the instrument is validated, an assay may be conducted in order to gather experimental results.

Validation

Three components of the instrument must be validated to ensure that design requirements are met: the centrifuge, the disc, and the heater. This subsection will detail the validation procedure for each of these components.

Centrifuge

The centrifuge is validated via the user interface. The motor is enabled and set to a range of speeds. The actual speed of the motor given by the motor driver is compared to the set-point. If the reported values match that of the set-point, the validation test is considered successful.

Disc

The disc is validated through the use of dyed water. A distilled water and food dye mixture is added to the reservoir using a pipette. The motor is enabled, and the disc is rotated at a range of angular velocities. If the sample is able to flow through the channels unimpeded, without leaks, the validation test is considered successful.

Heater

The heater is validated through the use of a FLIR thermal camera and the user interface. The heater is assigned a set-point and the temperature rise is observed both through a thermal camera and on the user interface. If the disc maintains a set point without under- or overshoot, and the values reported by the user interface and the thermal camera align, the validation test is considered successful.

Experimental Protocol

Once the instrument is validated as detailed above, a PCR assay will be completed on the instrument. The PCR assay will be completed per the following experimental protocol.

The sample is prepared using PCR master mix and a measure of EVARuby, per the relevant protocols. A $200\mu L$ sample is loaded onto the disc using a micropipette, followed by a layer of mineral oil. The rig is enclosed to prevent injury from moving components over the course of the assay. The heaters are set to preheat to the relevant temperature set-points. Once the

heaters are at temperature, the motor is enabled, and rotation is started. Once the sample has been processed, the instrument is stopped and locked-out. The fluorescence sensor is moved into position and fluorescence data is recorded.

References

- [1] J. Atencia and D. J. Beebe, "Controlled microfluidic interfaces," *Nature*, vol. 437, no. 7059, pp. 648–655, Sep. 2005, doi: 10.1038/nature04163.
- [2] E. K. Sackmann, A. L. Fulton, and D. J. Beebe, "The present and future role of microfluidics in biomedical research," *Nature*, vol. 507, no. 7491, pp. 181–189, Mar. 2014, doi: 10.1038/nature13118.
- [3] X. Wang *et al.*, "Microfluidics-based strategies for molecular diagnostics of infectious diseases," *Mil. Med. Res.*, vol. 9, p. 11, Mar. 2022, doi: 10.1186/s40779-022-00374-3.
- [4] "images (277×182)." Accessed: Mar. 26, 2025. [Online]. Available: <https://encrypted-tbn0.gstatic.com/images?q=tbn:ANd9GcT1xzZHkLzu9bUNFWT5twYRfTdAPO7FlX3WqA&s>
- [5] "ID-NOW.png (901×444)." Accessed: Mar. 26, 2025. [Online]. Available: <https://www.dbth.nhs.uk/wp-content/uploads/2021/12/ID-NOW.png>
- [6] P. P. Urone, R. Hinrichs, P. P. Urone, and R. Hinrichs, "14.2 Temperature Change and Heat Capacity - College Physics | OpenStax." Accessed: Mar. 26, 2025. [Online]. Available: <https://openstax.org/books/college-physics-2e/pages/14-2-temperature-change-and-heat-capacity>
- [7] "Figure-1-Microdevices-Blog.jpg (800×533)." Accessed: Mar. 26, 2025. [Online]. Available: <https://biotium.com/wp-content/uploads/2021/12/Figure-1-Microdevices-Blog.jpg>
- [8] "410214.jpg (688×517)." Accessed: Mar. 26, 2025. [Online]. Available: <https://cordis.europa.eu/docs/results/images/2019-10/410214.jpg>
- [9] D. Kinahan, "Introduction to Lab on a Disc," Accessed: Mar. 26, 2025. [Online]. Available: <https://docs.google.com/presentation/d/13FvzIOPoJ-j70C6mD6ByXidq4e72QwHi/edit#slide=id.p1>
- [10] L. Amirifar *et al.*, "Droplet-based microfluidics in biomedical applications," *Biofabrication*, vol. 14, no. 2, p. 022001, Jan. 2022, doi: 10.1088/1758-5090/ac39a9.
- [11] "dipstick.jpg (620×330)." Accessed: Mar. 26, 2025. [Online]. Available: <https://st1.thehealthsite.com/wp-content/uploads/2014/04/dipstick.jpg>
- [12] A. W. Martinez, S. T. Phillips, M. J. Butte, and G. M. Whitesides, "Supporting Information for".
- [13] L. Syedmoradi, M. Daneshpour, M. Alvandipour, F. A. Gomez, H. Hajghassem, and K. Omidfar, "Point of care testing: The impact of nanotechnology," *Biosens. Bioelectron.*, vol. 87, pp. 373–387, Jan. 2017, doi: 10.1016/j.bios.2016.08.084.
- [14] "iStock-1311297993640.jpg (640×410)." Accessed: Mar. 26, 2025. [Online]. Available: <https://www.qmul.ac.uk/media/qmul/media/news/iStock-1311297993640.jpg>
- [15] J. Budd *et al.*, "Lateral flow test engineering and lessons learned from COVID-19," *Nat. Rev. Bioeng.*, vol. 1, no. 1, pp. 13–31, Jan. 2023, doi: 10.1038/s44222-022-00007-3.
- [16] J. Zhang, Z. Shen, Y. Xiang, and Y. Lu, "Integration of Solution-Based Assays onto Lateral Flow Device for One-Step Quantitative Point-of-Care Diagnostics Using Personal Glucose Meter," *ACS Sens.*, vol. 1, no. 9, pp. 1091–1096, Sep. 2016, doi: 10.1021/acssensors.6b00270.

- [17] "Droplet Microfluidics Approach for Single-DNA Molecule Amplification and Condensation into DNA-Magnesium-Pyrophosphate Particles." Accessed: Mar. 26, 2025. [Online]. Available: <https://www.mdpi.com/2072-666X/8/2/62>
- [18] "A sample-to-answer droplet magnetofluidic assay platform for quantitative methylation-specific PCR | Biomedical Microdevices." Accessed: Mar. 26, 2025. [Online]. Available: <https://link.springer.com/article/10.1007/s10544-018-0276-6>
- [19] "High-throughput single-cell DNA sequencing of acute myeloid leukemia tumors with droplet microfluidics." Accessed: Mar. 26, 2025. [Online]. Available: <https://genome.cshlp.org/content/28/9/1345.short>
- [20] "Pathogenic Bacteria Detection Using RNA-Based Loop-Mediated Isothermal-Amplification-Assisted Nucleic Acid Amplification via Droplet Microfluidics | ACS Sensors." Accessed: Mar. 26, 2025. [Online]. Available: https://pubs.acs.org/doi/full/10.1021/acssensors.8b01206?casa_token=zCBtrQ2HakwAAAAA%3AfqvEx41vMYTUD767Urs0GYygBuT8P8NBNTndNjAntix8fjAmjbQz9kRrhPd1ArAoPOnqAsCcpbAYyvUN
- [21] D. Kinahan, "Introduction to Lab on a Disc,"
- [22] "Dissolvable Film-Controlled Buoyancy Pumping and Aliquoting on a Lab-On-A-Disc." Accessed: Mar. 26, 2025. [Online]. Available: <https://www.mdpi.com/2227-9717/11/1/128>
- [23] B. Alberts, *Molecular Biology of the Cell*, 6th ed. New York: W.W. Norton & Company, 2017. doi: 10.1201/9781315735368.
- [24] "DNA sequencing with chain-terminating inhibitors | PNAS." Accessed: Mar. 26, 2025. [Online]. Available: <https://www.pnas.org/doi/abs/10.1073/pnas.74.12.5463>
- [25] K. Mullis, F. Falooma, S. Scharf, R. Saiki, G. Horn, and H. Erlich, "Specific enzymatic amplification of DNA in vitro: the polymerase chain reaction," *Cold Spring Harb. Symp. Quant. Biol.*, vol. 51 Pt 1, pp. 263–273, 1986, doi: 10.1101/sqb.1986.051.01.032.
- [26] M. B. Kulkarni and S. Goel, "Advances in continuous-flow based microfluidic PCR devices—a review," *Eng. Res. Express*, vol. 2, no. 4, p. 042001, Dec. 2020, doi: 10.1088/2631-8695/abd287.
- [27] R. K. Saiki et al., "Primer-Directed Enzymatic Amplification of DNA with a Thermostable DNA Polymerase," *Science*, Jan. 1988, doi: 10.1126/science.2448875.
- [28] "images (627×489)." Accessed: Mar. 26, 2025. [Online]. Available: https://encrypted-tbn3.gstatic.com/images?q=tbn:ANd9GcRIETjAs3Nmk4i6YGo6KYcclsCqbc6Tk3srWiLXWpbXUth8wBvzr9OrGoN3T-ViCCsA_4kw1hh_RJEXxfSxiKPeyg
- [29] A. Chien, D. B. Edgar, and J. M. Trela, "Deoxyribonucleic acid polymerase from the extreme thermophile *Thermus aquaticus*," *J. Bacteriol.*, vol. 127, no. 3, pp. 1550–1557, Sep. 1976.
- [30] L. V. Wang and H. Wu, *Biomedical Optics: Principles and Imaging*. John Wiley & Sons, 2007.
- [31] R. Higuchi, C. Fockler, G. Dollinger, and R. Watson, "Kinetic PCR analysis: real-time monitoring of DNA amplification reactions," *Biotechnol. Nat. Publ. Co.*, vol. 11, no. 9, pp. 1026–1030, Sep. 1993, doi: 10.1038/nbt0993-1026.
- [32] H. Ihmels and D. Otto, "Intercalation of Organic Dye Molecules into Double-Stranded DNA -- GeneralPrinciples and Recent Developments," in *Supermolecular Dye*

- Chemistry*, F. Würthner, Ed., Berlin, Heidelberg: Springer, 2005, pp. 161–204. doi: 10.1007/b135804.
- [33] B. Bagchi, D. W. Oxtoby, and G. R. Fleming, “Theory of the time development of the stokes shift in polar media,” *Chem. Phys.*, vol. 86, no. 3, pp. 257–267, Jan. 1984, doi: 10.1016/0301-0104(84)80014-2.
 - [34] “rendition (500×308).” Accessed: Mar. 26, 2025. [Online]. Available: <https://digitalassets.avantorsciences.com/adaptivemedia/rendition?id=ad2825df9da b4e6bd031037cb8316e0f58cc3348&vid=376ac56d25ee632e82f61821865f562e7311 4d4f&prid=lowres&clid=SAPDAM>
 - [35] “Cat_31079_Packaging.jpg (1000×1000).” Accessed: Mar. 26, 2025. [Online]. Available: https://biotium.com/wp-content/uploads/2021/11/Cat_31079_Packaging.jpg
 - [36] A. I. Dragan *et al.*, “SYBR Green I: Fluorescence Properties and Interaction with DNA,” *J. Fluoresc.*, vol. 22, no. 4, pp. 1189–1199, Jul. 2012, doi: 10.1007/s10895-012-1059-8.
 - [37] “EvaRuby™ Dye, 20X in Water,” Biotium. Accessed: Mar. 26, 2025. [Online]. Available: <https://biotium.com/product/evaruby-dye-20x-in-water/>
 - [38] “SYBR_Green_I_spectra.png (1218×738).” Accessed: Mar. 26, 2025. [Online]. Available: https://upload.wikimedia.org/wikipedia/commons/2/28/SYBR_Green_I_spectra.png?2 0060929012306
 - [39] “PI-31079.pdf.” Accessed: Mar. 26, 2025. [Online]. Available: <https://biotium.com/wp-content/uploads/2021/10/PI-31079.pdf>
 - [40] P. J. Sykes, S. H. Neoh, M. J. Brisco, E. Hughes, J. Condon, and A. A. Morley, “Quantitation of targets for PCR by use of limiting dilution,” *BioTechniques*, vol. 13, no. 3, pp. 444–449, Sep. 1992.
 - [41] B. Vogelstein and K. W. Kinzler, “Digital PCR,” *Proc. Natl. Acad. Sci.*, vol. 96, no. 16, pp. 9236–9241, Aug. 1999, doi: 10.1073/pnas.96.16.9236.
 - [42] D. Moschou *et al.*, “All-plastic, low-power, disposable, continuous-flow PCR chip with integrated microheaters for rapid DNA amplification,” *Sens. Actuators B Chem.*, vol. 199, pp. 470–478, Aug. 2014, doi: 10.1016/j.snb.2014.04.007.
 - [43] Y. Xie *et al.*, “A Thermal Cycler Based on Magnetic Induction Heating and Anti-Freezing Water Cooling for Rapid PCR,” *Micromachines*, vol. 15, no. 12, p. 1462, Nov. 2024, doi: 10.3390/mi15121462.
 - [44] G. A. Nasser, A. L. Abdel-Mawgood, A. A. Abouelsoud, H. Mohamed, S. Umezawa, and A. M. R. F. El-Bab, “New cost effective design of PCR heating cycler system using Peltier plate without the conventional heating block,” *J. Mech. Sci. Technol.*, vol. 35, no. 7, pp. 3259–3268, Jul. 2021, doi: 10.1007/s12206-021-0646-5.
 - [45] F. Talebi, H. Ghafoorifard, S. Ghafouri-Fard, and A. Jahanshahi, “A straight-forward, inexpensive, low power continuous-flow μPCR chip using PCB-based heater electrodes with uniform temperature distribution,” *Sens. Actuators Phys.*, vol. 333, p. 113220, Jan. 2022, doi: 10.1016/j.sna.2021.113220.
 - [46] H. Bruus, *Theoretical Microfluidics*. London, England: Oxford University Press, 2007.
 - [47] “clear_acrylic.webp (1280×1280).” Accessed: Mar. 26, 2025. [Online]. Available: https://polytech-plastics.com.au/wp-content/uploads/2022/05/clear_acrylic.webp
 - [48] “zing-door.jpg (973×615).” Accessed: Mar. 26, 2025. [Online]. Available: <https://www.ilslaser.com/img/epilog/zing-door.jpg>

- [49] Mst. N. Bagum, Md. A. Habib, C. A. A. Rashed, Md. M. H. Kibria, and S. K. Nahar, “Optimizing laser-based micro-cutting for PMMA microfluidic device fabrication: thermal analysis and parameter optimization,” *Int. Polym. Process.*, vol. 39, no. 2, pp. 220–236, May 2024, doi: 10.1515/ipp-2023-4408.
- [50] R. Nigrovic, J. Mesko, R. Nikolic, V. Lazic, D. Arsic, and B. Hadzima, “Comparison of the PMMA mechanical properties after cutting by the laser beam and milling,” *FME Trans.*, vol. 46, no. 1, pp. 57–61, 2018, doi: 10.5937/fmet1801057N.
- [51] “paper-roll_66104_19078.1642677468.jpg (1280×1280).” Accessed: Mar. 26, 2025. [Online]. Available: https://cdn11.bigcommerce.com/s-obbu537zbn/images/stencil/1280x1280/products/262/821/paper-roll_66104_19078.1642677468.jpg?c=1
- [52] “Graphtec-CE7000-40_555x429.png (555×429).” Accessed: Mar. 26, 2025. [Online]. Available: https://colmanandcompany.com/Merchant2/graphics/00000001/Graphtec-CE7000-40_555x429.png
- [53] “hl-200_45degree_right_1_79564.1603385600.1280.1280_98072.1706206544.jpg (1280×844).” Accessed: Mar. 26, 2025. [Online]. Available: https://cdn11.bigcommerce.com/s-jpvxfjn9oz/images/stencil/1280x1280/products/605/672/hl-200_45degree_right_1_79564.1603385600.1280.1280_98072.1706206544.jpg?c=1
- [54] “Joule heating,” *Wikipedia*. Jan. 10, 2025. Accessed: Mar. 26, 2025. [Online]. Available: https://en.wikipedia.org/w/index.php?title=Joule_heating&oldid=1268663781
- [55] R. S. Khandpur, *Printed circuit boards: design, fabrication, assembly and testing*. New York: McGraw-Hill, 2006.
- [56] “Choosing the Best PCB Color-Enhancing Aesthetics and Functionality.” Accessed: Mar. 26, 2025. [Online]. Available: <https://jlpcb.com/blog/Choosing-the-Best-PCB-Color-Enhancing-Aesthetics-and-Functionality>
- [57] “PCB Heater - What You Need To Know About.” Accessed: Mar. 26, 2025. [Online]. Available: <https://www.linkedin.com/pulse/pcb-heater-what-you-need-know-antiraying-kh6wc>
- [58] F. P. T. team, “What is Flexible PCB Heater?,” Flex Plus FPC. Accessed: Mar. 26, 2025. [Online]. Available: <https://www.flexplusfpc.com/post/what-is-flexible-pcb-heater>
- [59] “FLX0PM1LACIFNG1-e1668572002136.jpg (800×449).” Accessed: Mar. 26, 2025. [Online]. Available: <https://hackaday.com/wp-content/uploads/2022/11/FLX0PM1LACIFNG1-e1668572002136.jpg?w=800>
- [60] T. Seyde *et al.*, “Is Bang-Bang Control All You Need? Solving Continuous Control with Bernoulli Policies,” in *Advances in Neural Information Processing Systems*, Curran Associates, Inc., 2021, pp. 27209–27221. Accessed: Mar. 26, 2025. [Online]. Available: https://proceedings.neurips.cc/paper_files/paper/2021/hash/e46be61f0050f9cc3a98d5d2192cb0eb-Abstract.html
- [61] Z. Yu, A. Mohammed, and I. Panahi, “A review of three PWM techniques,” in *Proceedings of the 1997 American Control Conference (Cat. No.97CH36041)*, Jun. 1997, pp. 257–261 vol.1. doi: 10.1109/ACC.1997.611797.
- [62] M. A. Johnson and M. H. Moradi, “Some PID Control Fundamentals,” in *PID Control: New Identification and Design Methods*, J. Crowe, K. K. Tan, T. H. Lee, R. Ferdous, M. R.

- Katebi, H.-P. Huang, J.-C. Jeng, K. S. Tang, G. R. Chen, K. F. Man, S. Kwong, A. Sánchez, Q.-G. Wang, Y. Zhang, Y. Zhang, P. Martin, M. J. Grimble, D. R. Greenwood, M. A. Johnson, and M. H. Moradi, Eds., London: Springer, 2005, pp. 47–107. doi: 10.1007/1-84628-148-2_2.
- [63] “UVVISNIR_1_ResizedImageWzYwMCwzNTId.jpg (600×359).” Accessed: Mar. 26, 2025. [Online]. Available: https://www.gigahertz-optik.com/assets/UVVISNIR_1_ResizedImageWzYwMCwzNTId.jpg
 - [64] J. Reichman, *Handbook of Optical Filters for Fluorescence Microscopy*. CHROMA TECHNOLOGY CORP, 2017. Accessed: Mar. 26, 2025. [Online]. Available: <https://www.chroma.com/assets/documents/chroma-handbook-of-optical-filters.pdf>
 - [65] “Optics Manufacturer & Supplier | Imaging Lens & Laser Optics Manufacturer | Edmund Optics.” Accessed: Mar. 26, 2025. [Online]. Available: <https://www.edmundoptics.eu/>
 - [66] “24V 3500RPM 0.23Nm 84W 5.0A Φ57x49mm Brushless DC Motor - 57BLR50-24-01 | StepperOnline.” Accessed: Mar. 26, 2025. [Online]. Available: <https://www.omc-stepperonline.com/24v-3500rpm-0-23nm-84w-5-0a-%D1%8457x49mm-brushless-dc-motor-57blr50-24-01>
 - [67] “Brushless DC (BLDC) Motor Fundamentals.pdf.” Accessed: Mar. 26, 2025. [Online]. Available: [https://electrathonoftampabay.org/www/Documents/Motors/Brushless%20DC%20\(BLDC\)%20Motor%20Fundamentals.pdf](https://electrathonoftampabay.org/www/Documents/Motors/Brushless%20DC%20(BLDC)%20Motor%20Fundamentals.pdf)
 - [68] “Digital Brushless DC Motor Driver 12-30VDC Max 8.0A 120W - BLD-305S | StepperOnline.” Accessed: Mar. 26, 2025. [Online]. Available: https://www.omc-stepperonline.com/digital-brushless-dc-motor-driver-12-30vdc-max-8-0a-120w-bld-305s?srsltid=AfmBOooD_jgeWc-_0Osg2LRiVX2WdJoVYqTfqQk6J9CVmGf0BmXjFudn
 - [69] “ESP32-S3-WROOM-1_1U_v0.5.1_Preliminary.pdf.” Accessed: Mar. 26, 2025. [Online]. Available: https://media.digikey.com/pdf/Data%20Sheets/Esspressif%20PDFs/ESP32-S3-WROOM-1_1U_v0.5.1_Preliminary.pdf
 - [70] “esp32-s3-devkitc-1-v1.1-isometric.png (800×695).” Accessed: Mar. 26, 2025. [Online]. Available: https://docs.espressif.com/projects/esp-idf/en/v5.2.2/esp32s3/_images/esp32-s3-devkitc-1-v1.1-isometric.png
 - [71] “Modbus_Application_Protocol_V1_1b3.pdf.” Accessed: Mar. 26, 2025. [Online]. Available: https://www.modbus.org/docs/Modbus_Application_Protocol_V1_1b3.pdf
 - [72] “Transistor-transistor logic,” *Wikipedia*. Feb. 27, 2025. Accessed: Mar. 26, 2025. [Online]. Available: https://en.wikipedia.org/w/index.php?title=Transistor%E2%80%93transistor_logic&oldid=1277889675
 - [73] “ESP-NOW - - — ESP-FAQ latest documentation.” Accessed: Mar. 26, 2025. [Online]. Available: <https://docs.espressif.com/projects/esp-faq/en/latest/application-solution/esp-now.html>
 - [74] J. Wu, “A Basic Guide to I2C,” 2022.
 - [75] M. Bishop, “HTTP/3,” Internet Engineering Task Force, Request for Comments RFC 9114, Jun. 2022. doi: 10.17487/RFC9114.

- [76] E. Rescorla and T. Dierks, “The Transport Layer Security (TLS) Protocol Version 1.2,” Internet Engineering Task Force, Request for Comments RFC 5246, Aug. 2008. doi: 10.17487/RFC5246.
- [77] A. Melnikov and I. Fette, “The WebSocket Protocol,” Internet Engineering Task Force, Request for Comments RFC 6455, Dec. 2011. doi: 10.17487/RFC6455.
- [78] “ECMAScript® 2024 Language Specification.” Accessed: Mar. 26, 2025. [Online]. Available: https://262.ecma-international.org/15.0/index.html?_gl=1*1xaqef8*_ga*MTc0NTU3NDEwNy4xNzQyOTkzNTg0*_ga_TDCK4DWEPP*MTc0Mjk5MzU4My4xLjAuMTc0Mjk5MzU4My4wLjAuMA..
- [79] “React Reference Overview – React.” Accessed: Mar. 26, 2025. [Online]. Available: <https://react.dev/reference/react>
- [80] “Introduction | Next.js.” Accessed: Mar. 26, 2025. [Online]. Available: <https://nextjs.org/docs>
- [81] “CN20137-40.jpg (1000×754).” Accessed: Mar. 26, 2025. [Online]. Available: https://cpcireland.farnell.com/productimages/large/en_GB/CN20137-40.jpg
- [82] “Hamamatsu C12666MA - Google Search.” Accessed: Mar. 26, 2025. [Online]. Available: https://www.google.com/search?sca_esv=83ceb05c68cf2c95&sxsrf=AHTn8zqyAYQHCme7vsYzXUqQ7xg2WsFQw:1742999380569&q=Hamamatsu+C12666MA&udm=2&fbs=ABzOT_CWdhQLP1FcmU5B0fn3xuWpA-dk4wpBWOGsoR7DG5zJBteutRhClwSdaS7of3GY5DR_y7mjIMia4GqlCEeMWtqGsAXllFStCZvJ1xN0vTFEYZt4bVUjvc8Jbh_KPsDQQO0qL5JUGSA4CcunuWkd8AR6d3fcLcFqHg7FM7TqoZWg-we_P3bBVi6m1mbQfgnFfJBgnMk9hYtbnhVSgU6FM9ap1afqLQ&sa=X&ved=2ahUKEwi6vbDX-qeMAXV0QUEAHXwKA9IQtKgLegQIIBAB&biw=2056&bih=1198&dpr=2#vhid=3ViwLSXs42yq9M&vssid=mosaic
- [83] “R2018344-01.jpg (1200×675).” Accessed: Mar. 26, 2025. [Online]. Available: <https://media.rs-online.com/R2018344-01.jpg>
- [84] “AS7265x-DS000612.pdf.” Accessed: Mar. 26, 2025. [Online]. Available: <https://look.ams-osram.com/m/76ce4c0d80cd1565/original/AS7265x-DS000612.pdf>
- [85] “4698-10.jpg (970×728).” Accessed: Mar. 26, 2025. [Online]. Available: <https://cdn-shop.adafruit.com/970x728/4698-10.jpg>
- [86] “AS7341-DS000504.pdf.” Accessed: Mar. 26, 2025. [Online]. Available: <https://look.ams-osram.com/m/24266a3e584de4db/original/AS7341-DS000504.pdf>

Appendix Three

Risk Assessment Forms

DCU Health and Safety Office

Project Title: DK3 - Development of a portable lab instrument

Researcher Name:

Conor Curley

Equipment/Process Name: Centrifugal Microfluidics

Preparation/Review Date:

11/29/24

Supervisor: Dr. David Kinahan | Technical Staff: Alan Meehan, Cian Merne

Location:

N/A

Who is affected by the Hazard: Staff, Research students, visitors														
Hazards	Is the Hazard present? Y/N	What is the risk?	Likelihood	Severity	Risk Rating (LxS)	Risk Rating -prior to having controls in place H= high M=Medium L= Low	Controls - Controls in place to reduce risks	Is the control in place? Y/N	Likelihood	Severity	Risk Rating (LxS)	L/M/H	Control measure implementation - Person/Office/Unit/Dept. responsible?	Approved by
Risk of Burn	Y	Minor risk of exposure to moderate-high temperatures on project rig	1	2	2	L	Hazard labels applied to hot rig components to inform user of risk	Y	1	1	1	L	Conor Curley	Dr. David Kinahan
							Rig enclosure is interlocked to prevent interaction with hot components while rig is in operation	Y					Conor Curley	Dr. David Kinahan
Risk of Crush, Pinch, Impact	Y	Minor risk of crush/pinch injury from interacting with centrifugal element of rig, minor risk of impact injury from rig failure	1	3	3	L	Rig fully enclosed in protective guarding to prevent interaction with rig during operation, and to prevent loose objects from being ejected from the rig during operation in the event of failure.	Y	1	1	1	L	Conor Curley	Dr. David Kinahan
							Rig enclosure is interlocked to prevent interaction with rig components while the rig is in operation.	Y					Conor Curley	Dr. David Kinahan

Researcher signature: C Curley

Technician signature(s): _____

Supervisor signature: _____

Date: _____

Date: _____

Date: _____

A copy of this form when completed should be submitted through the School Health & Safety Loop page. A copy should also be available where project work is undertaken.